METALLOPROTEASE REGULATION SHAPES THE BMP GRADIENT

IN SPACE AND TIME

Francesca Bartoloni Tuazon

A DISSERTATION

in

Cell and Molecular Biology

Presented to the Faculties of the University of Pennsylvania

in

Partial Fulfillment of the Requirements for the

Degree of Doctor of Philosophy

2019

Supervisor of Dissertation

_____

Mary Mullins, Professor and Vice Chair of Cell and Developmental Biology

Graduate Group Chairperson

_____

Daniel Kessler, Associate Professor of Cell and Developmental Biology

Dissertation Committee

Scott Poethig, John H. and Margaret B. Fassitt Professor of Biology

Peter Klein, Professor of Medicine

Matthew Good, Assistant Professor of Cell and Developmental Biology

Eileen Shore, Cali and Weldon FOP Research Professor of Orthopaedic Surgery

METALLOPROTEASE REGULATION SHAPES THE BMP GRADIENT IN SPACE AND TIME

Dedication

Inspiration move me brightly
light the song with sense and color,
hold away despair
More than this I will not ask
faced with mysteries dark and vast
statements just seem vain at last
some rise, some fall, some climb
to get to Terrapin

ACKNOWLEDGMENTS

This dissertation owes its life and journey to my thesis advisor, Mary Mullins. Remarkably, we built this research project based on my curiosity in a paper that I read and presented in her Development class. With Mary's enthusiastic support and her tireless dedication to rigorous science, this project and my own identity as a scientist blossomed. Beyond the bench, Mary remains an encouraging sponsor, recommending me for opportunities that allow me to grow. From TA-ing the Woods Hole Zebrafish course, to visiting our collaborators at Purdue University, to talk and panel positions, she continues to invest in my development and success. Mary also fostered and refined my existing passion for science writing. Through multiple grant applications (even a perfect score, one of my proudest accomplishments), abstracts, and manuscripts, she helped hone my skill and voice. We make an impressive team! Emerging from my graduate research training, I can confidently say that I am exceptionally well-trained and I am profoundly grateful to Mary for her time and effort.

Mary also cultivates an engaged, creative, and thorough lab thought-environment. I owe much to Mullins Lab members, past and present, for countless hours of suggestions, feedback, and troubleshooting at lab meetings and practice talks. Thank you. Beyond these invaluable contributions, I must acknowledge James Dutko for shepherding me through my rotation and sparking my love of zebrafish and BMP, Joe Zinski for paving the way in quantitative P-Smad imaging and analysis, Hannah Greenfeld for being an ever-encouraging and all around fun bay-mate, and AJ Lucy for being the figure design extraordinaire and a rock of sanity.

I have also been fortunate to have a wide net of support within the Penn community. First and foremost, I thank the DSRB graduate group. Sarah Millar brought me to Penn and Steve DiNardo was our enthusiastic leader, devoted to each students' success. Dan Kessler also served as a guiding voice for CAMB and has helped me navigate graduate school since my recruitment weekend. I also thank my thesis committee, Scott Poethig, Matt Good, Peter Klein, and Eileen Shore. You continually pushed me clarify and strengthen my story, while remaining inspiring and encouraging throughout, and I was able to thrive from your valuable insight.

I thank the CAMB Training Grant, both for its funding and the mentorship of Marisa Bartolomei and Mickey Marks, who had faith in me from my first year and continue to be some of my fiercest advocates. I was also privileged to be welcomed in BMB classes and their retreats, and I thank all BMB faculty for their open curiosity and encouragement, especially Kim Sharp who reminded me to never doubt my abilities. I also thank the DSRB and CDB administrators Meagan Schofer, Christina Strathearn, Megan Harrington, Stephanie Yuhasz, and Venetia Baldwin, who work continuously to support and improve our community.

Beyond Penn, I thank our collaborators at Purdue University, David Umulis and Xu Wang, for investing an incredible amount of work, skill, and patience in incorporating my results into a mathematical model. This is an impressive framework for future work, and I can't wait to see those results! I learned so much from our interdisciplinary collaboration (and many Skypes) and I am confident that I will continue to tap into the systems biology perspective throughout my career.

I would be remiss if I didn't acknowledge those who got me to graduate school: Sarah Kucenas, Mike Wormington, Tony Spano, and Jay Hirsh at the University of Virginia. They put graduate school on my radar as a serious career option and their

unbridled encouragement gave me the confidence to go for it. Sarah continues to be source of inspiration and reassurance and I look forward to remaining her colleague as part of the zebrafish research community. Relatedly, I must also thank Allan Goldberg for guiding me through the depths of my own resilience and for providing a critical framework for navigating life and graduate school.

My impressive and inspiring peers kept life lively and were always there to commiserate with the lows and celebrate the highs of graduate school (and life) together. Thank you: Isabel Sierra, Atrish Bagchi, Michael Herriges, Celine Santiago, Sarah Gwyn, Chris Bialas, Cat Debrosse, Joe Jordan, and John Welsh. After defenses and weddings, I am excited to see what the future holds for our friendships. Special thanks to Lyman Stebbins, a neighbor serendipitously turned friend for this Long Strange Trip, and Katie Welsh, whose unflagging support shows just how far #roomielove can go.

Finally, and most significantly, I thank my family. To my parents, Kata and Raul, your steadfast encouragement of my curiosity and creativity made me the scientist I am today. You have truly nurtured and protected a lifelong Sense of Wonder and your unconditional love continually empowers me to carve out my own path. To my in-laws, Jody and Bill, I cherish being embraced into your family and that you always make me smile as you cheer me (and my mutants) on. To my husband, Cory, your love and unwavering support feed my strength, motivation, and happiness. Thank you for being my rock in the most serious of moments and for making me laugh when I need to lighten up. I am immensely proud to say that I am the scientist and human being I am today because of you. Lastly, Arusha, thank you for always being my buddy. You were my thesis cat, too, even if only in spirit.

ABSTRACT

METALLOPROTEASE REGULATION SHAPES THE BMP GRADIENT

IN SPACE AND TIME

Francesca Tuazon

Mary Mullins

A fundamental question in developmental biology is how morphogens, such as Bone Morphogenetic Protein (BMP), form precise signaling gradients to impart positional and functional identity to the cells of the early embryo. The primary goal of this research is to employ recent advances in the quantitative measurement and visualization of the BMP signaling gradient to elucidate the mechanisms that shape the zebrafish BMP morphogen gradient in space and time. Specifically, I investigated the roles of Bmp1a and Tolloid, metalloproteases that promote BMP signaling by cleaving the critical BMP antagonist Chordin, and their competitive inhibitor Sizzled.

I combined rigorous mutant analyses with quantitative immunofluorescence to determine that the proteases Bmp1a and Tolloid spatially restrict Chordin in the early zebrafish gastrula. I discovered that maternally-deposited Bmp1a plays an unexpected and non-redundant role in establishing the BMP gradient, while Sizzled is surprisingly dispensable. Combining mathematical models and *in vivo* analyses with an immobile Chordin construct, I demonstrate that Chordin diffusion is dispensable for BMP gradient formation and DV patterning. These data exclude a counter-gradient of Chordin and instead favor a Chordin sink, established by Bmp1a and Tolloid, as the primary mechanism that drives BMP gradient formation.

I applied quantitative immunofluorescence to wild-type embryos and determined that the BMP signaling gradient steepens by the end of gastrulation. I discovered that Tolloid and Sizzled play separate roles in shaping the BMP gradient during gastrulation: they are first required at different stages and Tolloid steepens the BMP gradient while Sizzled limits the lateral extent of the highest BMP levels. These results suggest that gastrulation represents a new signaling environment that requires additional regulation by Tolloid and Sizzled. Taken together, I have defined distinct spatiotemporal roles for Bmp1a, Tolloid, and Sizzled in both establishing and then later shaping the BMP signaling gradient during zebrafish DV patterning.

TABLE OF CONTENTS

LIST OF TABLES

LIST OF ILLUSTRATIONS

CHAPTER 1. Spatiotemporal regulation of morphogen signaling patterns the early embryo

Contributions: This chapter contains figures and direct quotes from Tuazon and Mullins published in 2015 in *Seminars in Cell and Developmental Biology* (Tuazon and Mullins, 2015) and Tuazon, et al. under revision at *Cell Reports*.

1.1 Introduction: Orthogonal morphogen gradients pattern the early embryo

A fundamental question of developmental biology is how the un-patterned cells of the early embryo gain the positional and functional identity necessary to generate a mature organism (Wolpert, 1969). In this process distinct cell fates are specified by morphogens, signaling factors that form spatial gradients to direct cell fate (Ashe and Briscoe, 2006; Briscoe and Small, 2015; Rogers and Schier, 2011). Morphogens act in a concentration-dependent manner as a gradient of high, intermediate, and low activity specifies discrete cell fates. Morphogens are important for the initial patterning of the pluripotent cells of the early embryo, as well as for tissue and organ patterning later in development (Sansom and Livesey, 2009; Tuazon and Mullins, 2015). Furthermore, these developmental signaling molecules are often re-used during injury repair and exploited in disease progression. Thus, uncovering the mechanisms that underlie the generation and regulation of morphogen gradients has broad implications to our understanding of development and disease.

In vertebrates, distinct signaling proteins act as morphogens to pattern the dorsoventral (DV) axes and anteroposterior (AP), the foundation of the bilateral body plan. Since the amount of each signal at precise locations patterns the entire organism, the spatial regulation of individual morphogen levels is critical. Moreover, this precise distribution of morphogen signaling cannot be established instantaneously and entire embryo cannot be patterned all at once. Correct morphogen signaling levels must be maintained throughout the patterning process and cells must also be equipped to know exactly when to respond to morphogen signals to adopt their correct fate (Balaskas et al., 2012). Thus, temporal regulation of morphogen signaling and target cell competence are also essential to pattern a complete body axis. Furthermore, patterning of all DV and AP

tissues spans late blastula, gastrula, and somitogenesis stages, which are distinct and dynamic physical environments, so spatial and temporal regulation of morphogen signaling must be coordinated to navigate the challenges of early embryo development.

Although separate mechanisms exist for patterning the DV and AP axes, both axes are patterned concomitantly; these orthogonal patterning mechanisms must work in harmony across both space and time to properly pattern the organism. Patterning along the DV axis is directed by ventralizing Bone Morphogenetic Proteins (BMP) signaling, while patterning along the AP axis is directed by posteriorizing signals Wnt, fibroblast growth factor (FGF), Nodal, and retinoic acid (RA). This chapter addresses the current understanding of *Xenopus* and zebrafish DV and AP axial patterning during gastrulation as separate processes (Sections 1.2 and 1.3, respectively), as well as more recent advances in uncovering the mechanisms that coordinate DV and AP patterning in zebrafish (Section 1.4). This chapter also discusses the relationship between fate specification and the morphogenic movements of gastrulation (Section 1.5) and current techniques for visualizing morphogen gradients and manipulating spatial and temporal aspects of patterning (Section 1.6). The final section presents the goals of this dissertation research project within the context of DV patterning (Section 1.7).

1.2 A BMP morphogen gradient patterns the DV axis

1.2.1 Maternal establishment of the DV axis

In *Xenopus* and zebrafish, the initial DV axis is established by maternal Wnt/β-catenin signaling activating dorsal gene expression in prospective dorsal cells (Itoh et al., 1998; Langdon and Mullins, 2011; Moon and Kimelman, 1998; Schroeder and Yost, 1996;

Tao et al., 2005). This initial DV polarity depends on both the vegetal localization of dorsal determinants in the egg and their asymmetric transport via microtubules to the future dorsal side during embryonic cleavage stages. In zebrafish, maternal Wnt/β-catenin signaling dorsally activates the zygotic expression of dorsal genes *bozozok* and *fgf*, which establish and maintain the dorsal organizer (Langdon and Mullins, 2011). Another important organizer gene, *goosecoid*, is induced by Nodal signaling (Feldman et al., 1998; Gritsman et al., 2000; Zinski et al., 2018).

The dorsal organizer protects dorsal cell fates during axial patterning in two fashions. First, it induces the *chordin*, *noggin*, and *follistatin* genes, resulting in the expression of essential secreted BMP antagonists (Section 1.2.4). The dorsal organizer also inhibits the activity of *vox/vent/ved*, which transcriptionally repress dorsal genes (Section 1.3.5) (De Robertis, 2006; Flores et al., 2008; Kawahara et al., 2000; Melby et al., 2000; Melby et al., 1999; Onichtchouk et al., 1998; Shimizu et al., 2002; Trindade et al., 1999). As long as the dorsal organizer is correctly established by the aforementioned maternal mechanisms, the specification of DV cell fates is directed by BMP signaling in the embryo, as detailed below.

1.2.2 BMP signal transduction

Bone Morphogenetic Proteins (BMPs) are secreted growth factors belonging to the TGF-β superfamily (Zinski et al., 2018). While there are numerous distinct BMP ligands, the prominent BMP ligands during DV patterning are BMP2/4 and BMP7 (Dutko and Mullins, 2011). BMPs are secreted as either covalently linked homodimers or heterodimers, though in zebrafish the BMP2/7 heterodimer is the obligate ligand (Little and Mullins, 2009). BMPs bind a serine/threonine kinase receptor complex composed of two Type I (Bmpr1 and/or Acvr1l) and two Type II (Bmpr2 and/or Acvr2) receptors **(Figure**

1.1A) (Armes and Smith, 1997; Graff et al., 1994; Little and Mullins, 2009; Nikaido et al., 1999; Shi and Massague, 2003). In zebrafish, the BMP2/7 heterodimer is thought to signal through a heterotetrameric receptor complex comprised of both Bmpr1 and Acvr1l, and still unknown Type II receptors (Little and Mullins, 2009).

Upon BMP binding, the activated Type I receptors phosphorylate the C-terminus of the Smad1/5 transcription factor (P-Smad1/5), resulting in its nuclear accumulation **(Figure 1.1A)** (Feng and Derynck, 2005; Little and Mullins, 2009; Schmierer and Hill, 2007). In *Xenopus*, Smad1 is the primary transducer of BMP signaling during gastrulation, while in zebrafish *smad5* functions predominantly over *smad1* (Dick et al., 1999; Hild et al., 1999; Kramer et al., 2002; Wilson et al., 1997). Since Smad1 and Smad5 have equivalent phosphorylation sites and ventralizing activity (Hashiguchi and Mullins, 2013), they will be referred to as Smad1/5. After P-Smad5 subsequently accumulates in the nucleus, it induces BMP target genes (Hild et al., 1999; Massague et al., 2005; Schmierer and Hill, 2007).

1.2.3 A gradient of BMP signaling specifies ventrolateral cell fates

BMPs act as a morphogen to pattern the embryonic DV axis of all vertebrates (Bier and De Robertis, 2015; Tuazon and Mullins, 2015; Zinski et al., 2018). Specifically, a BMP signaling gradient specifies ventral cell fates (e.g. epidermis, blood, posterior somites) at high levels and lateral fates (e.g. neural crest) at intermediate levels, while dorsal fates (e.g. neural tissue, anterior somites) result from no BMP signaling **(Figure 1.1C)** (Bier and De Robertis, 2015; Dale et al., 1992; De Robertis and Sasai, 1996; Heasman, 2006; Knecht and Harland, 1997; Nguyen et al., 1998; Schier and Talbot, 2005; Schumacher et al., 2011; Tuazon and Mullins, 2015; Tucker et al., 2008). BMP signaling is essential to specify ventral cell fates: loss of BMP signaling results in the ablation of ventral tissues

with the concurrent expansion of dorsal tissues (Kishimoto et al., 1997; Schmid et al., 2000). In the zebrafish embryo, initial *bmp* expression is widespread and thus present dorsally, but it becomes restricted to the ventral half of the embryo during DV patterning (Dick et al., 2000; Schmid et al., 2000).

The BMP signaling gradient has been visualized by immunofluorescent staining for nuclear P-Smad1/5, a direct intracellular readout of BMP signaling. Use of this approach in *Xenopus* (Cho et al., 2013; Faure et al., 2000; Plouhinec et al., 2013; Schohl and Fagotto, 2002) and zebrafish (Hashiguchi and Mullins, 2013; Ramel and Hill, 2013; Tucker et al., 2008; Xue et al., 2014; Zinski et al., 2017; Zinski et al., 2019) reveals a gradient of P-Smad1/5 at mid-blastula stages that intensifies during gastrulation, exhibiting high P-Smad1/5 intensity ventrally and little to no P-Smad1/5 dorsally. In zebrafish there are differing reports for nuclear P-Smad1/5 in the dorsal organizer: most observe no dorsal P-Smad1/5 (Hashiguchi and Mullins, 2013; Ramel and Hill, 2013; Tucker et al., 2008; Zinski et al., 2017; Zinski et al., 2019), while another observes P-Smad1/5 in the dorsal organizer (Xue et al., 2014). Although all groups use the same antibody and dilution, there are differences in embryo pre-staining processing. An epitope recovery method (Xue et al., 2014) shows P-Smad1/5 in the dorsal organizer, whereas standard methods do not. The most recent advances in quantitative visualization of the P-Smad1/5 gradient (Zinski et al., 2017; Zinski et al., 2019), which were utilized throughout this project, are briefly summarized in Section 1.6.1 and detailed in Section 6.4.

1.2.4 Extracellular modulators generate and regulate the BMP gradient

The BMP signaling gradient is generated by extracellular mechanisms. In zebrafish embryos devoid of BMP signaling, BMP heterodimer protein can be injected directly into the extracellular space and completely rescue the P-Smad1/5 gradient before the onset

of gastrulation (Little and Mullins, 2009). Injection of exogenous heterodimer protein circumvents other potential mechanisms for gradient formation, such as graded *bmp* expression or transcriptional inputs (Section 1.3.5). This rescue by injected heterodimer protein suggests that the BMP gradient is generated largely by extracellular mechanisms. This is consistent with the rescue of severely dorsalized BMP mutants by injecting *bmp* RNA at the one-cell stage; although *bmp* RNA is initially present uniformly, the BMP gradient is still able to correctly pattern the DV axis (Dick et al., 2000; Nguyen et al., 1998).

Various secreted modulators are responsible for generating and further regulating the BMP ligand gradient (Little and Mullins, 2006; Umulis et al., 2009; Zakin and De Robertis, 2010; Zinski et al., 2018). These extracellular modulators promote or restrict BMP signaling in defined cellular domains across distinct phases of development, providing precise spatial and temporal control of signaling. An example of such precise control is the patterning of the preplacodal ectoderm (Section 4.1). BMP signaling is initially required to specify these tissues at the onset of gastrulation, but must be completely blocked after gastrulation for their final specification (Kwon et al., 2010; Reichert et al., 2013; Wawersik et al., 2005). Across vertebrates, this versatility of BMP regulation is important beyond DV patterning, too, since BMP gradients are later repurposed to direct patterning of specific organs, such as the neural tube and digits (Dutko and Mullins, 2011; Suzuki et al., 2008; Zagorski et al., 2017).

The primary extracellular modulators of BMP signaling are the BMP antagonists, which are secreted dorsally and bind and sequester BMPs to prevent ligand-receptor binding (Dutko and Mullins, 2011; Fainsod et al., 1997; Piccolo et al., 1996; Troilo et al., 2014; Zimmerman et al., 1996). The BMP antagonists include Chordin, Noggin, and Follistatin and they are fundamental to DV patterning since loss of all three antagonists

results in the ablation of dorsal tissues **(Figure 1.2C)** (Dal-Pra et al., 2006; Khokha et al., 2005; Little and Mullins, 2006). Chordin, however, is the central BMP antagonist since depletion of Chordin alone results in ventralization **(Figure 1.1A)** (Dal-Pra et al., 2006). Furthermore, Chordin is also required throughout various stages of DV patterning to continue to regulate BMP signaling (Connors et al., 2006; Fisher et al., 1997; Fisher and Halpern, 1999; Hammerschmidt et al., 1996a; Hammerschmidt et al., 1996b; Piccolo et al., 1996; Schulte-Merker et al., 1997). Finally, unlike Noggin and Follistatin, Chordin itself can be modulated by additional extracellular regulators, detailed below.

Chordin function is primarily modulated by two additional classes of proteins: (i) the metalloproteases Bmp1a and Tolloid, which cleave and inactivate Chordin (Blader et al., 1997; Jasuja et al., 2007; Muraoka et al., 2006; Piccolo et al., 1997; Wardle et al., 1999), and (ii) the metalloprotease inhibitor Sizzled, which binds the active site of Bmp1a and Tolloid to prevent them from cleaving Chordin **(Figure 1.1A)** (Lee et al., 2006; Muraoka et al., 2006). These genes are expressed in distinct domains: *bmp2/7* and *sizzled* ventrally (Schmid et al., 2000; Yabe et al., 2003), *chordin* dorsally (Schulte-Merker et al., 1997), and *bmp1a* and *tolloid* ubiquitously **(Figure 1.1B)** (Connors et al., 1999; Jasuja et al., 2007; Muraoka et al., 2006).

Additional Chordin regulators include BMP binding endothelial regulator (Bmper, also known as Crossveinless-2) and Twisted-gastrulation (Tsg). Bmper is known to both promote and inhibit BMP function in different contexts. In zebrafish, Bmper enhances BMP signaling when Chordin is present while inhibiting BMP signaling when Chordin is absent (Zhang et al., 2010) **(Figure 1.2C)**. Bmper may also antagonize Chordin activity in a complex with Tsg and BMP **(Figure 1.2C)** (Ambrosio et al., 2008; Ikeya et al., 2010; Reichert et al., 2013; Rentzsch et al., 2006). Finally, Twisted-gastrulation (Tsg), which

forms a ternary complex with Chordin and the BMP ligands, can either promote the cleavage of Chordin by Tolloid or, in the absence of Tolloid, inhibit BMP signaling **(Figure 1.2C)** (Larrain et al., 2001; Little and Mullins, 2004; Oelgeschlager et al., 2000; Oelgeschlager et al., 2003; Ross et al., 2001; Scott et al., 2001). Both Tsg and Bmper are expressed ventrally (Zinski et al., 2018).

This plethora of Chordin regulators suggests that regulating Chordin activity is key to shaping the BMP signaling gradient and DV patterning. Furthermore, there is emerging evidence that delimiting the Chordin expression domain is fundamental for establishing and maintaining a correct BMP signaling gradient (Genikhovich et al., 2015; Inomata et al., 2013; Plouhinec et al., 2013; Xue et al., 2014; Zinski et al., 2017). The partially-redundant roles of Bmp1a and Tolloid in restricting Chordin range and establishing the BMP signaling gradient are detailed in Chapter 2. The distinct roles of Tolloid and Sizzled in shaping the BMP signaling gradient during gastrulation are explored in Chapter 3. Finally, the role of Bmper in patterning the preplacodal ectoderm and the otic vesicle is investigated in Chapter 4.

1.3 Combinatorial Wnt, FGF, Nodal, and RA morphogenetic signaling pattern the AP axis

Although initial AP polarity in amphibians and fish is determined by the animal-vegetal axis of the egg, which is maternally established, the patterning of distinct AP cell fates in all vertebrates is controlled during late blastula and gastrula embryonic stages. By the end of gastrulation in *Xenopus*, zebrafish, chick, and mouse, a clear division of anterior and posterior cell fates has been established (Darnell et al., 1999; Gamse and Sive, 2000; Gawantka et al., 1998; Grinblat et al., 1998; Harland and Gerhart, 1997; Knoetgen et al.,

1999; Rowan et al., 1999; Simeone et al., 1993; Thomas and Beddington, 1996). AP patterning is mediated by Wnt, fibroblast growth factor (FGF), Nodal, and retinoic acid (RA) signaling. Specifically, Wnt, FGF, Nodal, and RA specify posterior cell fates and the specification of anterior cell fates relies on the graded inhibition of these signals.

During blastula and gastrula stages Wnt, FGF, and Nodal establish the broad regions of the AP body axis (the head, trunk, and tail as most posterior) **(Figure 1.2)**. Additionally, Nodal patterns the mesendoderm while Wnt, FGF, and RA specify distinct AP cell fates in the neural plate, dividing it into four distinct regions to establish the central nervous system (CNS). These four rostral (anterior) to caudal (posterior) subdivisions are the forebrain, midbrain, hindbrain, which is further subdivided into rhombomeres (numbered 1-7 from rostral to caudal in the zebrafish), and spinal cord **(Figure 1.2A)** (Green et al., 2015). Although the complete specification of CNS fates extends beyond gastrulation, these earlier subdivisions of the CNS can be used as a reliable readout of AP axial patterning. The roles of Wnt, FGF, Nodal, and RA signaling in patterning the AP body axis and/or the CNS are described below.

1.3.1 A Wnt gradient specifies posterior cell fates

Wnts are secreted cysteine-rich glycoproteins that bind to the Frizzled (Fz) family of receptors with the assistance of co-receptors such as low-density lipoprotein receptor-related proteins (LRPs) and heparin-sulphate proteoglycans (HSPGs) (Yamaguchi, 2001). During AP patterning, Wnt signaling activates the canonical Wnt/β-catenin pathway and promotes the expression of posterior genes (Hikasa and Sokol, 2013; Langdon and Mullins, 2011). During early and mid-blastula stages in the frog and zebrafish embryo, maternal Wnt signaling is localized dorsally and establishes the dorsal organizer, which establishes DV asymmetry (Sections 1.2.1 and 1.3.5) (Langdon and Mullins, 2011).

However, during late blastula and gastrula stages zygotic Wnt signaling is excluded from the dorsal organizer and localized to the ventrolateral embryo margin; this change in localization during gastrulation coincides with a dramatic change in Wnt function.

Zygotic Wnt functions in posterior tissue development **(Figure 1.2B)**: increasing zygotic Wnt signaling results in the loss of head structures (Christian and Moon, 1993; Dorsky et al., 2003; Glinka et al., 1998; Hikasa et al., 2010; Kim et al., 2000), whereas embryos deficient in Wnt signaling exhibit a dramatic loss of the tail and a reciprocally enlarged the head (Bellipanni et al., 2006; Heasman et al., 2000; Lekven et al., 2001; Shimizu et al., 2005). AP patterning by Wnt also depends on Wnt antagonists, including secreted Frizzled-related proteins (sFRPs) and Dickkopf (Dkk), which are localized anteriorly **(Figure 1.2B)** (Glinka et al., 1998; Hikasa and Sokol, 2013; Leyns et al., 1997). sFRPs are secreted proteins that contain domains homologous to the Wnt binding site of Fz receptors and thus bind Wnt and prevent Fz activation, while Dkk proteins are membrane-bound and bind LRP co-receptors to prevent the propagation of Wnt signaling (Yamaguchi, 2001).

Wnt signaling is also key to AP neural patterning, specifying caudal CNS cell fates (Bang et al., 1999; Dorsky et al., 2003; Itoh and Sokol, 1997; Kiecker and Niehrs, 2001; Kim et al., 2000; Lekven et al., 2001; McGrew et al., 1997; McGrew et al., 1995; Nordstrom et al., 2002; Rhinn et al., 2005). Studies of AP patterning in the CNS beautifully show that Wnt acts as a morphogen to specify caudal cell fates in a concentration-dependent manner (Erter et al., 2001; Itoh and Sokol, 1997; Kiecker and Niehrs, 2001; Lekven et al., 2001; Nordstrom et al., 2002; Rhinn et al., 2005). Remarkably, grafting Wnt-expressing cells or beads near forebrain progenitors (Nordstrom et al., 2002; Woo and Fraser, 1997) or incubating *Xenopus* animal cap explants (the most anterior tissue) with Wnt (Kiecker

and Niehrs, 2001) induces caudal cell fates that vary depending on the amount of Wnt expressed. This supports a prominent role for Wnt signaling in establishing the broad subdomains of the AP axis since Wnt can directly convey posterior positional information to specify the proportion and distribution of caudal cell fates in multiple regions of the developing CNS. Importantly, the most rostral cell fates, like the forebrain, require Wnt signal inhibition, which underscores the equal importance of Wnt antagonism in AP patterning (Houart et al., 2002; McGrew et al., 1997).

Although as a morphogen Wnt must function over a distance, Wnt is post-translationally modified with lipids that make it hydrophobic, insoluble, and poorly mobile, thus limiting its ability to form a signaling gradient by free diffusion (Port and Basler, 2010). Recent studies of fluorescently tagged Wnt in live zebrafish embryos offer an alternative mechanism for generating a gradient: short, actin-based filopodia can transport Wnt to the contact point between neighboring cells and activate Wnt signaling, increasing its effective signaling range (Stanganello et al., 2015).

1.3.2 An FGF gradient specifies posterior cell fates

FGFs are secreted growth factors that bind and activate FGF receptors (FGFRs). FGFRs are receptor tyrosine kinases (RTKs) and FGF binding results in receptor dimerization and intracellular *trans* phosphorylation (Pownall and Isaacs, 2010). Activated FGFRs recruit and activate a wide range of effectors, including Grb2 and Ras, which ultimately activate MAPK (mitogen activate protein kinase). Activated MAPK phosphorylates various transcription factors to regulate gene expression (Pownall and Isaacs, 2010). In zebrafish, FGF signaling is first induced during early blastula stages by maternal Wnt signaling (Langdon and Mullins, 2011). This initial FGF expression localizes

to the dorsal margin and contributes to inducing the dorsal organizer in DV axis formation (Sections 1.2.1 and 1.3.5).

However, similar to Wnt, FGF expression expands throughout the margin during gastrulation. This change in FGF expression coincides with a distinct role for FGF to promote posterior tissues development **(Figure 1.2B)** (Dorey and Amaya, 2010). Loss of FGF activity results in the loss of trunk and tail (Amaya et al., 1991; Draper et al., 2003; Griffin and Kimelman, 2003), while gain of FGF activity causes the loss of head tissues (Christen and Slack, 1997; Isaacs et al., 1994). FGF signaling is inhibited by Sprouty proteins, which interfere with the activation of the MAPK signaling cascade **(Figure 1.2B)** (Mason et al., 2006). Interestingly, since Sprouty can be localized in the cytosol or at the membrane, the mechanism of Sprouty inhibition of MAPK is context dependent and remains to be characterized during AP patterning (Cabrita and Christofori, 2008; Mason et al., 2006).

During CNS development, FGF maintains the midbrain-hindbrain boundary (Lamb and Harland, 1995; Reifers et al., 1998) and induces caudal cell fates like the hindbrain and spinal cord (Cox and Hemmati-Brivanlou, 1995; Doniach, 1995; Dyer et al., 2014; Kengaku and Okamoto, 1995; Kudoh et al., 2004; Labalette et al., 2011). Unlike Wnt signaling, FGF is not sufficient to ectopically induce caudal cell fates in the forebrain (Woo and Fraser, 1997) or in animal explants (McGrew et al., 1997). Although this supports a more prominent role for Wnt signaling in specifying the broad subdivisions of the CNS (Green et al., 2015), it is notable that FGF is required to generate a permissive environment for the caudalizing activity of Wnt (McGrew et al., 1997). The complex relationship between FGF and Wnt during neural patterning remains to be fully

characterized, but a recent study suggests that Wnt may regulate Sprouty expression, providing a mechanism to coordinate Wnt and FGF signaling (Dyer et al., 2014).

Evidence indicates that FGF functions as a morphogen, differentially activating posterior genes in a concentration- dependent manner (Dyer et al., 2014; Kengaku and Okamoto, 1995; Scholpp and Brand, 2004). Studies of tagged FGF and single molecule fluorescence correlation spectroscopy (FCS) suggest that the FGF gradient is generated by free diffusion of the ligand and receptor-mediated endocytosis (Scholpp and Brand, 2004; Yu et al., 2009).

1.3.3 A Nodal gradient specifies mesendoderm and posterior cell fates

Nodal proteins are secreted ligands belonging to the TGFβ superfamily. Nodal signaling is mediated by EGF-CFC (epidermal growth factor-Cripto-1/FRL-1/Cryptic) co-receptors and type I and type II Activin receptors, which are serine/threonine kinases (Gritsman et al., 1999; Schier, 2001; Zinski et al., 2018). Receptor activation results in the phosphorylation and nuclear accumulation of the Smad2 and Smad3 transcription factors, which then direct the transcriptional activity of target genes (Schier, 2003; Schier and Talbot, 2005; Zinski et al., 2018). The Nodal ligands identified in vertebrates are named as follows: Nodal in mouse; Nodal-related 1 (Ndr1, previously known as Squint), Ndr2 (previously known as Cyclops), and Ndr3 (previously known as Southpaw) in zebrafish; and *Xenopus* Nodal-related (Xnr) 1, 2,4,5, and 6 (Schier, 2003; Zinski et al., 2018). In early zebrafish and *Xenopus* embryos, Nodals are expressed around the margin and enriched dorsally and have region- and stage-specific functions (Bellipanni et al., 2006; Feldman et al., 1998; Jones et al., 1995; Joseph and Melton, 1997; Rebagliati et al., 1998; Shimizu et al., 2005; Smith et al., 1995).

Dorsally, Nodal is induced by maternal Wnt signaling during blastula stages (Kelly et al., 2000) and functions in formation of the dorsal organizer (Sections 1.2.1 and 1.3.5) (Erter et al., 1998; Feldman et al., 1998; Gritsman et al., 2000; Gritsman et al., 1999; Toyama et al., 1995). At the margin during gastrulation, Nodal is essential to induce and pattern the mesendoderm (Agius et al., 2000; Erter et al., 1998; Feldman et al., 1998; Green et al., 1992; Gritsman et al., 1999; Jones et al., 1995; Joseph and Melton, 1997; Kimelman and Griffin, 2000; Schier, 2009; Smith et al., 1995). In the mesendoderm, Nodal acts as a morphogen to differentially specify cell fates in a concentration-dependent manner: high levels of Nodal activity specify endoderm while lower levels specify mesoderm (Chen and Schier, 2001; Feldman et al., 2002; Green et al., 1992; Gritsman et al., 2000; Schier, 2009).

Nodal also directs AP axial patterning in the zebrafish by specifying posterior cell fates, such as the trunk and tail **(Figure 1.2B)** (Brennan et al., 2001; Schier, 2003; Schier and Talbot, 2005; Thisse et al., 2000). Mis-expressing Nodal and BMP in the most anterior domain of the embryo, the animal pole, ectopically induces trunk and tail tissues (Agathon et al., 2003; Fauny et al., 2009). The posterior fate of the induced tissue depends on the amount of BMP expressed, suggesting that the relative ratio of BMP to Nodal signaling in the margin directs trunk and tail patterning: an equal BMP/Nodal ratio specifies trunk, while a higher ratio specifies tail (Fauny et al., 2009). Since specific levels of BMP relative to Nodal are required, it remains unclear whether Nodal is functioning as a morphogen in this context. Furthermore, the ability of Nodal to induce trunk and tail tissues may be indirect: Nodal has been shown to induce Wnt and FGF expression, which promote posterior cell fates **(Figure 1.2B)** (Erter et al., 1998; Mathieu et al., 2004). Although these studies suggest a role for Nodal in AP patterning, Nodal is also patterning the

mesendoderm during the same time period. These two roles of Nodal require further investigation: do they cooperate or inform each other? are they independent and, if so, what mechanisms enable that independence? is Nodal acting as a morphogen in one context but not the other?

In the zebrafish gastrula, the endogenous Nodal signaling gradient has been visualized by fluorescence of Smad2 and Smad3 (intracellular readouts of Nodal activity) and is highest at the margin and decreases anteriorly (animally) (Harvey and Smith, 2009). Importantly, the Nodal signaling gradient is shaped by the Nodal antagonist, Lefty, which binds to Nodal and EGF-CFC coreceptors to attenuate Nodal signaling **(Figure 1.2B)** (Bisgrove et al., 1999; Chen and Shen, 2004; Chen and Schier, 2002; Feldman et al., 2002; Thisse et al., 2000; Thisse and Thisse, 1999). Furthermore, Nodal and Lefty, as an activator-inhibitor pair, exhibit characteristics described in reaction-diffusion models of pattern formation; mainly that Nodal acts at a short- to mid-range distance and induces its own expression and the expression of its inhibitor, Lefty, which acts at a long-range distance (Meinhardt and Gierer, 2000; Schier, 2009). Although the *in vivo* diffusion rates zebrafish Nodal and Lefty support this model (Chen and Schier, 2002; Muller et al., 2012), more recent studies suggest that alternative mechanisms that rely on temporal regulation, such as microRNA delay of *lefty* translation and/or the duration of Nodal signal may be more prominent (Dubrulle et al., 2015; van Boxtel et al., 2015)

1.3.4 An RA gradient specifies posterior CNS

RA, synthesized through the oxidation of retinol (vitamin A), acts as the ligand for nuclear RA receptors (RAR) (Rhinn and Dolle, 2012). Activated RARs dimerize with retinoid X receptors (RXR), then bind specific DNA motifs to regulate gene expression (Linville et al., 2009; Rhinn and Dolle, 2012). Although embryos lacking RA signaling still

develop posterior tissues and, therefore, RA does not play a role in the broad specification of the body plan, RA signaling is essential during gastrulation to correctly pattern the hindbrain (Begemann et al., 2004; Durston et al., 1989; Grandel et al., 2002; Schilling, 2008). Specifically, RA induces genes that specify the identity of more caudal hindbrain segments (rhombomeres 4-7 in the zebrafish) (Maves and Kimmel, 2005; Sirbu et al., 2005; White et al., 2007) and thus does not play a role in delineating the broad AP subdivisions of the CNS **(Figure 1.2A)** (Green et al., 2015; Kudoh et al., 2002; Maves and Kimmel, 2005).

In the context of the hindbrain, RA acts as a morphogen to directly specify distinct posterior cell fates in a concentration-dependent manner **(Figure 1.2B)** (White et al., 2007). Importantly, discrete levels of RA signaling depend on the active degradation of RA anteriorly by Cyp26 proteins, which degrade RA into its polar metabolites **(Figure 1.2B)** (Hernandez et al., 2007; White et al., 2007; White and Schilling, 2008). *cyp26* can be both induced by RA and suppressed by Wnt and FGF signaling, suggesting that Cyp26 integrates the three posterior neural signals to pattern the hindbrain (Kudoh et al., 2002; White et al., 2007). Additionally, cellular retinoic acid-binding proteins (Crabps), which transport RA to Cy26 enzymes for degradation, maintain the robustness of the RA gradient (Cai et al., 2012). Recently, a gradient of free, unbound RA has been directly observed in live zebrafish embryos by measuring fluorescence resonance energy transfer (FRET) of novel genetically encoded probes for RA (GEPRAs) (Shimozono et al., 2013). The observed RA gradient is highest in the trunk and then declines in a graded fashion both anteriorly and posteriorly, generating a two-tailed gradient (Shimozono et al., 2013).

1.3.5 Transcriptional regulation of BMP by Wnt, FGF, and Nodal signaling

Although Wnt, FGF, and Nodal are clearly required for AP patterning, these factors also affect BMP signaling and DV patterning through transcriptional regulatory relationships that persist from their role in establishing early DV polarity. For example *fgf*, which is initially induced by maternal Wnt/β-catenin, contributes to organizer formation by transcriptionally repressing *bmp2/7* expression and inducing *chordin* expression, thus antagonizing BMP signaling **(Figure 1.2D)** (Furthauer et al., 1997; Furthauer et al., 2004; Maegawa et al., 2006). Similarly, Nodal contributes to organizer formation by inducing *goosecoid* (Dixon Fox and Bruce, 2009; Feldman et al., 1998; Gritsman et al., 2000) and *chordin* (Sirotkin et al., 2000), which can inhibit BMP signaling **(Figure 1.2D)**. Notably, *chordin* is required for the dorsalizing activity of the organizer (Schulte-Merker et al., 1997), but *chordin* expression is not fully dependent on the organizer (Sirotkin et al., 2000).

On the other hand, the role of Wnt signaling changes when it is zygotically expressed. As opposed to its maternal role in establishing the dorsal organizer, zygotic Wnt signaling promotes *vox/vent/ved* expression to promote ventral cell fates (Ramel et al., 2005; Ramel and Lekven, 2004). *vox/vent/ved* maintain *bmp* gene expression ventrally and transcriptionally repress *bozozok, chordin,* and *goosecoid* restricting their expression to dorsal regions **(Figure 1.2D)** (Dixon Fox and Bruce, 2009; Gilardelli et al., 2004; Gonzalez et al., 2000; Imai et al., 2001; Kawahara et al., 2000; Melby et al., 2000; Shimizu et al., 2002). *bozozok*, initially induced by maternal Wnt/β-catenin, promotes dorsal cell fates by acting as a transcriptional repressor of *vox/vent/ved, bmp,* and zygotic *wnt,* while also stimulating *chordin* expression **(Figure 1.2D)** (Fekany-Lee et al., 2000; Leung et al., 2003; Maegawa et al., 2006; Sirotkin et al., 2000; Solnica-Krezel and Driever, 2001). Interestingly, BMP can also induce *vox/vent/ved* expression and thus positively regulate

its own expression **(Figure 1.2D)** (Gilardelli et al., 2004; Melby et al., 2000), though it acquires this ability after the BMP gradient has been established and it has begun patterning the DV axis (Nguyen et al., 1998; Schmid et al., 2000; Tucker et al., 2008). The stage-specific contribution of these transcriptional regulatory relationships remains to be fully characterized and integrated into our understanding of DV patterning.

1.4 Temporally coordinated progressive patterning of the AP and DV axes

Although it is well-characterized that tissues along the AP axis are patterned progressively from anterior to posterior (Stern et al., 2006), the temporal patterning of DV tissues has only recently been investigated. While it had been established in *Xenopus* and zebrafish that BMP signaling patterns most of the DV axis from mid-blastula through gastrula stages, there was only a general understanding of the broad tissue types that were being patterned and the tail is not completely specified within that time window (Marom et al., 2005; Pyati et al., 2005; Wawersik et al., 2005). Although tail progenitors are defined at the onset of gastrulation, their distinct cell fates are not specified until somitogenesis stages (10-24 hpf) (Agathon et al., 2003; Beck et al., 2001; Connors et al., 2006; Pyati et al., 2005; Tucker and Slack, 1995). Given this broad time window for DV patterning (mid-blastula to early somitogenesis stages), the dynamic nature of the BMP morphogen gradient, and the progressive patterning of the AP axis that occurs concomitantly, the field was lacking a precise understanding of the temporal control of DV patterning. A pivotal set of experiments tackled this issue and demonstrated that zebrafish DV patterning, similar to AP patterning, occurs in a temporally progressive manner (Hashiguchi and Mullins, 2013; Tucker et al., 2008).

1.4.1 The DV axis is progressively patterned from anterior to posterior

A direct approach to examine when BMP signaling patterns discrete DV tissues is to modulate BMP signaling levels over time. While Section 1.6.2 details multiple methods to exert temporal control of signaling, our group used heat shock inducible transgene expression in the zebrafish. One transgene used was the wild-type BMP receptor *acvr1l* (previously called *alk8*) under the control of the *hsp70* promoter in a maternal-zygotic *acvr1l* mutant (*hsp:acvr1l*; MZ-*acvr1l*) (Tucker et al., 2008). Heat shock induction of *acvr1l* expression can rescue the severely dorsalized MZ-*acvr1l* phenotype (Mintzer et al., 2001). Importantly, a normal embryo-wide BMP activity gradient is apparent 30 minutes after heat shock, demonstrating rapid control and robust rescue efficiency via *acvr1l* transgene induction (Tucker et al., 2008). Following a series of heat shock inductions at distinct time points, it was found that *acvr1l* induction as late as the late blastula or onset of gastrulation could fully rescue the gastrula pSmad1/5 gradient and the severe dorsalization of MZ-*acvr1l* mutant embryos (Tucker et al., 2008). Surprisingly, although pSmad1/5 is evident during mid-blastula stages, this BMP signaling is not necessary for patterning or to generate a robust pSmad1/5 gradient during gastrulation since *acvr1l* first expressed at the onset of gastrulation sufficed to pattern the embryo and generate a normal signaling gradient **(Figure 1.3A)**.

However, following heat shock induction, transgene expression persists for up to several hours (Connors et al., 2006; Pyati et al., 2005). To determine when BMP signaling is required to pattern tail tissues, the *hsp:acvr1l* transgene was induced in zygotic (Z) *acvr1l* mutants, which only display dorsalized tail tissue (Mintzer et al., 2001). By employing a similar developmental series of heat shock rescue experiments detailed above in *hsp:acvr1l*; Z-*acvr1l* embryos, *acvr1l* induction at the one-somite (10.5 hpf) stage

fully rescued all Z-*acvr1l* mutants, whereas induction at later somitogenesis stages only partially rescued the tail dorsalization or did not rescue (Tucker et al., 2008). This indicates that BMP signaling is sufficient during post-gastrula stages to pattern the tail **(Figure 1.3C)**. Therefore, the DV axis is patterned during at least two timeframes: BMP initiates patterning of the head and trunk beginning in the late blastula or at the onset of gastrulation and patterns the tail during early somitogenesis stages **(Figure 1.3)**.

1.4.2 BMP signaling progressively patterns the ectoderm and mesoderm from anterior to posterior

While the studies described above demonstrate that DV axial patterning initiates during late blastula/early gastrula stages and DV tail patterning initiates at the end of gastrulation, these experiments left open when distinct domains along the AP axis are patterned (i.e. are head and trunk DV tissues patterned concomitantly or sequentially). A developmental time series of BMP inhibition addressed this question. A transgene expressing the BMP antagonist *chordin* (Section 1.2.4) under the *hsp70* promoter (*hsp:chordin*), which can abolish BMP signaling in a wild-type embryo within 60 minutes of heat-shock induction, was used (Hashiguchi and Mullins, 2013; Tucker et al., 2008). In these experiments, *hsp:chordin* embryos were heat shocked at distinct 30-minute intervals from blastula through gastrula stages and then phenotyped to determine the extent of dorsalization. If a tissue remains properly patterned (i.e. not dorsalized) after heat-shock induction of Chordin at a specific stage, then BMP signaling has already patterned that tissue prior to the stage of heat shock.

The ventral expansion of dorsal neurectodermal markers was used to gauge the extent of dorsalization. Since neural tissues are dorsally derived and inhibited by BMP signaling **(Figures 1.1 and 1.2)**, complete dorsalization causes a clear phenotype:

neurectodermal markers are radially expanded and encircle the embryo **(Figure 1.4)**. Heat shock of *hsp:chordin* embryos at a mid-blastula stage (3 hpf) and the subsequent loss of BMP signaling by 4 hpf caused complete dorsalization **(Figure 1.4B)** (Hashiguchi and Mullins, 2013). Remarkably, loss of BMP signaling at time points at and after 4.5 hpf (resulting from heat shock at and after 3.5 hpf) resulted in the dorsal restriction of neurectodermal markers in a progressive (from rostral to caudal), time-dependent fashion.

Loss of BMP signaling at a late blastula stage (4.5 hpf) caused the radial expression of all markers except for the most rostral marker, *six3* (forebrain), which was restricted dorsally **(Figure 1.4B')** (Hashiguchi and Mullins, 2013). Therefore, BMP signaling acts prior to 4.5 hpf to properly pattern the forebrain, while it functions after 4.5 hpf to pattern more caudal tissues. Loss of BMP signaling at an early gastrula stage (6 hpf) caused the radial expansion of all markers except for *six3* and *pax2.1* (midbrain-hindbrain boundary, MHB), which were both restricted dorsally **(Figure 1.4C)**, demonstrating that BMP signaling patterns the MHB between 4.5 and 6 hpf (Tucker et al., 2008). Strikingly, hindbrain rhombomeres R3 and R5 (marked by *krox20*) are patterned in 30-minute intervals: R3 requires BMP signaling prior to 6.5 hpf **(Figure 1.4C')** and R5 prior to 7 hpf **(Figure 1.4D)** (Tucker et al., 2008). Finally, the most caudal hindbrain marker, *hoxb1b*, requires BMP signaling prior to 8.5 hpf **(Figure 1.4D')** (Hashiguchi and Mullins, 2013). Notably, at these later developmental stages, BMP signaling is required during specific intervals as opposed to being required for a longer duration (Hashiguchi and Mullins, 2013).

BMP signaling also patterns the mesoderm in a progressive, temporal manner. In the *hsp:chordin* experiments discussed above, the DV fates of the mesoderm are progressively patterned from anterior to posterior: the anterior pronephros requires BMP

signaling prior to 6 hpf, the posterior pronephros prior to 6.5 hpf, and blood precursors prior to 7 hpf (Tucker et al., 2008). Together with the previous section, these studies demonstrate that BMP signaling specifies the entire DV axis in a time-dependent, progressive fashion.

1.4.3 An identical patterning clock coordinates DV and AP progressive patterning

Since DV axial patterning progresses along the AP axis analogous to AP patterning, and both axes are patterned during gastrulation, a key question was whether DV and AP patterning are coordinated in time or are regulated by independent temporal mechanisms. This question was addressed by simultaneously manipulating DV and AP patterning and these studies demonstrated that the patterning of both axes is temporally coordinated (Hashiguchi and Mullins, 2013). These experiments relied on markers with expression domains dually specified by BMP and either FGF, Wnt, or RA. For example, *otx2* is a marker of anterior neurectoderm (forebrain and midbrain) (Li et al., 1994) that is restricted anteriorly by FGF and Wnt signaling and dorsally by BMP signaling, which together define its expression domain **(Figure 1.5A)**. In contrast, *hoxb1b* is a marker of caudal hindbrain that requires posterior FGF, Wnt, or RA signaling in conjunction with dorsal restriction by BMP signaling, to define its posterior-dorsal expression domain **(Figure 1.5C)**.

If AP and DV patterning are temporally coordinated, then alterations in AP patterning would similarly alter the temporal patterning of DV tissues. To evaluate this, embryos were either anteriorized by inhibiting FGF or Wnt, or posteriorized by overexpressing FGF, Wnt, or RA **(Figure 1.5A,C)**. These AP alterations were performed in *hsp:chordin* embryos (Section 1.4.2) to enable concurrent temporal manipulation of BMP signaling and DV patterning. Since BMP is required at late blastula stages (4.5 – 5

hpf), heat shock at 4 hpf in an already anteriorized or posteriorized embryo resulted in the ventral expansion of the anterior or posterior marker, respectively **(Figure 1.5B,D)**. These compound phenotypes can be described as anteriorized-dorsalized or posteriorized-dorsalized.

The key question was whether the anteriorized or posteriorized regions in the compound phenotypes would be patterned by BMP signaling simultaneously at the time point when BMP normally patterns the marker **(Figure 1.5B,D)**, or independently at the time point when BMP normally patterns each position along the AP axis **(Figure 1.5B',D')**. If patterning of the anteriorized or posteriorized regions occurs based on the normal timing of the marker, then DV and AP patterning are coordinated **(Figure 1.5B,D)**; conversely, if DV and AP patterning are not coordinated, then BMP would pattern the anteriorized or posteriorized regions of the marker at independent time points **(Figure 1.5B',D')**. Strikingly, the compound phenotype was always patterned simultaneously at the time point when BMP normally patterns the marker, showing that AP and DV patterning are temporally coordinated throughout gastrulation along these orthogonal axes (Hashiguchi and Mullins, 2013). This intimate coordinated patterning enables cells to adopt both an AP and DV identity simultaneously, integrating the positional information of two orthogonal axes to progressively pattern the embryo from head to tail **(Figures 1.2 and 1.3)**.

1.4.4 The Smad1/5 linker region coordinates AP and DV patterning

Several *in vitro* and *in vivo* studies offer a potential mechanism to coordinate AP and DV patterning: the phosphorylation state of Smad1/5. Although C-terminally phosphorylated Smad1/5 (referred to as Ct-pSmad1/5 in this section) is the primary downstream nuclear effector of BMP signaling (Section 1.2.2), FGF and Wnt signaling can also alter Smad1/5 phosphorylation in the linker region between its N- and C-terminal

domains **(Figure 1.6)**. MAPK, activated by FGF signaling, can phosphorylate four conserved sites in the Smad1/5 linker (pSmad1/5-L^{MAPK}) (Kuroda et al., 2005; Pera et al., 2003; Sapkota et al., 2007), while Wnt signaling inhibits GSK3 phosphorylation of the Smad1/5 linker (pSmad1/5-L^{GSK3}) (Fuentealba et al., 2007).

There is a model of sequential Smad1/5 phosphorylation: first by BMPR on the C-terminus, second by MAPK in the linker, and third by GSK3 in the linker **(Figure 1.6A)** (Fuentealba et al., 2007; Sapkota et al., 2007). Studies in *Xenopus* and MEFs demonstrate that pSmad1/5-L^{MAPK} represses Smad1/5 activity and that pSmad1/5-L^{GSK3} enhances this inhibition (Kuroda et al., 2005; Pera et al., 2003; Sapkota et al., 2007). Specifically, pSmad1/5-L^{MAPK} and dual pSmad1/5-$L^{MAPK+GSK3}$ promote Smad1/5 polyubiquitinylation by the Smurf1 E3 ligase, which results in Smad1/5 proteosomal degradation outside the nucleus **(Figure 1.6A)** (Fuentealba et al., 2007; Sapkota et al., 2007; Zhu et al., 1999). Thus, the Smad1/5 response to BMP signaling, which directs DV patterning, also depends on FGF and Wnt activity, which direct AP patterning.

Since the signaling molecules that direct AP and DV patterning converge on Smad1/5 phosphorylation at distinct sites (with either inhibitory or permissive effects, respectively), differential Smad1/5 phosphorylation could coordinate the timing of DV and AP patterning (Eivers et al., 2008). Antibody staining of mid- to late gastrula stage embryos for the three distinct Smad1/5 phosphorylation states reveals that each is spatially restricted: Ct-pSmad1/5 is only observed ventrally, pSmad1/5-L^{MAPK} is localized ventral-vegetally, and pSmad1/5-L^{GSK3} is predominantly restricted to ventral-animal regions **(Figure 1.6)** (Hashiguchi and Mullins, 2013). This spatial restriction is wholly dependent on the Smad1/5 phosphorylation state since Smad1/5 (phosphorylated and un-phosphorylated) is uniformly present across the embryo (Hashiguchi and Mullins, 2013).

Furthermore, the more vegetal localization of pSmad1/5-L^{MAPK} overlaps with the region of active BMP patterning at the margin **(Figure 1.3)**, while the animal localization of pSmad1/5-L^{GSK3} does not; therefore only FGF/MAPK activity is favorably positioned to temporally regulate BMP signaling.

Strikingly, experiments with mRNA encoding a human Smad1 resistant to MAPK phosphorylation (*hSmad1-MM*) disrupt coordinated DV and AP patterning. In zebrafish embryos deficient for endogenous Smad5, mis-expressed wild-type hSmad1 fully rescues the embryo, whereas hSmad1-MM results in anterior and posterior tissue markers being patterned by BMP 30 minutes earlier than normal (Hashiguchi and Mullins, 2013). This indicates that pSmad1/5-L^{MAPK} regulates the timing of DV patterning **(Figure 1.6B)**; presumably, pSmad1/5-L^{MAPK} slows or inhibits the cellular response to BMP signaling by 30-minutes to ensure that AP and DV patterning occur simultaneously. Exclusive MAPK phosphorylation of the Smad1/5 linker in the ventral-vegetal region is consistent with known FGF and Wnt activity at the margin. While FGF induces pSmad1/5-L^{MAPK}, Wnt inhibits additional pSmad1/5-L^{GSK3} possibly preventing pSmad1/5 degradation **(Figure 1.6B)**.

Conversely, at the animal pole the absence of both FGF and Wnt signaling results in pSmad1/5-L^{GSK3} localized animally **(Figure 1.6C)**. Thus, the localization of each phosphorylated Smad1/5 linker state is an amalgamation of the spatial distributions of BMP, FGF, and Wnt activity, providing a mechanism to coordinate AP and DV. This parallels regulatory mechanisms used by other TGFβ family members, which maximize different Smad2 or Smad3 phosphorylation states for distinct functions (Kamato et al., 2013; Matsuzaki, 2013). However, other mechanisms likely also modulate the temporal function of BMP signaling since DV tissues continue to be patterned progressively with

hSmad1-MM despite being precocious by 30 minutes. For example, temporal regulation of chromatin state could also contribute to the progressive patterning of DV tissues.

1.5 Do the morphogenetic movements of gastrulation impact cell fate specification?

The previous section discusses recent progress in understanding basic spatiotemporal features of AP and DV patterning: both AP and DV cell fates are 1) progressively patterned along the AP axis, 2) patterned in a coordinated manner by an identical patterning clock, which is 3) mediated in part by FGF phosphorylation of the Smad1/5 linker in ventral regions of the embryo. However, this coordinated AP and DV patterning takes place during the dynamic and rapid process of gastrulation. Gastrulation shapes the germ layers of the embryo through the conserved morphogenetic movements of cell internalization, epiboly, convergence, and extension, all of which result in dramatic cell movements and rearrangements of cellular contacts (Solnica-Krezel, 2005). The relationship between these morphogenetic movements and concurrent AP and DV cell fate specification is key to fully understand these processes, yet this relationship is complex and requires further investigation.

1.5.1 Morphogenetic movements and AP and DV signaling and patterning

Evidence suggests that Wnt, Nodal, FGF, and BMP signaling can direct morphogenetic cell movements independently of their roles in cell specification (Heisenberg and Solnica-Krezel, 2008). For example, the BMP signaling gradient, in addition to DV fate specification, also directs domains of distinct convergent extension movements (Myers et al., 2002), possibly through the regulation of cell-cell adhesion (von

der Hardt et al., 2007). However, since cell fate specification is difficult to truly uncouple from cell behavior experimentally, differential cell movements may still be a result of DV cell specification. Alternatively, the DV positional information supplied by the BMP gradient may independently inform cell movements (Solnica-Krezel, 2005). Further studies are needed to distinguish between these two possibilities. There are similar studies and open questions concerning AP patterning and gastrulation associated with Nodal signaling (Solnica-Krezel, 2005).

Some cells dramatically change their position during dorsal convergence and extension and are exposed to different levels of morphogen signaling. It remains mostly unknown whether these cells are already specified, bring their fate with them, and are refractory to the new signaling environment they move through. Interestingly, BMP signaling patterns prospective head DV tissues prior to the major cell movements of dorsal convergence. Thus these rostral cells are expected to sense the same BMP signaling level during the first half of gastrulation and are specified at the time they converge dorsally (Section 1.4.2) **(Figure 1.4)** (Tucker et al., 2008). In other contexts, cells may be specified by morphogen signals during discrete time windows, responding to gradient thresholds, or may measure signal over a window of time as they move through a gradient. Lastly, cells may require exposure to multiple morphogen signaling levels for their specification. Further studies are required to decipher precisely the relationships between cell movements, morphogen gradients, and cell specification and the mechanisms that intertwine these processes.

1.5.2 Morphogenetic movements reorganize the DV axis established by the onset of gastrulation

It is worth noting that, due to the massive cell movements during gastrulation, the dorsal-ventral axis defined in late blastula/early gastrula stages **(Figures 1.1C and 1.2A)** is distinct from the dorsoventral axis of the post-gastrula embryo, which has a body plan that resembles the mature organism. That is, while the broad territories of the embryo can be mapped by the onset of gastrulation **(Figures 1.1C and 1.2A)**, these tissues are dramatically reorganized during gastrulation and neurulation (Kimelman and Martin, 2012; Kimmel et al., 1990). In particular, dorsal convergence combined with extension along the AP axis results in many tissues being oriented along the AP axis after gastrulation and during somitogenesis. However, this does not mean that there is only one axis (Kumano and Smith, 2002; Lane and Sheets, 2000, 2002; Lane and Smith, 1999). Prior to the onset of gastrulation, these tissues are oriented along a coordinate orthogonal to the AP axis, i.e. the DV axis in **Figure 1.2A, gray arrows**. For example, by the onset of gastrulation the somites are oriented along the DV axis of the early gastrula **(Figure 1.2A)** and this orientation informs the organization of the somites along the AP axis: dorsal somitic mesoderm develops into more anterior somites, while ventral somitic mesoderm develops into more posterior somites. Moreover, the epidermis is specified by BMP signaling ventrally during gastrulation, but later is present throughout all regions of the embryo; the neural crest is specified by BMP signaling in lateral regions of the gastrula embryo but comes to lie dorsally in the neural tube following neurulation. Thus, the DV axis of the early gastrula is an independent coordinate system to that of the post-gastrula and neurula embryo.

Furthermore, visualization of morphogen gradients (Section 1.6.1) demonstrates that there are indeed two orthogonal axes of the embryo at the onset of gastrulation. Gradients of Nodal (Dubrulle et al., 2015; Harvey and Smith, 2009) and Wnt (Dorsky et al., 2003; Shimizu et al., 2012) signaling are observed along the AP axis and a gradient of BMP signaling is observed orthogonally, revealing two distinct axial coordinate systems **(Figure 1.2A,C)** (Hashiguchi and Mullins, 2013; Tucker et al., 2008). Moreover, AP patterning continues in the absence of DV patterning (e.g. in BMP loss-of-function contexts), making evident the independent patterning of these axes **(Figures 1.4 and 1.5)**. Thus, the DV and AP axes are essential coordinates for cell fate specification and patterning of the body plan during gastrulation. Organization of tissues along the AP axis at the end of gastrulation results from integrating orthogonal morphogen gradients with dorsal convergence and extension morphogenetic movements. Further studies are needed to understand how these distinct axes are integrated to coordinate progressive patterning of the embryo (Section 1.4) and how they account for cell movements.

1.5.3 Changes in DV signaling pole proximity and gastrulation movements may affect BMP gradient formation

Gastrulation from fish to mammals entails dramatic rearrangements in cellular contacts. Though the types of cell movements during gastrulation are diverse, each type consistently results in a change in cell-cell contacts, which may impact the functionality of morphogen gradients (Solnica-Krezel, 2005). A clear example arises in the BMP gradient during gastrulation in the zebrafish **(Figures 1.3 and 1.7, yellow arrows)**. Gastrulation begins at the vegetal margin (50% epiboly) where the ventral-most cells, which have the highest levels of BMP signaling, are the farthest possible distance (~675 μm, embryo diameter) from the dorsal-most cells, which have no BMP signaling **(Figure 1.7A,**

compare white and black asterisks). As gastrulation and epiboly proceed, the margin progresses vegetally (posteriorly) and the ventral- and dorsal-most cells continuously move closer to each other until they eventually meet (100% epiboly) **(Figure 1.7B-D)**. The distance between these cells of opposing signals drastically decreases from ~675 μm at the onset of gastrulation to their direct apposition in the tailbud at the end of gastrulation. Thus, the cells presumed to have the highest and lowest levels of BMP signaling progressively converge until meeting in the tailbud. This dramatic increase in the proximity of cells with opposing signal may have profound effects on the shape of the BMP morphogen gradient during gastrulation (Connors et al., 1999; Connors et al., 2006) and is further investigated in Chapter 3.

Epiboly also likely plays a key role in regulating the temporal patterning of DV tissues through FGF signaling. As epiboly proceeds, pSmad1/5-L^{MAPK} is localized to progressively more posterior (vegetal) regions **(Figure 1.6B)**, which would enable both the temporal progressivity and coordination of DV and AP tissue patterning (Hashiguchi and Mullins, 2013). Future studies are needed to address whether these changing signaling contexts (i.e. the proximity of cells with opposing signals or the progressively posterior restriction of pSmad1/5-L^{MAPK}) are a principal spatial mechanism to direct the shape and timing of morphogen gradients throughout gastrulation.

1.6 Current and emergent methods of visualization and manipulation

In this section we focus on *in vivo* genetic and fluorescent visualization approaches and methods of spatial and temporal signal manipulation used to study AP and DV patterning, the majority of which have been developed in zebrafish.

1.6.1 Morphogen visualization and use of reporters

A major difficulty in studying the morphogens that pattern the AP and DV axes is that they are secreted and difficult to visualize by immunostaining at endogenous levels. Most studies of ligand expression and dynamics rely on overexpression of fluorescently labeled constructs (Muller et al., 2012; Plouhinec et al., 2013; Stanganello et al., 2015; Yu et al., 2009) or the use of antibodies that recognize the immature ligand, as opposed to its fully processed form (Ramel and Hill, 2013; Xue et al., 2014). While the endogenous RA gradient has recently been visualized and quantified (Shimozono et al., 2013), that approach relies on FRET from a direct ligand-receptor interaction, which is less applicable for the Wnt, FGF, and BMP gradients since these ligands signal through more complex mechanisms (i.e. ligand bound to receptor may not be indicative of active signaling depending on the presence of co-receptors or complex stoichiometry, Sections 1.2.2 and 1.3.1-1.3.2). However, the advent of CRISPR/Cas9 genome editing offers a new approach to tag these ligands at their endogenous loci and even employ signal amplification techniques to visualize the endogenous morphogen gradient in fixed or live samples (Cong et al., 2013; Hwang et al., 2013; Mali et al., 2013).

A complementary approach to ligand visualization is the visualization of downstream readouts of the morphogen. For example, the intracellular transducer of BMP signaling is nuclear P-Smad1/5, which can be directly visualized by immunofluorescence (Faure et al., 2000; Hashiguchi and Mullins, 2013; Persson et al., 1998; Tucker et al., 2008). Recently, our lab has developed quantitative imaging and analysis of P-Smad1/5 immunoflourescence (Zinski et al., 2019). Importantly, our imaging approach avoids common artifacts such as spherical aberration and intensity drop off, yielding measurements of P-Smad1/5 fluorescence with single-cell resolution while maintaining

each cell's position in 3D. Further, our post-acquisition algorithms enable population analyses so we can quantitate the BMP signaling gradient shape across mutants and time points (Zinski et al., 2017) (Chapters 2 and 3). The full methodology is summarized in Section 6.4 (Zinski et al., 2019) and can be applied to the fluorescent imaging of other morphogen gradients in the early embryo and the quantitation of P-Smad1/5 at later developmental stages (Chapter 4).

There are also various transgenic reporters in zebrafish for Wnt (Dorsky et al., 2002; Korinek et al., 1997; Shimizu et al., 2012), FGF (Molina et al., 2007), Nodal (Harvey and Smith, 2009), RA (Perz-Edwards et al., 2001; White et al., 2007), and BMP signaling (Collery and Link, 2011; Korchynskyi and ten Dijke, 2002; Monteiro et al., 2004; Ramel and Hill, 2013). These reporter transgenes utilize sequences from a promoter that responds to the morphogen signal to drive reporter expression e.g. of *luciferase* or GFP. But, how rapidly the reporter is expressed after signal induction and how long the reporter signal persists after signal repression must be carefully characterized to determine the responsiveness of each reporter. To visualize morphogen signaling, which can change in a relatively short time period, it is likely best to use rapidly folding (e.g. Venus) or destabilized fluorescent proteins (Collery and Link, 2011; Dorsky et al., 2002; Harvey and Smith, 2009; Molina et al., 2007; Shimizu et al., 2012).

1.6.2 Temporal manipulation of signaling

Our knowledge of when Wnt, FGF, RA, Nodal and BMP signals are required for AP and DV patterning comes from experiments that activate or inhibit these signals at specific developmental time points. A particularly expedient approach in *Xenopus* and zebrafish is to incubate embryos in media containing various chemical inhibitors or activators. These pharmacological treatments include SU5402 (inhibits FGFR), LiCl

(inhibits the Wnt inhibitor GSK3), DEAB (inhibits RA processing), Dorsomorphin DMH1 (inhibit BMP type I receptors), and RA itself (Hashiguchi and Mullins, 2013). Although these chemicals have well-characterized direct effects, studies of temporal function must determine the delay between drug application and complete inhibition or activation of signaling. This delay is infrequently defined and it is assumed that inhibition/activation ensues immediately after drug application, which may not be the case. For example, DMH1 takes 3 hours to fully inhibit BMP signaling during gastrulation (Hashiguchi and Mullins, 2013). Furthermore, one must account for the multiple functions of a signaling pathway during development. For example, since Wnt establishes the dorsal organizer during mid- to late blastula stages, which is unrelated to its role directing AP patterning during gastrula stages (Sections 1.2.1), any experiment that aims to understand the posteriorizing role of Wnt signaling must manipulate Wnt signaling *after* blastula stages.

Another method of temporal manipulation is to generate transgenic lines that can be induced to either inhibit or activate signaling. Previously we discussed *hsp70* promoter driven genes that inhibit or activate BMP signaling (Sections 1.4.1 and 1.4.2) (Connors et al., 2006; Hashiguchi and Mullins, 2013; Pyati et al., 2005; Row and Kimelman, 2009; Tucker et al., 2008). When using heat shock-inducible transgenes, it is important to determine the appropriate duration of heat shock to activate or inhibit signaling, which can vary from 10 minutes (Connors et al., 2006) to an hour (Pyati et al., 2005; Tucker et al., 2008). Here, too, it is important to factor in the time it takes for signaling to be effectively induced or fully repressed. Finally, inducing heat shock results in embryo-wide expression of the transgene. To achieve spatially restricted gene control, one may induce local heat shock by sublethal laser irradiation (Shoji and Sato-Maeda, 2008) or a microheater (Placinta et al., 2009). Alternatively, one may transplant cells from the transgenic line into

a background without a heat shock transgene and heat shock the entire embryo after transplantation.

1.6.3 Spatial manipulation of signaling

Morphogen signaling relies on the restricted localization and differential mobility of the morphogens themselves and their regulators. An elegant, direct, and versatile method to investigate spatial mechanisms is by generating chimeric organisms by grafting or transplanting donor cells into a host embryo (Kemp et al., 2009). First, cell transplantation or grafting assays can determine the importance of localization by altering the spatial expression of the protein of interest. For example, to determine where *tolloid* must be expressed to inhibit Chordin function, *tolloid*-expressing cells were transplanted into *tolloid* -/- embryos. Only cells transplanted into the ventral vegetal region rescued the *tolloid* mutant phenotype, thus revealing the region where Tolloid cleaves Chordin to promote BMP signaling (Connors et al., 2006). Second, cell transplantation assays can be used to further evaluate whether a signaling factor functions directly at a distance. Such studies clearly established that the zebrafish Nodal signal, Squint, functions directly on its gene targets at a distance and therefore is a morphogen (Chen and Schier, 2001). Regional expression may also be generated by injecting single blastomeres during cleavage stages (Section 2.2.8).

Additionally, the cell transplantation approach may be extended to address questions not only of space but also of time. As noted in the previous section, cells from heat shock-inducible transgenic lines may be used as transplant donors to incorporate temporal and spatial control of gene expression (Pyati et al., 2005; Row and Kimelman, 2009). Furthermore, transplantation of various regions of the zebrafish blastula-gastrula margin has revealed there are distinct cell fate organizing centers in the margin, and that

these organizing centers are fully active by the onset of gastrulation, including the one that specifies tail tissue (Agathon et al., 2003; Fauny et al., 2009).

1.7 Conclusion and Project Goals

Establishing the vertebrate body plan requires the coordination and integration of AP and DV axial patterning across the entire length of the embryo and over multiple developmental stages. The spatiotemporal regulation of this process is complex, but it can reveal the essential and conserved mechanisms used to generate and maintain morphogen signaling gradients. With the advent of quantitative measurement and visualization techniques, we are closer to understanding the mechanisms that drive patterning and body plan formation.

This project focuses exclusively on DV patterning by the BMP morphogen gradient. The primary goal of this research is to employ recent advances in the quantitative measurement and visualization of the BMP signaling gradient (Zinski et al., 2017; Zinski et al., 2019) (Section 1.6.1) to elucidate the mechanisms that shape the BMP morphogen gradient in space and time. Specifically, this project investigates the roles of known extracellular regulators of the BMP antagonist Chordin (Section 1.2.4) at the onset of gastrulation (Chapter 2), during gastrulation (Chapter 3), and during otic vesicle patterning after gastrulation (Chapter 4). Respectively, these timepoints represent distinct stages of the BMP morphogen gradient: when it is first established, when it changes shape during gastrulation, and lastly when it becomes restricted to an individual organ, as opposed to being embryo-wide. The partially-redundant roles of Bmp1a and Tolloid in restricting Chordin range to establish the BMP gradient are detailed in Chapter 2. The distinct roles of Tolloid and Sizzled in shaping the BMP signaling gradient during gastrulation are

investigated in Chapter 3. Finally, the role of Bmper in BMP patterning the otic vesicle is explored in Chapter 4.

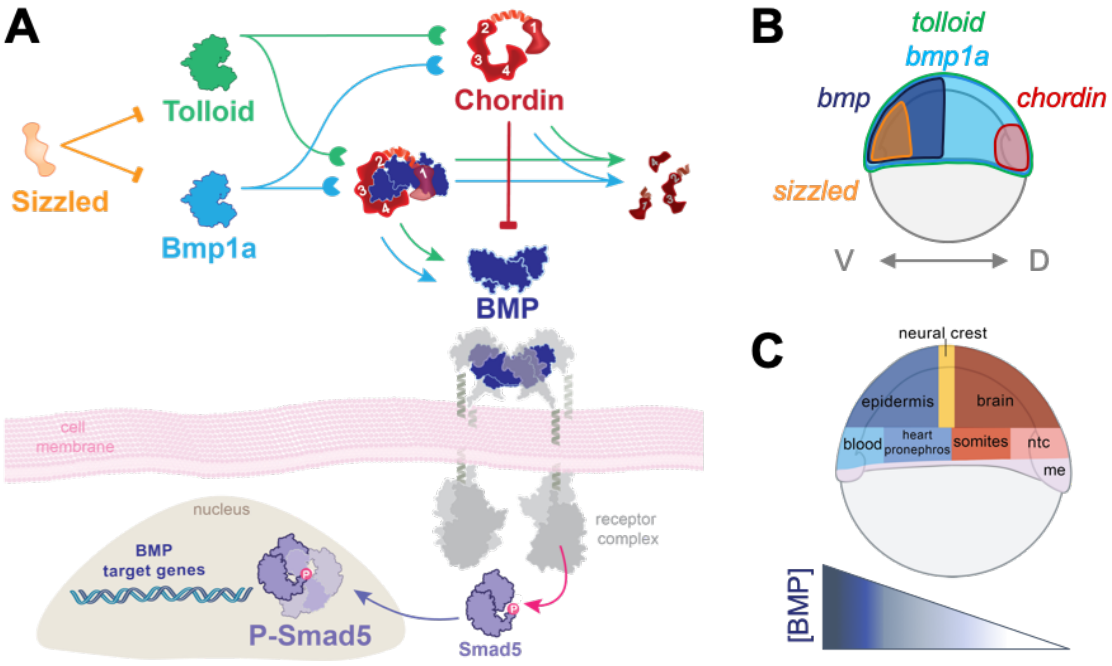

Figure 1.1 Extracellular regulation of the BMP morphogen gradient patterns DV tissues.

(A) Schematic of the extracellular BMP regulators explored in this project, adapted from (Dutko and Mullins, 2011), and (B) their published mRNA expression domains in the zebrafish gastrula (6.3 hpf, see Section 1.2.4 for references). (C) Fatemap of the early zebrafish gastrula (ntc.: notochord, me: mesendoderm).

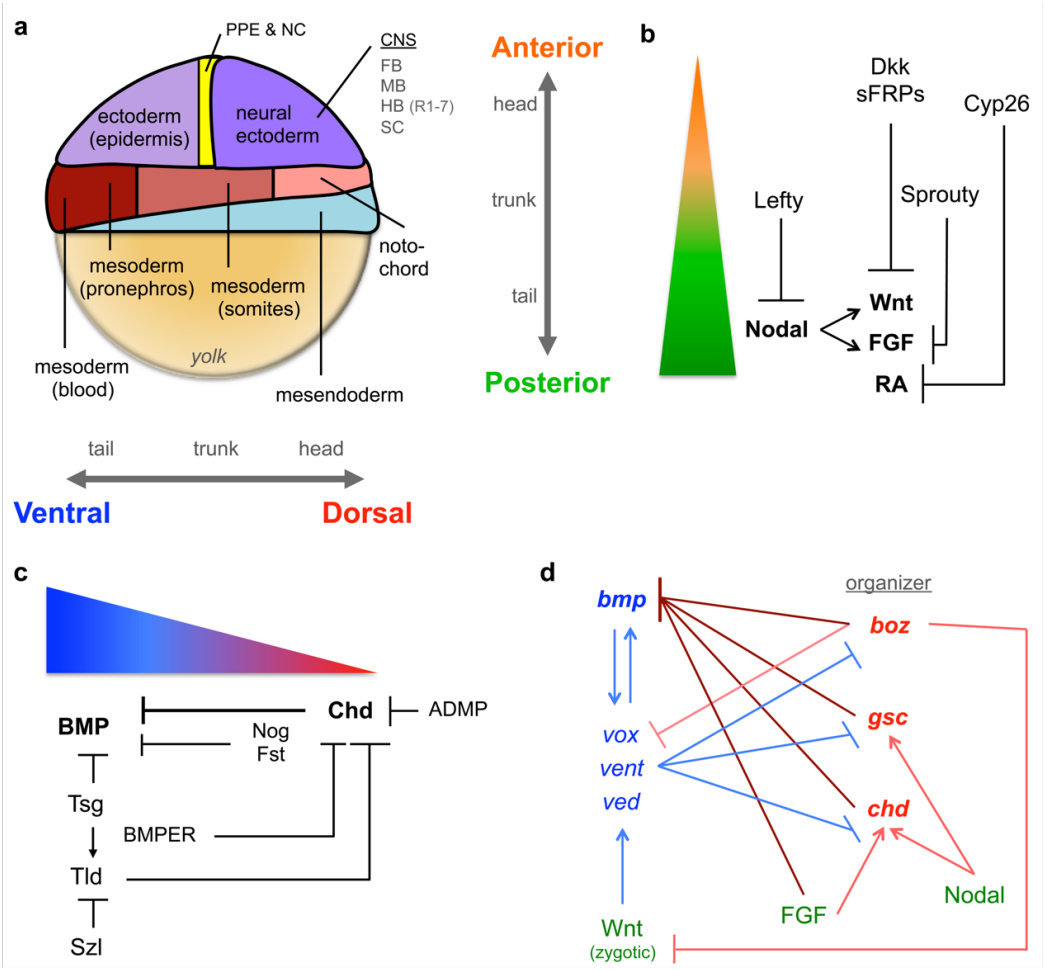

Figure 1.2 The AP and DV axis are patterned by morphogens and their regulators.

(A) Fate map of a zebrafish gastrula (6.3 hpf) with the orientation of the AP and DV axes. The neural ectoderm can be divided into four regions of the CNS: forebrain (FB), midbrain (MB), hindbrain (HB), which is further subdivided into rhombomeres 1-7 in zebrafish, and spinal cord (SC). (B) Wnt, FGF, Nodal, and RA specify posterior fates (green) in a concentration-dependent manner, while their inhibition is required for anterior fate specification (orange). (C) The BMP morphogen gradient specifies ventral cell fates (blue) at high levels and allows dorsal fate specifcation (red) at low levels. BMP signaling is regulated by extracellular factors; the DV localization of their transcriptional domains (detailed in Section 1.2.4) is depicted. Chordin (Chordin) activity is key since it acts as a BMP antagonist and as the substrate for other extracellular modulators. (D) Transcriptional regulation of bmp and dorsal organizer genes. By activating different transcriptional repressors, zygotic Wnt promotes while FGF and Nodal antagonize BMP signaling. Blue lines indicate activity that promotes BMP signaling and red lines indicate activity that limits it (dark shades describe a direct effect, light shades an indirect effect).

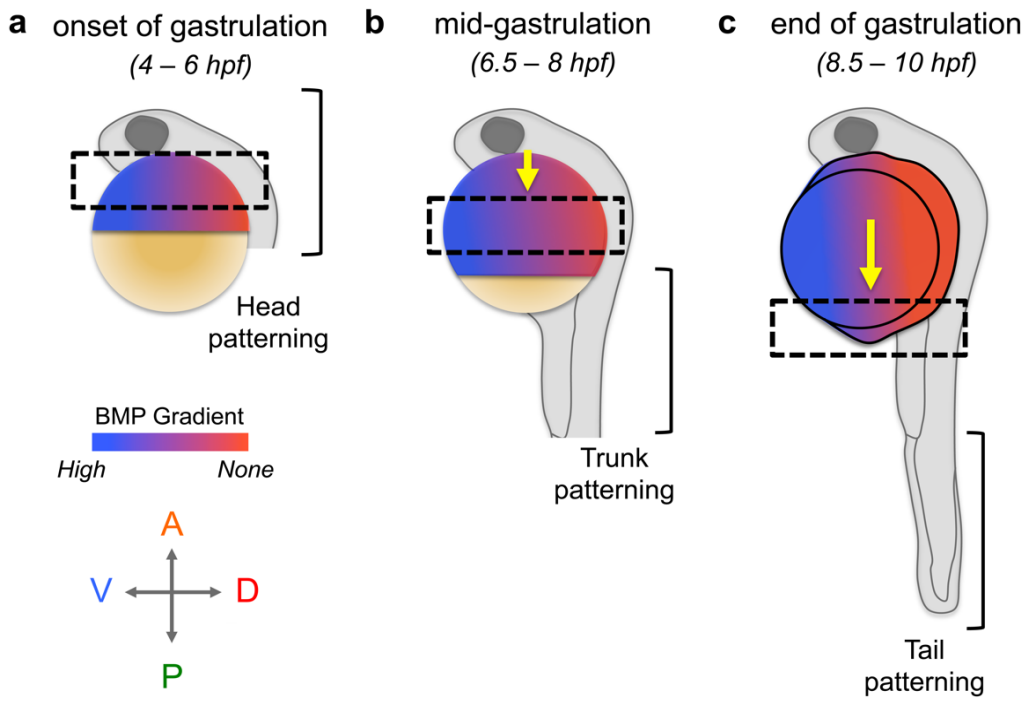

Figure 1.3 BMP signaling patterns DV cell fates from anterior to posterior.

AP and DV coordinates refer to the zebrafish gastrula embryos (A-B), which are depicted with cells atop the yolk. The dashed box indicates the region of active DV patterning with the corresponding portion of the body plan represented by the larval zebrafish (24 hpf). During gastrulation, cells undergo epiboly wherein the multilayered tissue thins and spreads posteriorly to completely envelop the yolk. (A) From late blastula to early gastrula stages (30-65% epiboly), the most anterior tissues, i.e. the head, are patterned. (B) As gastrulation proceeds, the region of active patterning progresses posteriorly (yellow arrow). At mid-gastrula stages (65-85% epiboly), trunk tissues are patterned. (C) From late gastrula (85-100% epiboly) to early somitogenesis, the most posterior tissues, i.e. the tail, are patterned.

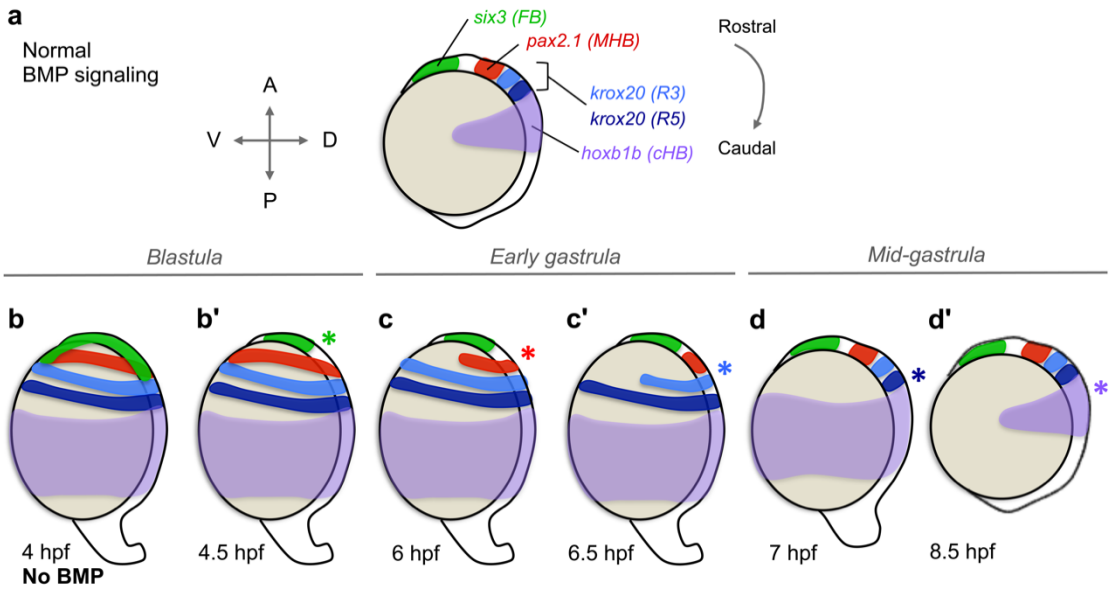

Figure 1.4 BMP signaling progressively patterns the anterior neurectoderm.

(A) Wild-type expression pattern of anterior neurectoderm markers. (B-D') Summary of a developmental time series of BMP inhibition demonstrating that BMP signaling patterns the neurectoderm progressively, from rostral to caudal, in a time-dependent manner. (B) Loss of BMP signaling beginning at a mid-blastula stage (4 hpf) causes severe dorsalization and radial expansion of the neurectoderm. (B') Loss of BMP signaling at a late blastula stage (4.5 hpf) causes radial expansion of all markers except *six3*, which is restricted dorsally (green asterisk). Therefore, BMP patterns *six3* between 4-4.5 hpf. (C) Loss of BMP signaling at the onset of gastrulation (6 hpf) restricts *pax2.1* expression (red asterisk), indicating that BMP patterns the MHB between 4.5-6 hpf. (C') Loss of BMP signaling at 6.5 hpf restricts R3 (light blue asterisk) and (D) loss of BMP signaling at 7 hpf additionally restricts R5 (dark blue asterisk), indicating that BMP patterns R3 and R5 in 30-minute intervals from 6-7 hpf. (D') Loss of BMP signaling at 8.5 hpf restricts *hoxb1b* expression (purple asterisk), indicating that BMP patterns *hoxb1a* between 7-8.5 hpf.

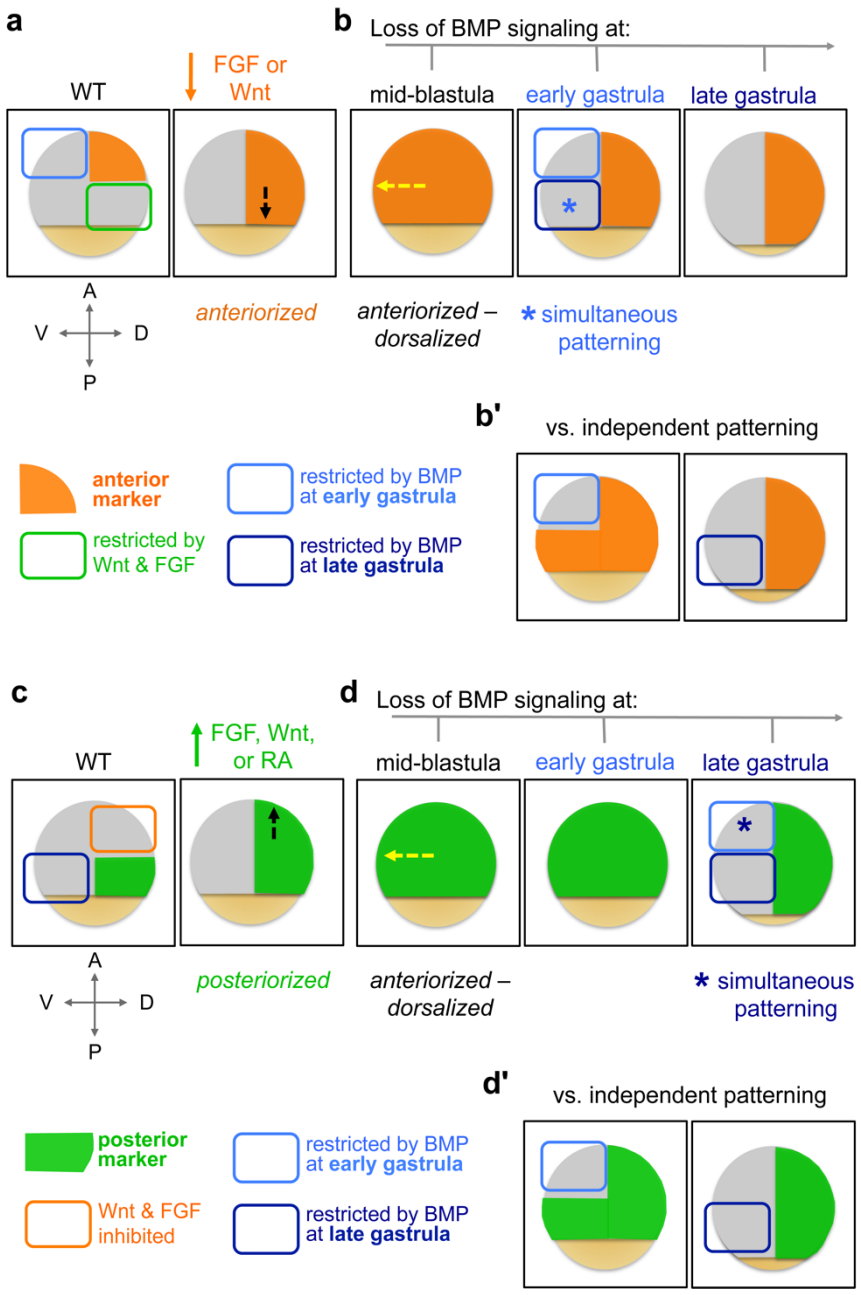

Figure 1.5 AP and DV patterning are temporally coordinated.

Marker expression is depicted in embryos at mid- or late gastrula stage. (A) BMP restricts anterior marker expression (orange) at early gastrula stages. Embryo anteriorized by inhibiting FGF or Wnt (dashed black arrow: posterior expansion of anterior marker). (B) Inhibiting BMP signaling in an anteriorized embryo at a mid-blastula stage causes a compound anteriorized-dorsalized phenotype (dashed yellow arrow: ventral expansion of the anterior marker). Since AP and DV patterning are temporally coordinated, inhibiting BMP at an early gastrula stage (when the anterior marker is normally patterned) causes complete dorsal restriction of the anterior marker. (B') If AP and DV patterning were

temporally independent, inhibiting BMP at an early gastrula stage would restrict the normal domain and the posteriorly expanded region would be restricted at a later gastrula stage. (C) BMP restricts posterior marker expression (green) at late gastrula stages. Embryo posteriorized by overexpressing FGF, Wnt, or RA (dashed black arrow: anterior expansion of posterior marker). (D) Inhibiting BMP signaling in a posteriorized embryo at a mid-blastula stage causes a compound posteriorized-dorsalized phenotype (dashed yellow arrow: ventral expansion of the posterior marker). Since AP and DV patterning are temporally coordinated, inhibiting BMP signaling only at a late gastrula stage (when the posterior marker is normally patterned) causes complete dorsal restriction of the posterior marker. (D') If AP and DV patterning were temporally independent, inhibiting BMP at an early gastrula stage would still restrict the anteriorly expanded domain, but not the normal domain of the posterior marker.

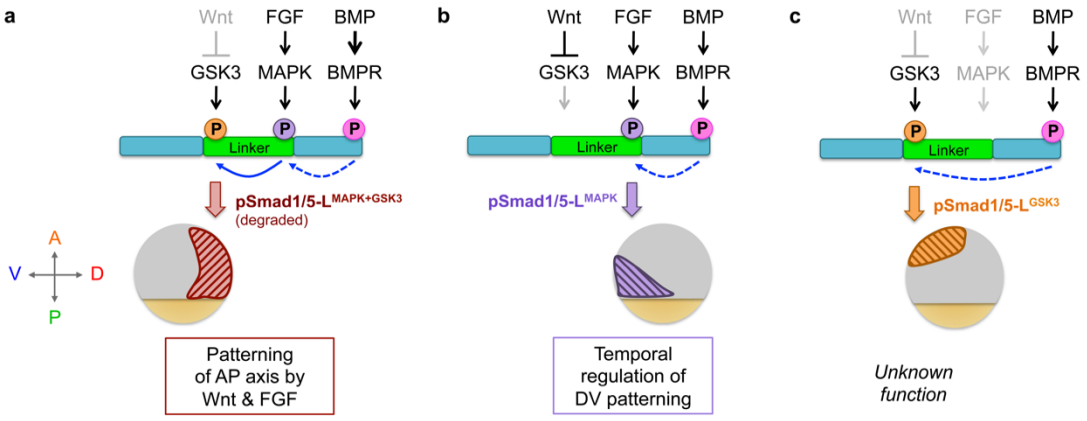

Figure 1.6 Function of pSmad1/5 linker forms is spatially restricted.

The N- and C-termini of Smad1/5 are shown in teal and the linker region is in green. C-terminal phosphorylation of Smad1/5 (Ct-pSmad1/5) a prerequisite to linker phosphorylation (dashed blue arrow). (A) In dorsal regions, MAPK and GSK3 sequentially phosphorylate the Smad1/5 linker (solid blue arrow), leading to pSmad1/5-L$^{MAPK+GSK3}$ degradation and blockage of BMP signaling. This mechanism may be most important during blastula stages when BMP signaling is more widespread and present dorsally (Section 3.1). (B) In ventral-posterior regions both FGF and Wnt are present, activating MAPK and inhibiting GSK3, respectively, to generate pSmad1/5-L^{MAPK}. pSmad1/5-L^{MAPK} may have reduced activity, which regulates timing of DV patterning. During epiboly, pSmad1/5-L^{MAPK} localizes progressively more posteriorly with the margin, patterning anterior DV tissues in its wake (not shown). (C) In animal regions GSK3 is uninhibited by Wnt, resulting in pSmad1/5-L^{GSK3}, though its significance remains unknown. Since pSmad1/5-L^{GSK3} does not overlap with pSmad1/5-L^{MAPK}, it is possible that in the zebrafish embryo (versus *in vitro* studies) either GSK3 does not require MAPK to prime the linker or those residues may be rapidly de-phosphorylated.

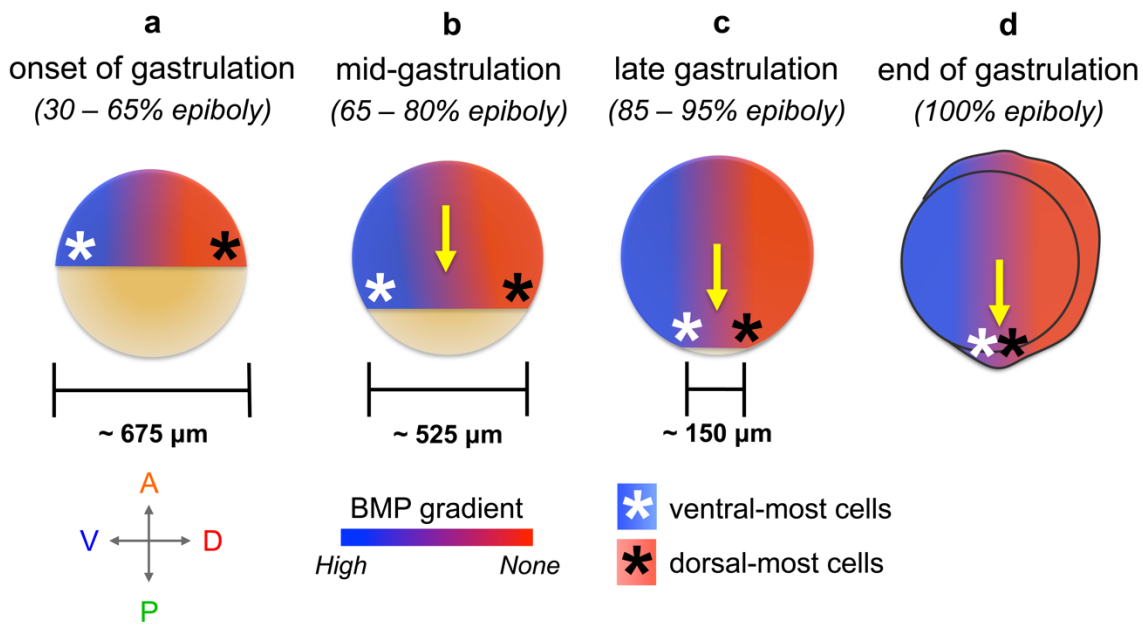

Figure 1.7 During gastrulation, there is a dramatic decrease in distance between ventral- and dorsal-most cells.

During gastrulation, there is a dramatic decrease in distance between the ventral- and dorsal-most cells. (a) From late blastula to early gastrula stages (4 – 6 hpf), the ventral-most cells (white asterisk), which have the highest levels of BMP signaling, are farthest (approximately 675 µm) from the dorsal-most cells (black asterisk), which have the lowest levels of BMP signaling. (b – d) As gastrulation proceeds (6 – 10hpf), epiboly movements advance the margin posteriorly (yellow arrow) and the distance between the ventral- and dorsal-most cells decreases rapidly until, by the end of epiboly, they are in direct contact.

CHAPTER 2. Proteolytic restriction of Chordin range underlies BMP gradient formation

Contributions: This chapter contains figures and direct quotes from Tuazon, et al. under revision at *Cell Reports*.

Summary

A fundamental question in developmental biology is how morphogens, such as Bone Morphogenetic Protein (BMP), form precise signaling gradients to impart positional and functional identity to the cells of the early embryo. We combined rigorous mutant analyses with quantitative immunofluorescence to determine that the proteases Bmp1a and Tolloid spatially restrict Chordin in the early zebrafish gastrula. We discovered that maternally-deposited Bmp1a plays an unexpected and non-redundant role in establishing the BMP gradient, while Sizzled is surprisingly dispensable. Combining mathematical models and *in vivo* analyses with an immobile Chordin construct, we demonstrate that Chordin diffusion is dispensable for BMP gradient formation and DV patterning. These data exclude a counter-gradient of Chordin and instead favor a Chordin sink, established by Bmp1a and Tolloid, as the primary mechanism that drives BMP gradient formation.

2.1 Introduction

The roles of Bmp1a, Tolloid, and Sizzled (Section 1.2.4) in generating the zebrafish BMP gradient warrant further investigation. Bmp1a and Tolloid likely have partially redundant functions since their amino acid sequences are highly similar (93.4%) **(Supplemental Figure 2.1A)** and their expression domains overlap, though *bmp1a* alone is maternally deposited **(Figure 2.1A'-B)** (Connors et al., 1999; Jasuja et al., 2006; Muraoka et al., 2006; Xie and Fisher, 2005). However, the extent of Bmp1a/Tolloid redundancy during BMP gradient formation, and any impact Sizzled may have on it, were unclear. To this end, we utilized a quantitative immunofluorescence approach that we recently developed to quantify nuclear P-Smad5, the direct intracellular readout of BMP

signaling (Zinski et al., 2017; Zinski et al., 2019) **(Figure 2.1A)**. We can visualize the P-Smad5 gradient at single cell resolution embryo-wide and compare differences across mutant populations (Zinski et al., 2017; Zinski et al., 2019). This approach provides the comprehensive, high resolution analysis required to determine the spatial and temporal contributions of Bmp1a, Tolloid, and Sizzled.

Furthermore, we combined our quantitative P-Smad5 analysis with mathematical modeling and large-scale computational screens to distinguish between potential mechanisms of BMP gradient formation. The predominant model in the field has been a counter-gradient mechanism, where dorsally secreted Chordin diffuses ventrally in a gradient to generate an inverse gradient of BMP signaling (De Robertis and Moriyama, 2016; Plouhinec et al., 2013) **(Figure 2.8)**. We recently excluded two alternative models of BMP gradient formation by computational modeling in zebrafish: a mechanism that relies on a gradient of *bmp* transcript and a mechanism acting in Drosophila DV patterning relying on facilitated BMP diffusion with Chordin (Zinski et al., 2017). The final model is a source-sink mechanism, where BMP diffuses from its source ventrally to be captured by a sink of Chordin dorsally (Zinski et al., 2017) **(Figure 2.8)**. Since BMP and Chordin both rapidly diffuse (Inomata et al., 2013; Pomreinke et al., 2017; Zinski et al., 2017), a Chordin counter-gradient and a Chordin sink both remain viable mechanisms for BMP gradient formation, and how a dorsal sink of Chordin could be established was unknown.

Here, we combined rigorous maternal-zygotic double mutant analyses with P-Smad5 quantitation to determine that Bmp1a and Tolloid are required to spatially restrict Chordin in the early zebrafish gastrula. We discovered that maternally-deposited Bmp1a plays an unexpected and non-redundant role in establishing the BMP gradient, while Sizzled is surprisingly dispensable. Incorporating Bmp1a, Tolloid, and Sizzled into a

computational model screen of zebrafish BMP gradient formation revealed that, despite its high diffusivity, Chordin has a limited effective range. This excludes the counter-gradient mechanism and instead favors a restricted Chordin sink, generated by Bmp1a and Tolloid. We directly tested this by regionally expressing an immobile Chordin construct in embryos deficient in Bmp1a, Tolloid, and endogenous Chordin. Remarkably, immobile Chordin was able to pattern the DV axis of these embryos, consistent with our model that Bmp1a and Tolloid proteases are key to restrict Chordin and establish the sink that drives BMP gradient formation.

2.2 Results

2.2.1 Tolloid and maternal Bmp1a are required for early DV patterning

Previous studies evaluating Bmp1a/Tolloid redundancy relied solely on morpholino (MO)-mediated knockdown of *bmp1a* and had conflicting phenotypes: one found no DV patterning defects (Jasuja et al., 2006), while the other reported severe dorsalization, lysis, and death (Muraoka et al., 2006). To resolve this discrepancy and circumvent any non-specific morpholino effects, we utilized two nonsense mutations: *bmp1a*^{t31169}, a characterized null (Bowen et al., 2012), and *bmp1a*^{sa2416}, from the Zebrafish Mutation Project (Kettleborough et al., 2013) **(Supplemental Figure 2.1A)**. We generated maternal-zygotic (MZ) mutants of each allele and both displayed a wild-type phenotype at 36 hours post fertilization (hpf) **(Figure 2.1C and Supplemental Figure 2.1B)**, concurring that *bmp1a* loss has no anatomical effect on DV patterning (Jasuja et al., 2006). Furthermore, *bmp1a*^{sa2416} mutants phenocopied *bmp1a*^{t31169}, displaying a ruffled tail fin by 5 days post fertilization (dpf) and adult craniofacial, tail, and body axis defects

(Supplemental Figure 2.1B-D) consistent with its later role in skeletal development, unrelated to DV patterning (Asharani et al., 2012; Bowen et al., 2012; Gistelinck et al., 2018; Hur et al., 2017).

We evaluated whether Bmp1a and Tolloid function redundantly during DV patterning by generating double mutants with either zygotic (Z), maternal (M), or maternal-zygotic (MZ) loss of *bmp1a* **(Figure 2.1D)** and assaying the embryonic phenotype. Double zygotic mutants were generated by intercrossing *bmp1a*^{t31169}*;tolloid* double heterozygotes **(Figure 2.1D)**. Dorsalized progeny were classified on an established scale, with C1 being mild and C5 being most severe (Mullins et al., 1996), and subsequently genotyped for *bmp1a* and *tolloid*. Since the progeny were not all dorsalized, only a subset of wild-type embryos was also genotyped **(Figure 2.1E, columns 1-3)**. Single Z-*bmp1a* homozygotes were wild-type and additional heterozygosity for *tolloid* had no effect **(Figure 2.1E, columns 2-3)**. In contrast, single *tolloid* homozygotes were C1 and additional heterozygosity for *bmp1a* resulted in mostly C2 phenotypes **(Figure 2.1C and E, columns 4-5)**. Homozygous *bmp1a;tolloid* double mutants were C3 dorsalized, a moderately severe phenotype, indicating that zygotic *bmp1a* and *tolloid* function redundantly **(Figure 2.1E, column 6 and Supplemental Figure 2.1E-F)**.

We generated embryos lacking maternal *bmp1a* and zygotic *tolloid* (M-*bmp1a;tolloid*) by crossing a female homozygous for *bmp1a*^{t31169} and heterozygous for *tolloid* with a male heterozygous for *tolloid* **(Figure 2.1D)**. Strikingly, all M-*bmp1a;tolloid* embryos were C5 dorsalized, the most severe dorsalization phenotype, while siblings remained wild-type **(Figure 2.1E columns 7-9)**. We confirmed that C5 embryos were radially dorsalized by wholemount *in situ* analysis of neurectoderm markers *pax2.1* (mid-hindbrain boundary) and *krox20* (hindbrain rhombomeres 3 and 5). Expression of *pax2.1*

and *krox20* is normally restricted dorsally, as seen in wild-type controls and M-*bmp1a* siblings; however, in the majority of M-*bmp1a;tolloid* embryos, these markers were expanded around the entire embryo **(Figure 2.1F)**. We saw the same phenotype when injecting an antisense morpholino targeting *tolloid* (*tll1*MO) (Kok et al., 2015; Lele et al., 2001) into M-*bmp1a* embryos **(Supplemental Figure 2.2A-B)**. The same concentration (2ng) of *tll1*MO that phenocopied *tolloid* mutants when injected into wild-type embryos **(Supplemental Figure 2.2A)** caused C5 radial dorsalization in M-*bmp1a* embryos **(Supplemental Figure 2.2A-B)**. These data indicate that maternally-deposited *bmp1a* alone is redundant with *tolloid* and both are absolutely required to pattern the DV axis.

Finally, we generated embryos lacking maternal-zygotic *bmp1a* and zygotic *tolloid* (MZ-*bmp1a;tolloid*) by crossing a female homozygous for *bmp1a*^{t31169} and heterozygous for *tolloid* with a *bmp1a*^{t31169}*;tolloid* double heterozygous male **(Figure 2.1D)**. All MZ-*bmp1a;tolloid* embryos were C5 dorsalized while MZ-*bmp1a* siblings remained wild-type **(Figure 2.1E, columns 10 and 12)**. As with Z-*bmp1a* and M-*bmp1a*, additional heterozygosity for *tolloid* had no effect on MZ-*bmp1a* embryos **(Figure 2.1E, column 11)**. Furthermore, in MZ-*bmp1a* embryos injected with *tll1*MO, *chordin* expression remained unchanged **(Supplemental Figure 2.2C)**, which excludes that an expanded *chordin* expression domain contributes to the observed dorsalization. Together, with the Z-*bmp1a;tolloid* and M-*bmp1a;tolloid* phenotypes, these data reveal that maternally-deposited *bmp1a* is primarily redundant with *tolloid*, and that Bmp1a/Tolloid are essential for BMP signaling and DV patterning.

2.2.2 Bmp1a/Tolloid shield BMP signaling from Chordin embryo-wide

To understand how Bmp1a/Tolloid shape the BMP signaling gradient, we quantified P-Smad5 in all nuclei of the early gastrula at 5.7 hpf. By this time-point in wild-

type embryos, the gradient is firmly established (Zinski et al., 2017; Zinski et al., 2019) **(Figure 2.2A)**. We found that loss of M- or MZ-Bmp1a and Tolloid caused a dramatic loss of P-Smad5 across the embryo **(Figure 2.2E)**, consistent with their radial dorsalization **(Figure 2.1E-F)**. This was observed in MZ- or M-*bmp1a* embryos with *tll1*MO and in M-*bmp1a;tolloid* double mutants **(Figure 2.2E and Supplemental Figure 2.2D-G)**. We quantified P-Smad5 levels around the embryo margin **(Figure 2.2F)** and compared the distribution in wild-type to the loss-of-function conditions. This analysis revealed that the P-Smad5 gradient is effectively ablated in all embryos deficient for both maternal Bmp1a and zygotic Tolloid activity, even in the ventral-most regions where BMP is produced **(Figure 2.2I and Supplemental Figure 2.2H)**. These results indicate that without Bmp1a/Tolloid, Chordin can reach the ventral-most regions of the embryo and inhibit all BMP signaling there **(Figure 2.2L)**. This suggests that a key function of Bmp1a/Tolloid is to restrict Chordin to protect BMP signaling ventrolaterally **(Figure 2.2L)**.

2.2.3 Bmp1a alone modulates the early BMP signaling gradient and DV patterning

We also quantified the P-Smad5 gradient in both *tolloid* and *bmp1a* single mutants. *tolloid* mutants are mildly dorsalized, with the phenotype restricted to the tail **(Figure 2.1C)** (Connors et al., 1999). While previous work indicates that BMPs pattern the tail at the end of gastrulation (9-10 hpf) (Connors et al., 2006; Pyati et al., 2005; Tucker et al., 2008), an earlier change in the P-Smad5 gradient could affect tail patterning (Agathon et al., 2003). However, even with our highly sensitive quantification, *tolloid* mutants displayed a wild-type P-Smad5 gradient at 5.7 hpf (early gastrula) **(Figure 2.2B,G)**. This indicates that Tolloid alone does not contribute to BMP gradient formation and that Bmp1a is sufficient at this stage.

In contrast, the P-Smad5 gradients of M- and MZ-*bmp1a* embryos were wholly unexpected. Given that MZ-*bmp1a* mutants exhibit a wild-type phenotype at 36 hpf **(Figure 2.1C)** and are viable and fertile through multiple generations as adults, we expected to see a wild-type P-Smad5 gradient. However, M- and MZ-*bmp1a*^{t31169} embryos displayed a significantly reduced P-Smad5 gradient at 5.7 hpf **(Figure 2.2C-D)**. They were compared to stage-matched wild-type controls, which were stained and processed in the same tube as mutants and identified by genotyping after P-Smad5 imaging (indicated by asterisk in all figures, see Methods). At the margin, where peak P-Smad5 levels were observed **(Figure 2.2F)** (Tucker et al., 2008; Zinski et al., 2017), M- and MZ-*bmp1a* embryos exhibited similar P-Smad5 gradients that were both shallower and lower in amplitude than wild-type **(Figures 2.2H and Supplemental Figure 2.3A-B)**. In a more animal region, M-*bmp1a* embryos exhibited higher ventral P-Smad5 intensities than MZ-*bmp1a*, though both gradients were still greatly reduced compared to wild-type **(Figure 2.2K)**. Consistent with their reduced P-Smad5 gradients, M-*bmp1a* embryos displayed previously unknown DV patterning defects, with a loss of ventral marker *gata2* and concomitant expansion of dorsal marker *foxb1a* at 6.3 hpf **(Figure 2.2J-J')**. Together, these results show that maternal Bmp1a plays a key role in establishing the BMP gradient and in DV patterning **(Figure 2.2L)**.

Surprisingly, we found that embryos derived from M-*bmp1a*^{t31169}/+ heterozygous females (crossed to wild-type males) also displayed a significantly reduced P-Smad5 gradient **(Supplemental Figure 2.3F, H)**. Further, this gradient closely resembles that of embryos derived from homozygous M-*bmp1a* ^{t31169} females crossed to wild-type males (M-*bmp1a*^{t31169} embryos), differing only in the ventral-most regions **(Supplemental Figure 2.3E-F, I)**. It was also observed in M-*bmp1a*^{sa2416}/+ embryos **(Supplemental Figure 2.3G,**

J)**, supporting that the reduced P-Smad5 gradient is independent of the *bmp1a* mutation or strain background. Furthermore, *in situ* hybridization analysis revealed that *bmp1a* expression is diminished in both M-*bmp1a*^{t31169} and M-*bmp1a*^{t31169}/+ embryos compared to in-tube controls **(Supplemental Figure 2.3K-L)**, which may explain their similarly reduced P-Smad5 gradients. We explored whether maternal *bmp1a* is targeted for degradation by known mechanisms such as by miR-430 (Bazzini et al., 2012; Giraldez et al., 2006), which could result in the aberrant degradation of wild-type *bmp1a* in M-*bmp1a*^{t31169}/+ embryos. However, based on existing RNA-sequencing (Mishima and Tomari, 2016) and miR target scanning, *bmp1a* is not a target of miR-430, leaving the underlying mechanism to be determined.

2.2.4 M-*bmp1a* embryos rapidly recover peak BMP signaling levels

The early DV patterning defects in M-*bmp1a* embryos **(Figure 2.2J-J')** were difficult to reconcile with their normal body plan **(Figure 2.1C)** unless BMP signaling and the P-Smad5 gradient recovered at a later stage. To investigate this, we quantified the P-Smad5 gradient 1.3 hours later, at 7 hpf **(Figure 2.3)**. The accurate staging of embryos at this time-point (and all others) was confirmed by relative nuclei density, which reveals clear landmark features that readily distinguish 5.3, 5.7, 6.3, and 7 hpf embryos **(Supplemental Figure 2.4)**. At 7 hpf (mid-gastrulation), M-*bmp1a* embryos recovered peak P-Smad5 levels ventrally and approached wild-type levels laterally **(Figure 2.3B,D)**. The same recovery pattern was also observed at the margin of M-*bmp1a*^{sa2416}/+ embryos **(Supplemental Figure 2.5A-F)**. Interestingly, at a more animal position, M-*bmp1a*/+ embryos display a similar recovery of P-Smad5 levels compared to at the margin, while M-*bmp1a* embryos display a weaker recovery compared with the margin **(Supplemental Figure 2.5G-I)**. In contrast, in embryos deficient for both M-Bmp1a and Tolloid the P-

Smad5 gradient remained effectively ablated embryo-wide **(Figure 2.3C-D)**. Overall, the rapid and significant recovery of the P-Smad5 gradient in M-*bmp1a* embryos demonstrates that BMP signaling, and its regulation, is highly dynamic.

However, despite the recovery of peak P-Smad5 levels by 7 hpf, DV patterning defects in M-*bmp1a* and M-*bmp1a*/+ embryos persisted. The cranial neurectoderm markers *otx2* and *gbx1* remained expanded at 8 hpf **(Figure 2.3E-F and Supplemental Figure 2.4J-K)**. This is consistent with previous studies showing that BMP signaling patterns anterior tissues such as the head earliest, between 4.7 and 6 hpf, compared to more caudal tissues (Bhat et al., 2013; Hashiguchi and Mullins, 2013; Tucker et al., 2008). Dorsal marker expansion may also persist because P-Smad5 levels in the lateral region (between 45° and 90°), though recovering, remain significantly below wild-type **(Figure 2.3D and Supplemental Figure 2.4F)**. Thus, M-*bmp1a* mutants provide a powerful context to investigate the recovery of BMP signaling, the plasticity of the early gastrula, and how the embryo may compensate for an early expansion of neural tissues later during development.

2.2.5 Sizzled is dispensable for early BMP gradient formation in zebrafish

In M-*bmp1a* and M-*bmp1a/*+ embryos, which exhibit significantly reduced P-Smad5 at 5.7 hpf **(Figure 2.2 and Supplemental Figure 2.3)**, we also observed reduced *sizzled* expression **(Figure 2.4A)**. This is consistent with *sizzled* being induced by BMP signaling and Sizzled's role as a feedback inhibitor (Collavin and Kirschner, 2003; Inomata et al., 2013; Lee et al., 2006; Martyn and Schulte-Merker, 2003; Yabe et al., 2003). *sizzled* mutants are mildly ventralized and, similar to *tolloid* mutants, this phenotype primarily affects the tail **(Figure 2.1C)** (Hammerschmidt et al., 1996a). However, although *sizzled* expression is responsive to BMP levels, we found that the P-Smad5 gradient in *sizzled*

mutants remained unchanged in two null alleles **(Figure 2.4B-E)**. Since both *sizzled* and *tolloid* mutants displayed wild-type P-Smad5 gradients in the early gastrula (5.7 hpf) **(Figures 2.2 and 2.4)**, and both mutants do not display DV patterning defects until mid- to late-gastrula stages (8-10 hpf) (Connors et al., 1999; Connors et al., 2006; Hammerschmidt et al., 1996a; Miller-Bertoglio et al., 1999), Sizzled and Tolloid likely shape the BMP gradient later in gastrulation to correctly pattern tail tissues.

Although Sizzled alone may not play a role in establishing the early BMP gradient, we postulated that Sizzled may contribute to the reduced P-Smad5 gradient in M-*bmp1a* and M-*bmp1a/+* embryos **(Figure 2.2 and Supplemental Figure 2.3)**. In M-Bmp1a deficient embryos, Sizzled could be inhibiting Tolloid, which is still present, resulting in increased Chordin activity and a shallower P-Smad5 gradient. To directly test this, we quantified the P-Smad5 gradient in embryos deficient for both Bmp1a and Sizzled to determine if the additional loss of *sizzled* ameliorated, or even rescued the decreased M-*bmp1a/+* P-Smad5 gradient. However, at 5.7 hpf we found no discernable difference between M-*bmp1a/+;sizzled* homozygotes and their M-*bmp1a/+* and M-*bmp1a/+;sizzled* heterozygous siblings **(Figure 2.4F-I)**. This indicates that Sizzled, on its own and in the sensitized M-*bmp1a/+* background, is dispensable for early BMP gradient formation in zebrafish, though this does not preclude an early role for Sizzled under other perturbations.

2.2.6 Expression dynamics likely account for distinct requirements of Bmp1a/Tolloid function

To incorporate Bmp1a and Tolloid into a mathematical model of BMP gradient formation, we determined the dynamics of *tolloid* gene expression in late blastula and early gastrula embryos using RNAscope. Previous *in situ* methods describing *tolloid*

distribution in the early gastrula yielded limited spatial and temporal resolution due to intense puncta that dominated the chromogenic alkaline phosphatase signal (Connors et al., 1999). In contrast, RNAscope offers whole-mount fluorescence microscopy, enabling detection within individual nuclei and across distinct anteroposterior positions. Importantly, we found that *tolloid* expression is very low in the late blastula (4.7 hpf) but increases significantly in the early gastrula (5.7 hpf) **(Figure 2.5A-C)**. We also found that *tolloid* puncta correspond to nuclear transcripts **(Supplemental Figure 2.7A-D)**. Interestingly, segmenting and extracting *tolloid* distribution at the margin revealed graded ventral-to-dorsal expression at 5.7 hpf **(Figure 2.5A-C)**.

We used an updated mathematical model, described in the next section, to evaluate the roles of Tolloid and Bmp1a expression dynamics in BMP signaling gradient formation. We performed several computational screens (100,000 simulations each) with: (i) varied distribution and onset of Tolloid and (ii) ubiquitous Bmp1a either constant or degrading **(Supplemental Figure 2.6F-I, Tables 1-2).** Though graded Tolloid modestly improved the number of solutions that fit our P-Smad5 gradient data, we found the most solutions that fit our results exhibited a later onset of Tolloid expression and constant Bmp1a expression **(Supplemental Figure 2.6F, Table 2)**. This is consistent with our measurements of *tolloid* mRNA **(Figure 2.5A-C)** and existing RNA-sequencing that includes *bmp1a* (Mishima and Tomari, 2016). Furthermore, we identified the optimal Tolloid onset time to be 5.3 hpf **(Supplemental Figure 2.6G-I)**, which is consistent with the less prominent role of Tolloid and its inability to substitute for loss of Bmp1a at 5.7 hpf **(Figure 2.2)**. Taken together, these results support that temporal differences in Bmp1a and Tolloid expression may be key to their distinct roles in shaping the early BMP gradient.

2.2.7 Computational screen endorses limited Chordin range during BMP gradient formation

In our previous mathematical model of BMP gradient formation (Zinski et al., 2017), we used a linear model of Chordin proteolysis by a single metalloprotease, Tolloid, and did not consider Sizzled regulation. Since we found that Bmp1a plays an independent role in gradient formation **(Figure 2.2)**, we updated our model and tested it against an expanded cohort of mutant P-Smad5 gradients. First, we incorporated distinct Bmp1a and Tolloid expression patterns and dynamics **(Figure 2.5D-E)**. Second, we explicitly used enzyme saturation kinetics to describe Bmp1a and Tolloid processing of Chordin and their competitive inhibition by Sizzled **(Supplemental Figure 2.6A)**. Third, since *sizzled* expression is regulated by BMP signaling, we estimated Sizzled expression based on BMP signaling levels using a gene control feedback term **(Supplemental Figure 2.6B)**. Though loss of Sizzled did not have an early P-Smad5 phenotype, it was still included because it is expressed at 5.7 hpf **(Figure 2.4 and Supplemental Figure 2.6C)** and therefore may potentially affect Bmp1a/Tolloid.

With this updated model, we performed a large-scale computational screen (1 million simulations) of BMP gradient formation from 3.5 hpf, when wholesale zygotic transcription initiates, to 5.7 hpf, the early gastrula stage when we measured the P-Smad5 gradient in multiple mutant conditions. For each simulation, we solved a system of partial differential equations **(Supplemental Figure 2.6A-B)** with a distinct combination of randomly varied values for unknown parameters **(Tables 3-5)**. That same parameter combination was then re-simulated to predict the BMP signaling gradient in mutant conditions. Finally, simulated BMP signaling gradients were compared to respective measured P-Smad5 profiles for wild-type; *chordin*, *sizzled*, *tolloid*, and M-*bmp1a* single

mutants; and M-*bmp1a;tolloid* double mutants **(Figure 2.5H, Table 6)**. Loss of *noggin* was compared to the wild-type P-Smad5 profile as an additional control, as in (Zinski et al., 2017). In this updated model, 23 individual parameters are varied compared to 19 previously (Zinski et al., 2017), increasing the number of simulations required. Furthermore, model solutions are now compared against eight wild-type or mutant P-Smad5 profiles **(Figures 2.2 and 2.4)**, compared to four previously (Zinski et al., 2017).

In our initial computational modeling screens, we found that BMP and Chordin production rates (ϕ_B and ϕ_C) were limited to 0.01–1 nM/s and 0.1–10 nM/s, respectively. Furthermore, ϕ_C was consistently higher than ϕ_B. Thus, we performed our finalized computational screen using these production value ranges and constrained ϕ_C to be greater than ϕ_B, which increased model fitness **(Figure 2.5F, Tables 3-6)**. From this computational screen, the median ratio of ϕ_C to ϕ_B was 8.77 in the solutions fitting the P-Smad5 profiles **(Figure 2.5F')**. Interestingly, the M-*bmp1a* P-Smad5 profile was the most challenging to fit, consistently constraining the number of best-fit solutions **(Tables 2, 6)**. Impressively, with only 1 million simulations and the additional parameters incorporated, we were able to generate model solutions, 16 in total, that simultaneously fit all mutant P-Smad5 profiles within the experimentally observed error **(Figure 2.5H)**.

Additionally, fitting the M-*bmp1a;tolloid* P-Smad5 profile refined another important system parameter, Chordin diffusion. High rates of Chordin diffusion (D_C), up to 50 $\mu m^2/s$, were required to recapitulate the embryo-wide P-Smad5 decrease seen in M-*bmp1a;tolloid* embryos **(Tables 3, 4, and 6)**. The mean D_C of our solutions, 23.42 $\mu m^2/s$ **(Figure 2.5G)**, suggests a higher rate of Chordin diffusion than the recently measured effective diffusion rate in zebrafish, 6 $\mu m^2/s$ (Pomreinke et al., 2017). These previous measurements were performed in the presence of Bmp1a/Tolloid, suggesting that

Bmp1a/Tolloid could limit Chordin's effective range to restrict Chordin function. Furthermore, in *Xenopus* D_C measurements indicate a highly mobile (31 $\mu m^2/s$) and less mobile fraction of Chordin, suggesting that higher rates of Chordin diffusion are achievable (Inomata et al., 2013).

Although D_C values from both zebrafish and *Xenopus* show that Chordin is highly diffusive (Inomata et al., 2013; Pomreinke et al., 2017), the distribution of Chordin in our computational solutions is restricted to the dorsal half (from 90° to 180°) of the embryo **(Figure 2.5J)**. Importantly, the distribution of Chordin clearly differentiates between the counter-gradient and source-sink models: in the counter-gradient model, Chordin diffuses the length of the embryo, while in the source-sink model Chordin remains dorsally limited to act as an immobile sink **(Figure 2.5I)** (Zinski et al., 2017). Thus, our modeling solutions are exclusively consistent with predictions from a source-sink model and thus exclude the counter-gradient as a model of BMP gradient formation in the early zebrafish embryo **(Figure 2.5J)**. Furthermore, these data implicate that Bmp1a/Tolloid restrict the effective mobility of Chordin to generate a dorsal sink.

2.2.8 Chordin mobility is dispensable for DV patterning

A defining feature of the source-sink model is that Chordin is not required to diffuse to the ventral regions of the embryo; in fact, it must be prevented from doing so, presumably by Bmp1a/Tolloid **(Figure 2.5I-J)**. Thus, we predict that, in the absence of Bmp1a/Tolloid, non-diffusible Chordin is sufficient to generate a normal BMP gradient when localized correctly. We tested this in our mathematical model by expressing non-diffusing Chordin (D_C=0) in a M-*bmp1a;tolloid* background **(Table 7)**. We performed 1 million simulations with varied immobile Chordin expression domains and, surprisingly, found that many solutions (40,615) can generate a wild-type BMP gradient **(Figure 2.6A-**

A'). This suggests that Chordin diffusion may be dispensable to generate a functional BMP gradient.

As expected, the majority (79%) of immobile Chordin domains in these solutions, which were varied in both size and location, were dorsally localized **(Figure 2.6A-A')**. However, the dorsal domain sizes were consistently broad, with most individual solutions extending from least 180° to at least 100° **(Figure 2.6A, red)**. In fact, the mean length of all dorsal regions extended to 90°, or halfway across the embryo **(Figure 2.6A', red)**, which is consistent with the Chordin distribution observed from solutions in our earlier screen **(Figure 2.5J)**. Furthermore, there were many (20%) lateral solution domains **(Figure 2.6A, green)** and the majority of these (70%) also had a mean length that reached 90° **(Figure 2.6A', green)**. In contrast, there were very few (1%) ventral solution domains **(Figure 2.6A-A', blue)**. Together, the individual and mean domain lengths of our modeling solutions suggest that non-diffusing Chordin is primarily required in the dorsolateral region of the embryos from 90-135° **(Figure 2.6A-A')**.

To directly test whether Chordin diffusion is required for DV patterning *in vivo*, we generated a membrane-tethered Chordin protein **(Figure 2.6B)**. This construct had an N-terminal epitope tag and the rat integral-membrane protein, CD2, at the C-terminus (HA-Chordin-CD2) (Ashe and Levine, 1999). mRNA microinjection of *HA-chordin-cd2* in M-*bmp1a*/+ and wild-type embryos resulted in membrane localization at 5.7 hpf, which was absent when the epitope-only (*HA-chordin*) mRNA was injected **(Figure 2.6C-D)**. Notably, HA-Chordin-CD2 membrane localization was more clearly visible in M-*bmp1a*/+ embryos **(Figure 2.6C-D)**, indicating that endogenous Bmp1a is very efficient at cleaving HA-Chordin-CD2 in wild-type embryos.

Both HA-Chordin and HA-Chordin-CD2 were functional. The epitope-only control rescued *chordin* mutants **(Supplemental Figure 2.7E)** while HA-Chordin-CD2 dorsalized embryos lacking endogenous Chordin, M-Bmp1a, and Tolloid **(Figure 2.6E-F)**. Consistent with our earlier double mutant analysis **(Figure 2.1)**, embryos deficient for M-Bmp1a and Tolloid, but wild-type or heterozygous for *chordin*, were severely dorsalized **(Figure 2.6F and Supplemental Figure 2.7F, column 2)**. Additional microinjection of *HA-chordin-cd2* mRNA had no adverse effects, even enhancing dorsalization in *chordin* heterozygotes **(Figure 2.6E-F and Supplemental Figure 2.7F, column 3)**. However, *chordin* mutant siblings, which were also deficient for M-Bmp1a and Tolloid, displayed the ventralized *chordin* mutant phenotype **(Figures 2.6F, columns 4-5, and 2.7B)**. Importantly, this confirms that Bmp1a and Tolloid function exclusively through Chordin. Furthermore, microinjection of *HA-chordin-cd2* in *chordin* mutant embryos also severely dorsalized them **(Figure 2.6E-F, column 6)**. Thus, HA-Chordin-CD2, despite being localized to the membrane, can function like endogenous Chordin, fully inhibiting BMP signaling embryo-wide in the absence of M-Bmp1a and Tolloid.

Our mathematical model predicts that non-diffusible Chordin, in the absence of Bmp1a/Tolloid, can recapitulate a normal BMP gradient if expressed in dorsal-lateral regions **(Figure 2.6A-A')**. To determine if localized immobile Chordin can correctly pattern the DV axis, we regionally expressed membrane-tethered Chordin construct in embryos lacking endogenous Chordin, M-Bmp1a, and Tolloid **(Figure 2.7A)**. To regionally express *HA-chordin-cd2* mRNA, we injected it into a single blastomere between the 8- and 16-cell stages **(Figure 2.7A)**. Only cells descendant from the injected blastomere will express HA-Chordin-CD2, resulting in regional expression **(Figure 2.7A-A')**. The expression region was determined at 6.3 hpf, when the dorsal shield is apparent as a landmark, based

on the fluorescence of H3.3-mCherry, which was co-injected as a lineage tracer **(Figure 2.7A)**. The embryo phenotype was then evaluated at 12 hpf and 1-2 dpf before identifying the *chordin* mutants by genotyping.

Remarkably, we found that three of four identified *chordin* homozygous mutants displayed a near wild-type phenotype at 2 dpf **(Figure 2.7C-D)**. *chordin* mutants normally display distinct DV patterning defects: reduced eyes, expansion of the posterior somites, yolk extension, and blood island, and duplication of the ventral tail fin **(Figure 2.7B)**, which persist with or without M-Bmp1a/Tolloid **(Figure 2.6F, columns 4-5)**. However, regional expression of HA-Chordin-CD2 impressively rescued these defects **(Figure 2.7C, column 9)**. Notably, dorsal-lateral expression of HA-Chordin-CD2 resulted in rescue **(Figure 2.7D)**, which is consistent with our model of immobile Chordin that predicts that the rescuing region extends to halfway across the embryo **(Figure 2.6A-A')**. Also consistent with this prediction, much smaller regions of strictly dorsal HA-Chordin-CD2 expression did not rescue **(Supplemental Figure 2.7H)**. Importantly, dorsal-lateral expression of HA-Chordin (the epitope-only control) in embryos deficient in Chordin, M-Bmp1a and Tolloid did not rescue *chordin* mutants to a wild-type phenotype and instead dorsalized them **(Figure 2.7C, columns 7-8)**.

Additionally, M-*bmp1a;chordin* +/- and +/+ embryos were radially dorsalized when injected with the *tll1*MO, confirming that *tll1*MO blocked Tolloid activity **(Figure 2.6F and Supplemental Figures 2.7F, column 2 and 2.7G, columns 2 and 5)**. Enough HA-Chordin-CD2 was injected to radially dorsalize embryos deficient for Chordin, Bmp1a, and Tolloid when expressed ubiquitously **(Figure 2.6F, column 6 and Supplemental Figure 2.7G, column 9)**, so a sufficient amount was injected regionally. This demonstrates that the ability of dorsolaterally-expressed HA-Chordin-CD2 to rescue the *chordin* mutant

phenotype to wild-type is due to the presence of the CD2 membrane tether. And, that the inability of HA-Chordin to rescue *chordin* mutants to a wild-type phenotype is due to its capacity to diffuse throughout the embryo in the absence of Bmp1a/Tolloid and block all BMP signaling. Together, these results show that dorsolateral regional expression of immobile Chordin can pattern the DV axis and suggests that Chordin diffusion is not required for BMP gradient formation. This supports our model that Bmp1a/Tolloid restrict Chordin mobility to dorsal regions, thus generating the sink that drives BMP gradient formation.

2.3 Discussion

Here, we resolve the roles of the metalloproteases Bmp1a and Tolloid in BMP gradient formation. Our mutant analyses show that Tolloid is partially redundant to Bmp1a: both are required for DV patterning but Bmp1a plays a non-redundant role in shaping the BMP gradient **(Figures 2.1-2.2)**. Importantly, use of *bmp1a* mutants confirmed the epistatic relationship between Bmp1a, Tolloid, and Chordin **(Figures 2.6-2.7)**. This is important because Bmp1a/Tolloid metalloproteases process additional substrates, such as procollagens (Hopkins et al., 2007), and because of the identification of potential gene duplicates, namely *chordin-like* (Branam et al., 2010). However, concomitant loss of Bmp1a, Tolloid, and Chordin resulted in a stereotypical *chordin* mutant phenotype **(Figure 2.7)**, indicating that Chordin is the sole relevant substrate for Bmp1a and Tolloid proteolysis during gastrulation.

2.3.1 Implications from quantitative mutant P-Smad5 analyses

Quantitation of the P-Smad5 gradient in *bmp1a*, *tolloid*, and *sizzled* single mutants provided unprecedented spatial and temporal clarity. First, M-*bmp1a* embryos had a significantly diminished P-Smad5 gradient in the early gastrula that remarkably recovered by mid-gastrulation **(Figures 2.2-2.3)**. This revealed an individual, albeit unexpected, role for Bmp1a in BMP gradient formation and early DV patterning. Additionally, given their wild-type 1 dpf appearance, M-*bmp1a* mutants present a biologically relevant context for future studies into the mechanisms, and patterning consequences, of BMP gradient recovery. Interestingly, the similarities between M-*bmp1a* homozygous and heterozygous mutants **(Supplemental Figures 2.3-2.5)** also warrant future investigation.

Second, both *tolloid* and *sizzled* single mutants, which have tail DV patterning defects, displayed normal P-Smad5 gradients at 5.7 hpf **(Figures 2.2 and 2.4)**. This is consistent with previous studies describing later DV patterning defects in these mutants (Connors et al., 1999; Connors et al., 2006; Hammerschmidt et al., 1996a; Miller-Bertoglio et al., 1999) and the model that more posterior tissues are progressively patterned later in development (Hashiguchi and Mullins, 2013; Tuazon and Mullins, 2015; Tucker et al., 2008). Future studies will have to address the roles of Tolloid and Sizzled during gastrulation. Since *sizzled* is expressed earlier **(Figure 2.4)**, it may be translationally repressed to time its activity, similar to Lefty in the Nodal morphogen system (van Boxtel et al., 2015), though *sizzled* is not a miR-430 target based on our analysis of existing RNA-sequencing (Mishima and Tomari, 2016). Additionally, as the embryo progresses through gastrulation there is a rapid and dramatic reorganization of cells, which may affect BMP gradient shape and require specific regulators, such as Tolloid and Sizzled (Connors et al., 2006; Tuazon and Mullins, 2015).

2.3.2 Mathematical modeling predictions with *in vivo* analysis: Bmp1a/Tolloid, the keepers of a Chordin sink

Combining our updated mathematical model of BMP gradient formation **(Supplemental Figure 2.6)** and RNAscope analysis, we identified and validated previously uncharacterized complexity in *tolloid* expression dynamics, specifically that it is non-uniform and likely first expressed close to 5.3 hpf **(Figure 2.5 and Supplemental Figure 2.7)**. This may account for our finding that Tolloid cannot compensate for the loss of Bmp1a, which is maternally deposited, during BMP signaling gradient formation **(Figure 2.2)**. Iterative large-scale mathematical screens also revealed likely ranges, and even a relative ratio, for BMP and Chordin production rates, which are valuable for any future mathematical modeling in the field since these rates are difficult to measure *in vivo* **(Figure 2.5)**.

Both models with either diffusing and non-diffusing Chordin **(Figure 2.5 and 2.6)** support that regionally-restricted Chordin is required to generate the BMP gradient. First, despite likely being produced at almost 10-fold higher rates than BMP, and being highly diffusive **(Figure 2.5)** (Inomata et al., 2013; Pomreinke et al., 2017), Chordin distribution in our solutions remained restricted to the dorsal half of the embryo. This compels the exclusion of the counter-gradient as a viable mechanism for BMP gradient formation in the early zebrafish embryo. Furthermore, this implicates Bmp1a/Tolloid as the keepers of a Chordin sink, essentially preventing a counter-gradient of Chordin from forming.

Our results that regional, non-diffusing Chordin can correctly pattern the embryo **(Figure 2.7)** provide pivotal *in vivo* support for this mechanism. The rescuing regions extend through the dorsolateral and lateral regions, consistent with our model results **(Figure 2.5)**. However, when compared to the smaller area of Chordin production

(Figures 2.1A and 2.5D), this suggests that some limited diffusion is required during normal development to generate a correctly-sized Chordin sink. Future studies have the opportunity to define the spatial and temporal characteristics of a Chordin sink.

2.3.3 Employing the Bmp1a/Tolloid modality across systems

The use of Bmp1a/Tolloid to limit Chordin mobility provides an exciting glimpse into how BMP can readily form a morphogen gradient in diverse biological contexts. Using the zebrafish as an example, Chordin's high diffusivity can first be restricted in the early gastrula to pattern the DV body axis (as we show here) and then be utilized later, in the absence of Bmp1a/Tolloid, to pattern other organs, such as the neural tube or digits (Dutko and Mullins, 2011; Suzuki et al., 2008; Zagorski et al., 2017). Thus, Bmp1a/Tolloid represent a module of mechanistic flexibility, enabling the same signal (BMP) and antagonist (Chordin) to be employed throughout a single organism's lifespan in environments of distinct shapes and sizes during development, homeostasis, or even disease.

Furthermore, the requirement for a restricted Chordin sink in the zebrafish gastrula may reveal underlying principles, such as spatial expression profiles or time-scales, differentiating mechanisms of gradient formation when compared to other organisms. In contrast to zebrafish and *Xenopus*, BMP gradient formation in *Drosophila* relies on a counter-gradient of the Chordin ortholog Sog and the facilitated diffusion of BMP that is mediated by Tolloid and Sog (Mullins, 1998; Peluso et al., 2011). While in sea urchins and sea anemones, BMP and Chordin are co-expressed (Lapraz et al., 2009; Meinhardt, 2015a), the roles for Bmp1a/Tolloid remain undescribed although they are expressed (Angerer et al., 2006; Reynolds et al., 1992). Overall, Bmp1a/Tolloid may be fundamental

to delineate distinct mechanisms of BMP gradient formation, within and across organisms, and offer an exciting perspective for a broad range of future studies in the field.

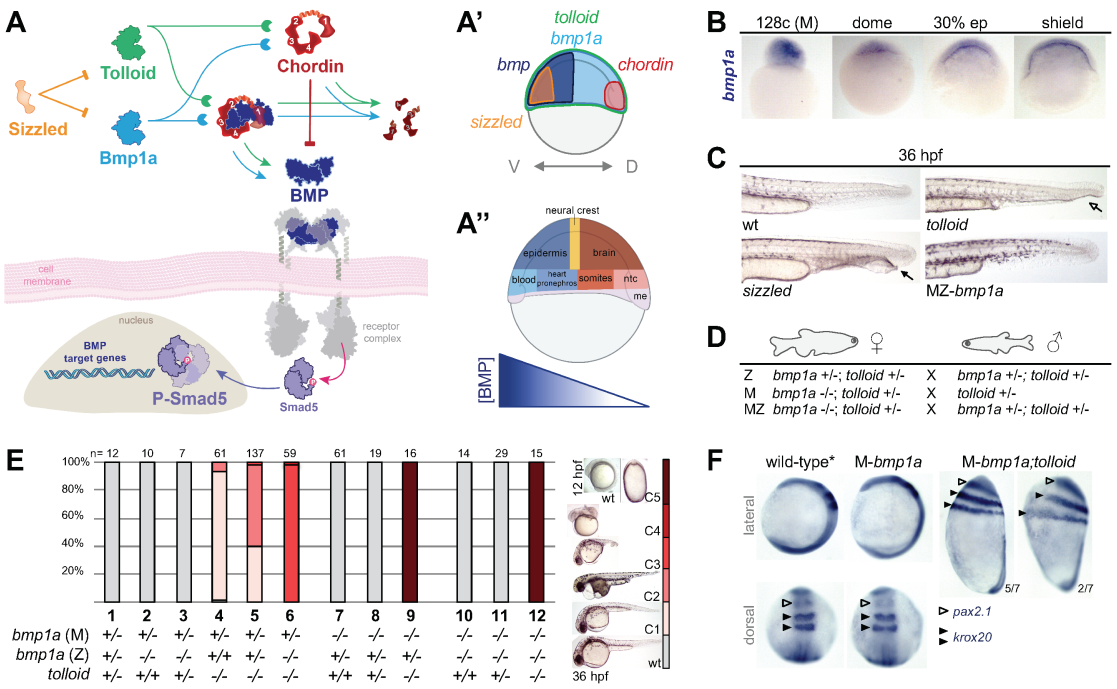

Figure 2.1 Bmp1a and Tolloid are redundant in DV patterning

(**A**) Schematic of the extracellular BMP regulators explored in this paper, adapted from (Dutko and Mullins, 2011), and (**A'**) their published mRNA expression domains in the zebrafish gastrula (6.3 hpf, see text for references). (**A''**) Fatemap of the early zebrafish gastrula (ntc.: notochord, me: mesendoderm). (**B**) *bmp1a* mRNA expression in wild-type embryos at 128-cell (2.5 hpf), dome (4.3 hpf), 30% epiboly (4.7 hpf) and shield (6.3 hpf) stages. (M: maternal expression) (**C**) 36 hpf tail phenotypes of wild-type and *tolloid*, *sizzled*, and MZ-*bmp1a*^{t31169} mutants. Open arrow: loss of ventral tail fin in *tolloid* mutants. Solid arrow: duplication of ventral tail fin in *sizzled* mutants. (**D**) Adult fish crosses used to generate zygotic (Z), maternal (M), and maternal-zygotic (MZ) depletion of *bmp1a* and zygotic *tolloid*. (**E**) Dorsalization of embryos resulting from Z-, M-, and MZ-*bmp1a*^{t31169}*;tolloid* crosses (columns 1-6, 7-9, and 10-12 respectively). *bmp1a* (M) indicates genotype of the mother while *bmp1a* (Z) and *tolloid* indicate embryo genotype. (**F**) Lateral view of wholemount *in situ* analysis of neurectoderm markers at 5-somite stage (12 hpf). In wild-type (n=9) and M-*bmp1a* (n=4) embryos, *pax2.1* (open arrowhead) is expressed in the forebrain and *krox20* (black arrowheads) in the hindbrain. *pax2.1* and *krox20* are radially expanded in M-*bmp1a;tolloid* embryos (n=7). Asterisk (*) indicates in-tube controls.

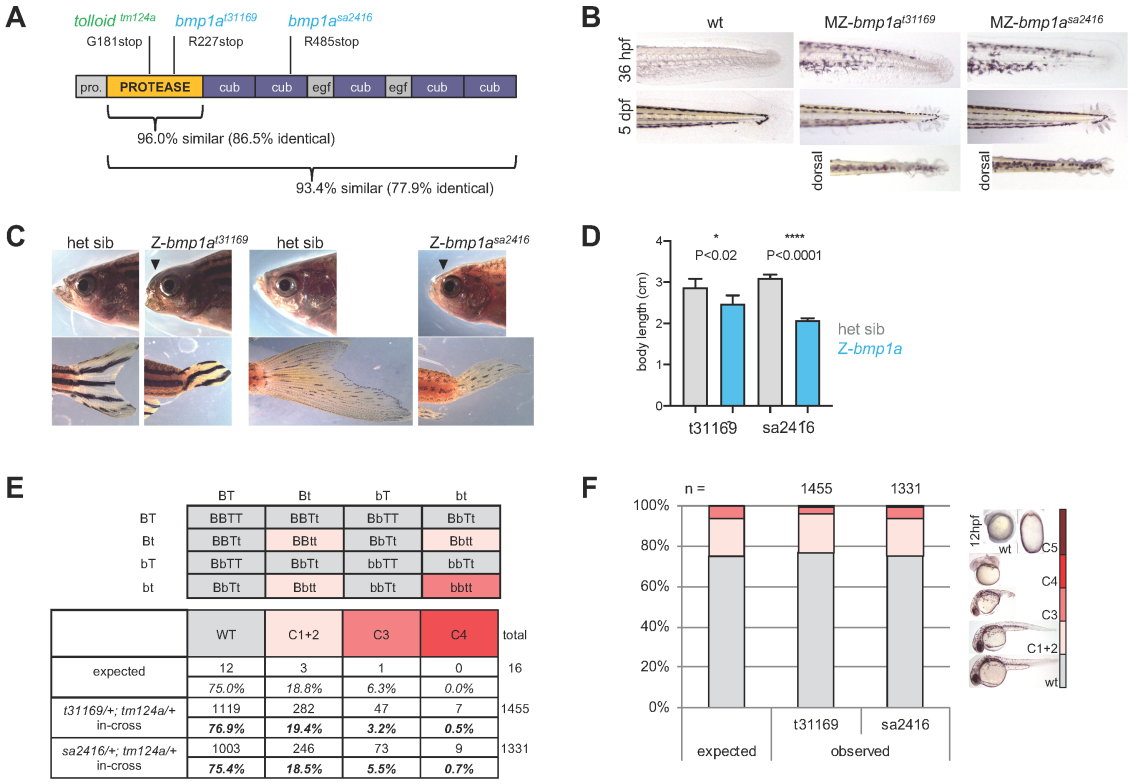

	WT	C1+2	C3	C4	total
expected	12	3	1	0	16
	75.0%	*18.8%*	*6.3%*	*0.0%*	
t31169/+; tm124a/+ in-cross	1119	282	47	7	1455
	76.9%	***19.4%***	***3.2%***	***0.5%***	
sa2416/+; tm124a/+ in-cross	1003	246	73	9	1331
	75.4%	***18.5%***	***5.5%***	***0.7%***	

Supplemental Figure 2.1 Equivalent *bmp1a* alleles confirm Bmp1a/Tolloid redundancy

Related to Figure 2.1. (**A**) Schematic of the shared domain structure of zebrafish Bmp1a and Tolloid proteins and the location of the mutant alleles used in this paper (pro: prodomain). Brackets indicate regions where the Bmp1a and Tolloid amino acid sequences were compared. (**B**) At 36 hpf, MZ-*bmp1a* mutants of both alleles appear phenotypically wild-type and by 5 dpf display a characteristic ruffling of the tail fin, resulting from the known role for Bmp1a in processing collagens (Asharani et al., 2012; Bowen et al., 2012). (**C**) Adult Z-*bmp1a*^{sa2416} fish display deformed tail fins compared to their heterozygous siblings, phenocopying Z-*bmp1a*^{t31169}. Similarly, Z-*bmp1a*^{sa2416} mutants also display frontonasal shortening (arrowheads), though it is more pronounced in Z-*bmp1a*^{t31169}. (**D**) Adult Z-*bmp1a*^{sa2416} mutants have significantly shorter body axes, similar to Z-*bmp1a*^{t31169}. (**E-F**) Dorsalization of embryos resulting from *bmp1a*^{t31169}*/+;tolloid/+* or *bmp1a*^{sa2416}*/+;tolloid/+* intercrosses. Approximately 1/16th of embryos are C3 dorsalized, consistent with Mendelian ratios for the double mutant phenotype.

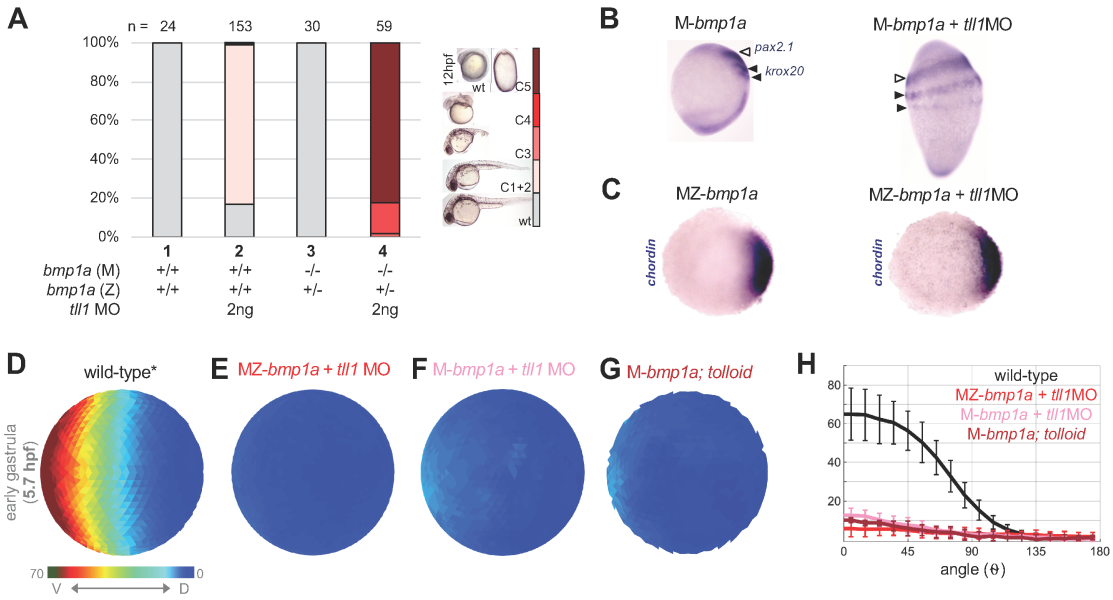

Supplemental Figure 2.2 A *tolloid* morpholino phenocopies the M-*bmp1a;tolloid* double mutant

Related to Figures 2.1 and 2.2. (**A**) *tll1*MO recapitulates the *tolloid* single mutant phenotype (column 2) (Kok et al., 2015; Lele et al., 2001). Injection of this concentration (2ng) into M-*bmp1a*^{t31169} mutants (column 4) also results in severe, radial dorsalization, as observed in **Figure 1E, column 9**. (**B**) Lateral views of wholemount *in situ* analysis of neurectoderm markers at 5-somite stage (12 hpf). In un-injected M-*bmp1a*^{t31169} controls (n=6), *pax2.1* (open arrowhead) is expressed in the forebrain while *krox20* (black arrowheads) is expressed in the hindbrain. *pax2.1* and *krox20* are radially expanded in M-*bmp1a*^{t31169}+*tll1*MO embryos (n=18). (**C**) Wholemount *in situ* analysis of *chordin* expression in un-injected MZ-*bmp1a*^{t31169} (n=11) and MZ-*bmp1a* ^{t31169}+*tll1*MO (n=15) embryos. (**D-G**) Animal view of mean P-Smad5 intensities at early gastrula stage (5.7 hpf) in: (**D**) Wild-type controls (n=29), pooled from all experiments in figure (also shown in **Figure 2A**). Asterisk (*) indicates in-tube controls. (**E**) MZ-*bmp1a* ^{t31169}+*tll1*MO embryos (also shown in **Figure 2E**, n=9). (**F**) M-*bmp1a* ^{t31169}+*tll1*MO embryos (n=9). (**G**) M-*bmp1a* ^{t31169}*;tolloid* double mutants (n=3). (**H**) Average marginal P-Smad5 intensities of **D-G**. Error bars indicate standard deviation.

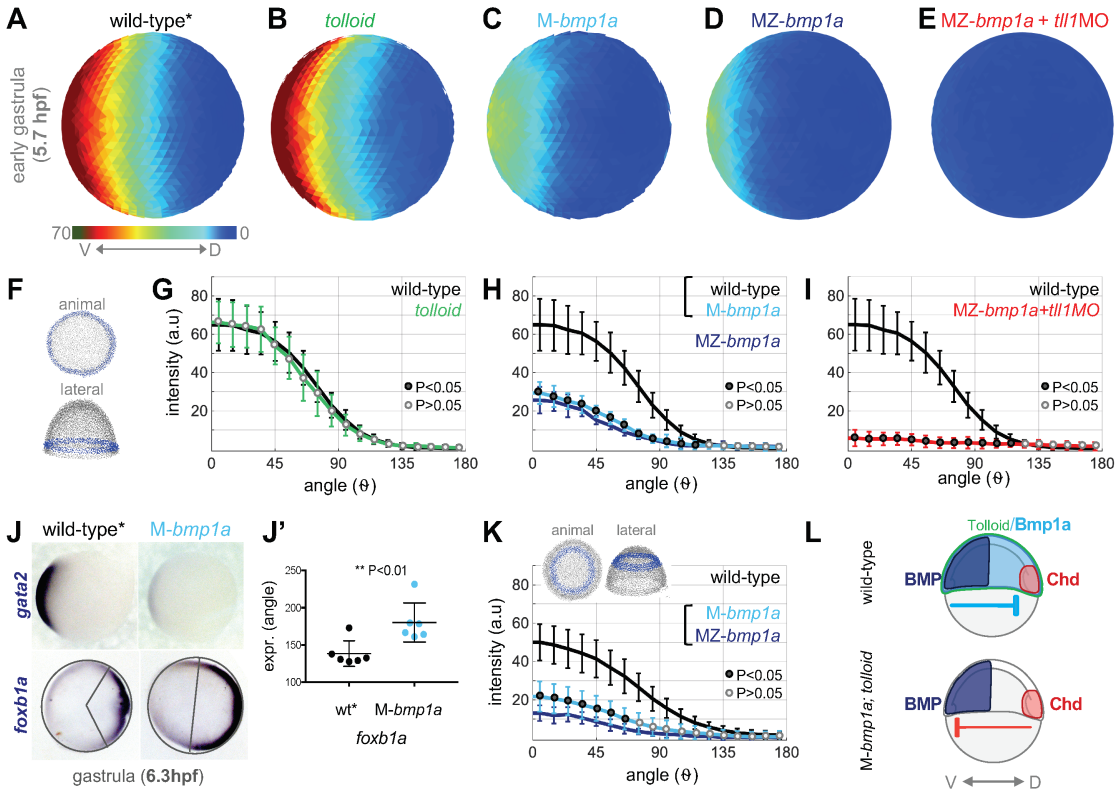

Figure 2.2 Maternal Bmp1a is required for a normal P-Smad5 Gradient and functions redundantly with Tolloid

Asterisk (*) indicates in-tube controls. (**A-E**) Animal view of mean P-Smad5 intensities at early gastrula stage (5.7 hpf) in: (**A**) Wild-type controls (n=29), pooled from all experiments in figure. (**B**) *tolloid* mutants (n=10, 3 replicates). (**C**) M-*bmp1a*^{t31169} mutants (n=11, 4 replicates). (**D**) MZ-*bmp1a*^{t31169} mutants (n=8, 2 replicates). (**E**) MZ-*bmp1a*^{t31169} embryos injected with 2ng *tll1*MO (n=9, 2 replicates). (**F**) Standard location of 30μm band of cells used to generate marginal P-Smad5 profiles. (**G-I, K**) Average marginal P-Smad5 intensities of **A-E**. Wild-type controls are shown in black. Error bars indicate standard deviation. Filled circles indicate a significant (P<0.05) difference at each position compared to wild-type, unless a bracket indicates another comparison. (**J**) Animal view of wholemount *in situ* analysis of ventral marker *gata2* (wt n=5, M-*bmp1a*^{t31169} n=10) and dorsal marker *foxb1a* (wt n=6, M-*bmp1a* n=6) at 6.3 hpf. (**J'**) Quantification of *foxb1a* angle of expression. (**K**) M- and MZ-*bmp1a*^{t31169} P-Smad5 profiles at an animal position. (**L**) Our model that Tolloid/Bmp1a normally restrict Chordin dorsally (top) and that in M-*bmp1a;tolloid* (bottom), Chordin is unrestricted and inhibits BMP signaling in ventral regions.

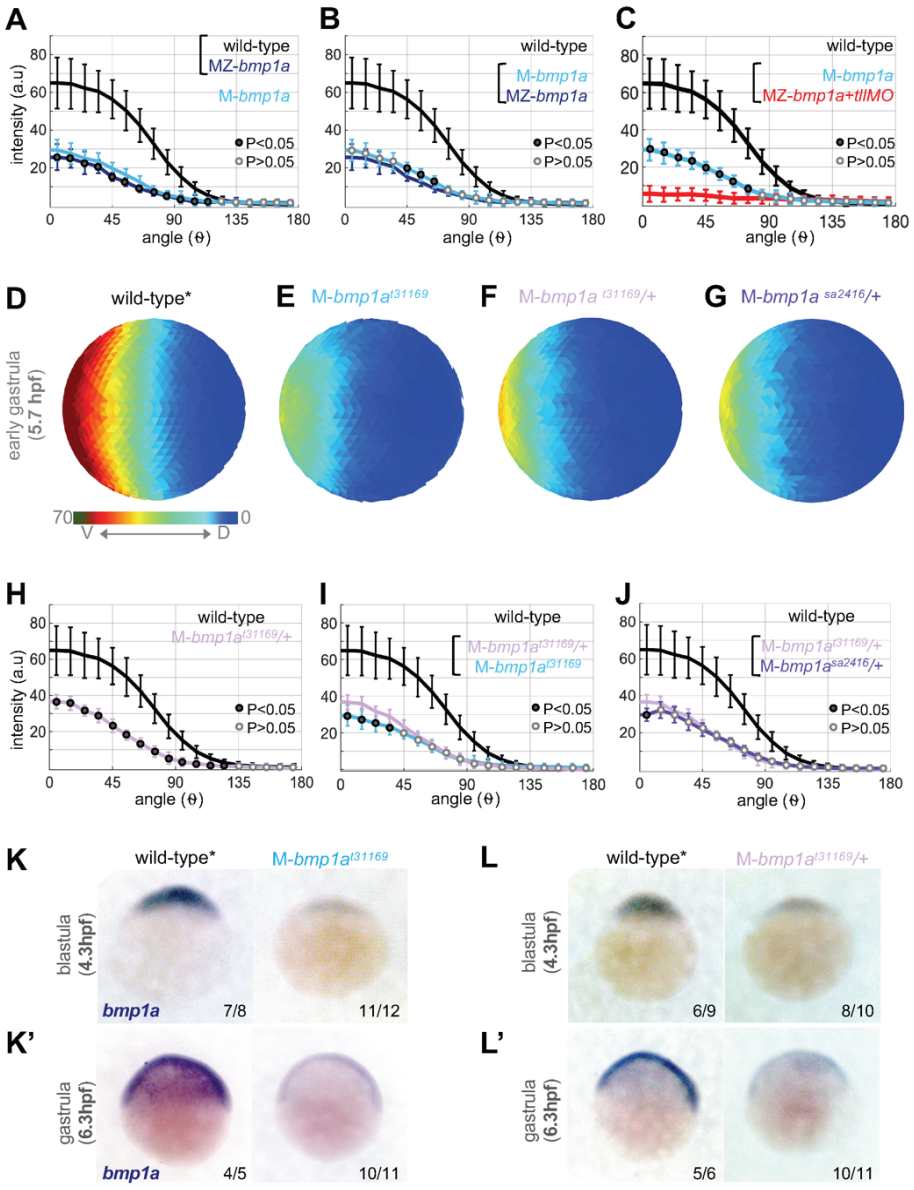

Supplemental Figure 2.3 M-, MZ-, and Heterozygous *bmp1a* mutants display similarly diminished P-Smad5 gradients

Related to Figure 2.2. (**A-C**) Extended analysis of marginal P-Smad5 intensities shown in **Figure 2 A, C-E**. Wild-type controls are shown in black. Error bars indicate standard deviation. Filled circles indicate a significant (P<0.05) difference at each position compared to wild-type, unless a bracket indicates another comparison. (**D-G**) Animal view of average P-Smad5 intensities at early gastrula stage (5.7 hpf) in: (**D**) Wild-type controls (n=29), pooled from all experiments in figure (also shown in **Figure 2A**). Asterisk (*) indicates in-tube controls. (**E**) M-*bmp1a*^{t31169} from **Figure 2D**, for comparison (n=11, 4 replicates). (**F**) M-*bmp1a*^{t31169}/+ (n=5). (**G**) M-*bmp1a*^{sa2416}/+ (n=3). (**H-J**) Comparison of the average marginal intensities in **D-G**. Wild-type controls are shown in black. Error bars

indicate standard deviation. Filled circles indicate a significant ($P<0.05$) difference at each position compared to wild-type, unless a bracket indicates another comparison. (**K-L'**) Lateral views of wholemount *in situ* analysis of *bmp1a* expression at 4.7 and 6.3 hpf in M-*bmp1a*^{t31169} homozygotes (**K-K'**) and heterozygotes (**L-L'**).

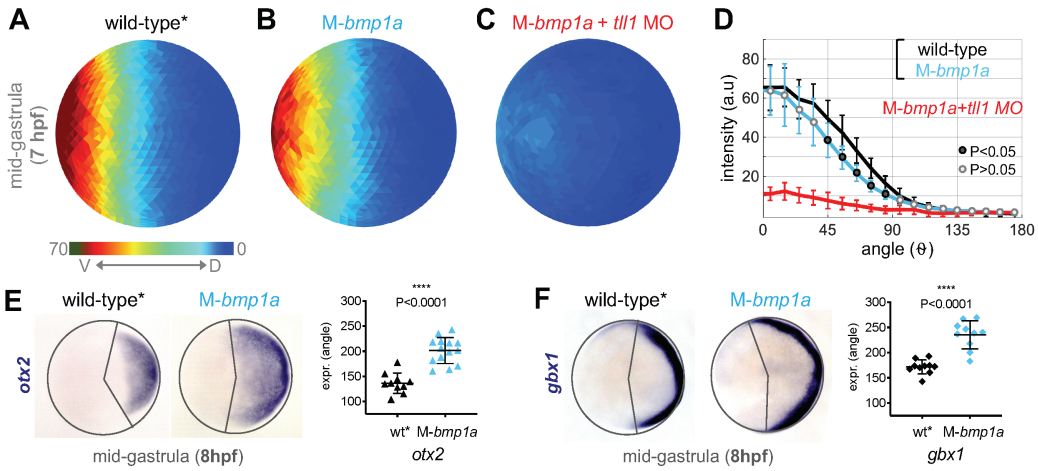

Figure 2.3 M-*bmp1a* embryos rapidly recover peak P-Smad5 levels while patterning defects persist

Asterisk (*) indicates in-tube controls. (**A-C**) Animal view of mean P-Smad5 intensities at gastrula stage (7 hpf) in: (**A**) Wild-type controls (n=11), pooled from all experiments in figure. (**B**) M-*bmp1a*^{t31169} mutants (n=6, 2 replicates). (**C**) M-*bmp1a*^{t31169} embryos injected with 2ng *tll1*MO (n=4). (**D**) Average marginal P-Smad5 intensities of **A-C**. Error bars indicate standard deviation. Filled circles indicate a significant (P<0.05) difference at each position compared to wild-type. (**E-F**) Animal view and quantification of wholemount *in situ* analysis at 8 hpf of dorsal markers (**E**) *otx2* (wt n=10, M-*bmp1a*^{t31169} n=14) and (**F**) *gbx1* (wt n=10, M-*bmp1a*^{t31169} n=10).

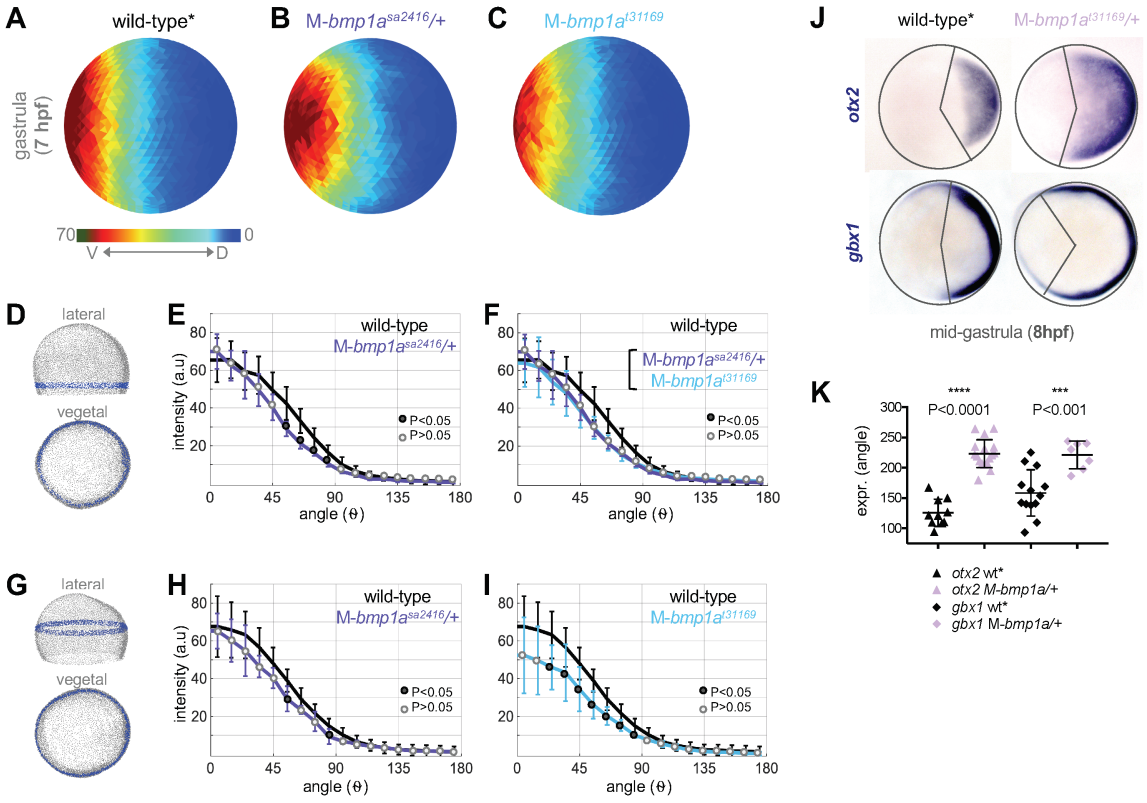

Supplemental Figure 2.4 M-*bmp1a* heterozygote also display P-Smad5 gradient recovery

Related to Figure 2.3. Asterisk (*) indicates in-tube controls. (**A-C**) Animal view of mean P-Smad5 intensities at gastrula stage (7 hpf) in: (**A**) Wild-type controls (n=11), pooled from all experiments in figure (also shown in **Figure 3A**). (**B**) M-*bmp1a*^{sa2416}/+ (n=5). (**C**) M-*bmp1a*^{t31169} from **Figure 3B**, for comparison (n=6, 2 replicates). (**D**) Location of 30μm band of cells used to generate marginal profiles in **E-F** (same position as in **Figure 3D**). (**E-F**) Average marginal intensities of **A-C**. Wild-type controls are shown in black. Error bars indicate standard deviation. Filled circles indicate a significant (P<0.05) difference at each position compared to wild-type, unless a bracket indicates another comparison. (**G**) Location of a more animal 30μm band of cells (located near the equator of the embryo) used to generate marginal profiles in **H-I**. (**H, I**) Average equatorial intensities of **A-C**. Wild-type controls are shown in black. Error bars indicate standard deviation. Filled circles indicate a significant (P<0.05) difference at each position compared to wild-type.

(**J**) Animal view of wholemount *in situ* analysis for dorsal markers *otx2* (wt=10, M-*bmp1a* ^{t31169}/+=17) and *gbx1* (wt=13, M-*bmp1a* ^{t31169}/+=7) at 8 hpf. (**K**) Quantification of *otx2* and *gbx1* angle of expression in (**J**). Can be compared to **Figure 3E-F**.

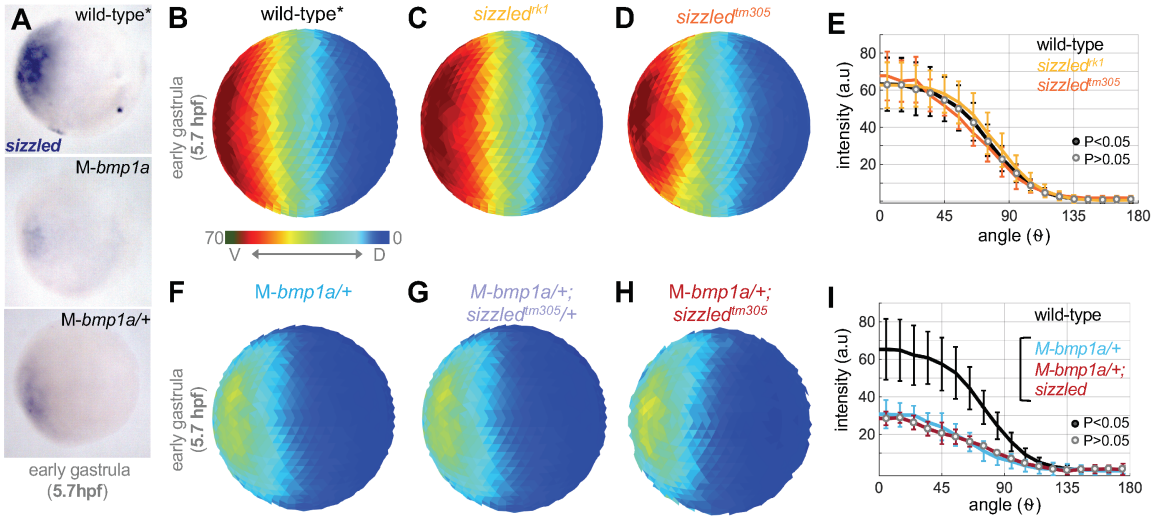

Figure 2.4 Sizzled is dispensable for early BMP gradient formation

Asterisk (*) indicates in-tube controls. (**A**) Animal view of wholemount *in situ* analysis of *sizzled* (wt=26, M-*bmp1a* ^{t31169}=9, M-*bmp1a* ^{t31169}/+=8) at 5.7 hpf. (**B-C**) Animal view of mean P-Smad5 intensities at early gastrula stage (5.7 hpf) in: (**B**) Wild-type controls (n=36), pooled from all experiments in figure. (**C**) *sizzled*^{rk1} mutants (n=34 from 3 replicates). (**D**) *sizzled*^{tm305} mutants (n=8 from 2 replicates). (**E**) Average marginal intensities of **B-D**. Wild-type controls are shown in black. Error bars indicate standard deviation. Open circles indicate no significant (P>0.05) difference at any position in each mutant compared to wild-type. (**F-H**) Animal view of mean P-Smad5 intensities at early gastrula stage (5.7 hpf) in siblings from a *bmp1a*^{t31169}/+;*sizzled*^{tm305}/+ female crossed to a *sizzled*^{tm305}/+ male: (**F**) M-*bmp1a*/+ (n=4), (**G**) M-*bmp1a*/+;*sizzled*/+ (n=4), (**H**) M-*bmp1a*/+;*sizzled* (n=3). (**I**) Average marginal intensities of **F-H**. Wild-type controls are shown in black. Error bars indicate standard deviation. Open circles indicate no significant (P>0.05) difference at any position between M-*bmp1a*/+ and M-*bmp1a;sizzled* siblings.

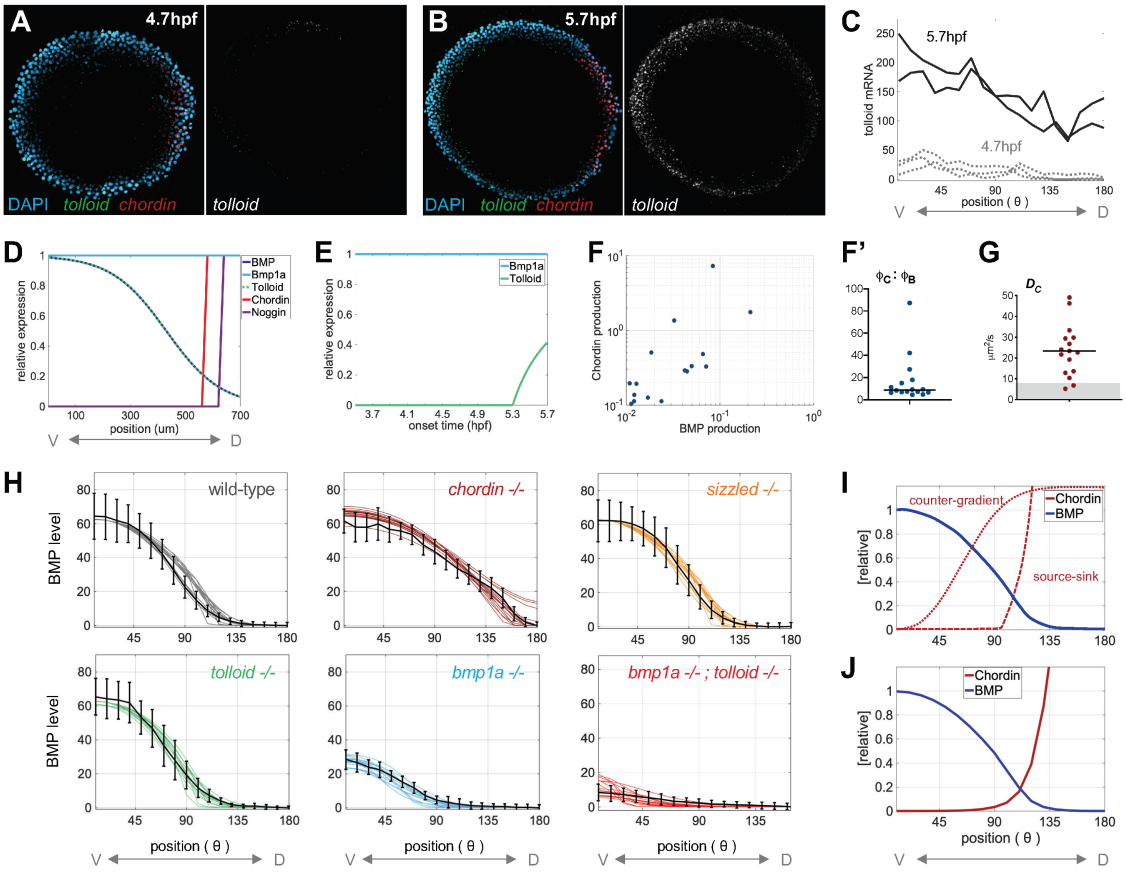

Figure 2.5 Incorporating differential *tolloid* and *bmp1a* expression into a mathematical model of BMP gradient formation

(**A-B**) RNAscope analysis of wild-type *tolloid* expression at 4.7 hpf (n=3) and 5.7 hpf (n=2). (**C**) Quantification of (**A-B**). (**D**) Spatial expression of model input domains. (**E**) Distinct temporal dynamics of Bmp1a and Tolloid expression in model input. (**F**) Rates (nM/s) of BMP (ϕ_B) and Chordin production (ϕ_C) in model solutions. (**F'**) The relative ratio of ϕ_C to ϕ_B (median=8.77 nM/s). (**G**) Rates of Chordin diffusion (D_C) in model solutions (mean=23.42, median=23.04). Gray box indicates previously measured effective diffusion rate, 6 $\mu m^2/s$ (Pomreinke et al., 2017). (**H**) BMP distribution in the 16 best-fit model solutions under wild-type and the indicated mutant conditions compared to the respective measured P-Smad5 profiles. (**I**) Schematic of the distinct Chordin distributions predicted in the counter-gradient and source-sink mechanisms. (**J**) Mean Chordin distribution (normalized to maximum BMP concentration) in the 16 best-fit model solutions.

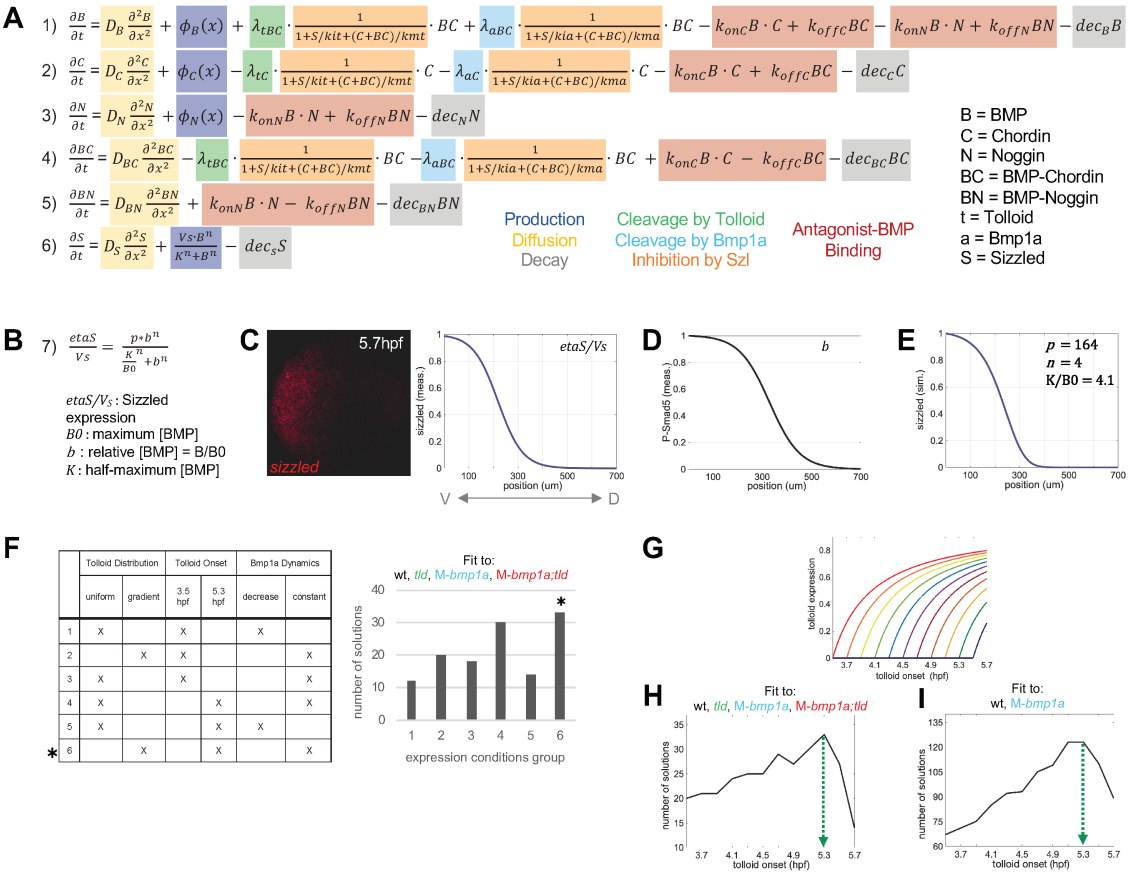

Supplemental Figure 2.5 Incorporating Bmp1a, Tolloid, and Sizzled into a mathematical model of BMP gradient formation

Related to Figure 2.5 and Tables 1-7. (**A**) System of partial differential equations solved based on fixed and varied parameter values detailed in **Tables 1, 3-5, and 7**. (**B**) Gene feedback term used to calculate Sizzled expression based on BMP levels. (**C**) Marginal *sizzled* expression (by RNAscope) and (**D**) corresponding P-Smad5 profile at 5.7 hpf used in (**E**). (**E**) Simulated Sizzled expression and cooperativity parameter terms based on solving Equation 7 with the values determined in (**C-D**), detailed in Methods. (**F**) Number of solutions in screens of differential Bmp1a and Tolloid expression, also presented in **Table 2**. The number of solutions was determined by simultaneously fitting to wild-type, *tolloid*, M-*bmp1a*, and M-*bmp1a;tolloid* P-Smad5 profiles (NRMSD <0.12). (**G**) Differential onset times of Tolloid expression. We ran eleven screens (100,000 simulations each) with the onset time for each screen set at distinct 12-minute intervals. (**H-I**) Number of fitting solutions with each time-point of graded Tolloid expression, with constant Bmp1a, to find the optimal Tolloid onset time. (**H**) The number of solutions that fit measured WT, M-*bmp1a* and *tolloid* single mutant, and M-*bmp1a;tolloid* double mutant P-Smad5 profiles (NRMSD<0.12). (**I**) The number of solutions that fit measured WT and M-*bmp1a* single mutant P-Smad5 profiles (NRMSD<0.12).

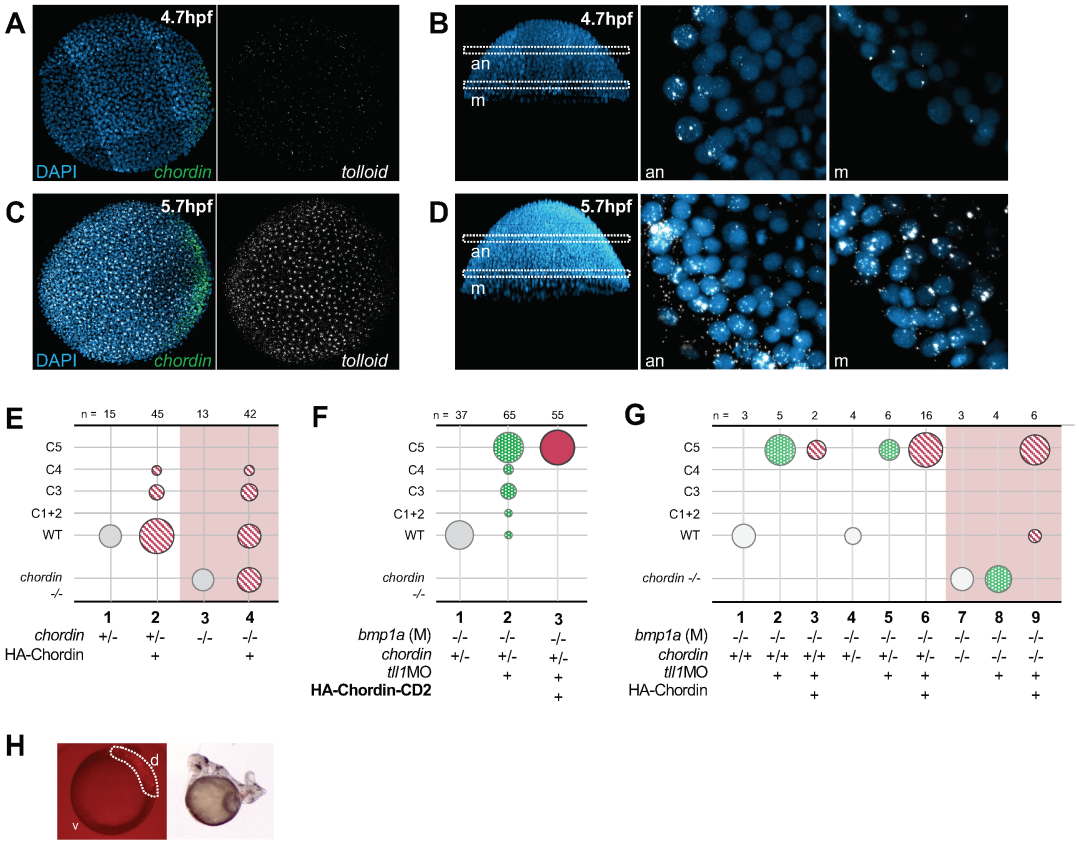

Supplemental Figure 2.6 Additional RNAscope and HA-Chordin/HA-Chordin-CD2 microinjection analysis

Related to Figures 2.5-7. (**A, C**) Maximum projections of *tolloid* RNAscope expression at 4.7 hpf (**A**) and 5.7 hpf (**C**). (**B, D**) Higher magnification view of single confocal slices at the indicated animal and marginal positions demonstrating that *tolloid* puncta are in the nucleus. (**E**) Phenotypes of *chordin* -/- X *chordin* +/- embryos injected with 300-900pg of *HA-chordin* mRNA, sorted by genotype. Epitope-tagged Chordin can rescue, and even dorsalize, *chordin* -/-. (**F**) *chordin* +/- siblings from the cross (*bmp1a*^{t31169}*; chordin*/+ female crossed to a *chordin*/+ male) and injections (3ng *tll1*MO and 250-800pg *HA-chordin-cd2*) in **Figure 6E-F**; n is from 3 replicates. While the majority of M-*bmp1a-/-;chordin+/-* embryos are radially dorsalized after injection with the *tll1*MO (column 2), there are consistently more intermediately dorsalized phenotypes than M-*bmp1a* siblings **(Figure 6F, column 2)**. However, additional injection of 250-800pg *HA-chordin-cd2* enhanced dorsalization (column 3), confirming that the construct is functional. These injections include the controls performed in parallel to the regional injections in **Figure 7C**. (**G**) Ubiquitous expression of epitope-only (460pg HA-Chordin) controls cause radial dorsalization, even in *chordin-/-* siblings. This confirms that HA-Chordin is functional (shown in **E**) and acts as a control performed in parallel to the regional injections in **Figure 7C**. (**H**) Dorsal expression of HA-Chordin-CD2 in M-*bmp1a*^{t31169}*;chordin+/-* embryos with the *tll1*MO caused an undetermined phenotype that is not clearly dorsalized or ventralized; d: dorsal, v: ventral.

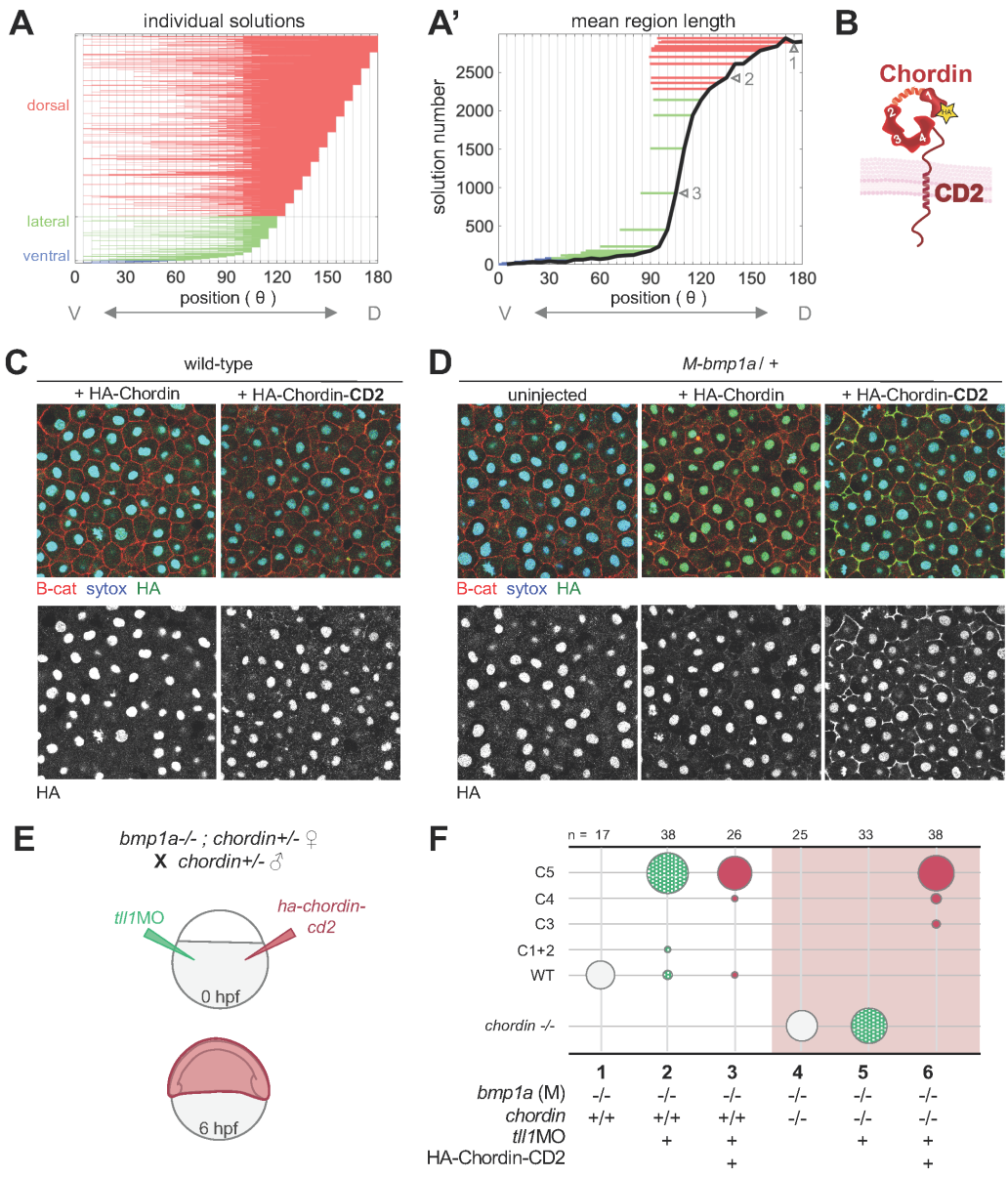

Figure 2.6 Immobile Chordin is a viable modulator of BMP signaling

(**A**) Display of 1/20th of the 40,615 immobile Chordin model screen solutions. Each line represents an individual immobile chordin domain and was sorted along the *y*-axis by its dorsal-most (initiating) position, in 5° intervals: 0-60° was classified as ventral (blue), 61-120° as lateral (green), and 121-180° as dorsal (red). (**A'**) The mean length of all immobile Chordin regions binned in 5° intervals. The number of solutions within each interval is

shown on the *y*-axis and the frequency of solutions is denoted by the solid black line. The gray numbers with arrowheads denote the location of HA-Chordin-CD2 rescuing cells in the embryos from Figure 7D. (**B**) Schematic of our membrane-tethered Chordin construct with N-terminal HA tag. (**C**) Anti-HA immunostaining of wild-type embryos injected at the 1-cell stage with *HA-chordin* or *HA-chordin-cd2* mRNAs. (**D**) Anti-HA immunostaining of M-*bmp1a*^{sa2416}/+ embryos injected at the 1-cell stage with *HA-chordin* or *HA-chordin-cd2* mRNAs. (**E**) Schematic of the cross (*bmp1a*^{t31169}*; chordin/+* female crossed to a *chordin/+* male) and injection conditions (3ng *tll1*MO and 250-800pg *HA-chordin-cd2*) used to generate (**F**). (**F**) Phenotypes of M-*bmp1a*^{t31169} embryos injected in (**E**) separated by *chordin* genotype. Ubiquitous expression of HA-Chordin-CD2 (column 6) resulted in equivalent dorsalization as endogenous Chordin (column 3); n is from 3 replicates. These injections include the controls performed in parallel to the regional injections in **Figure 7C**.

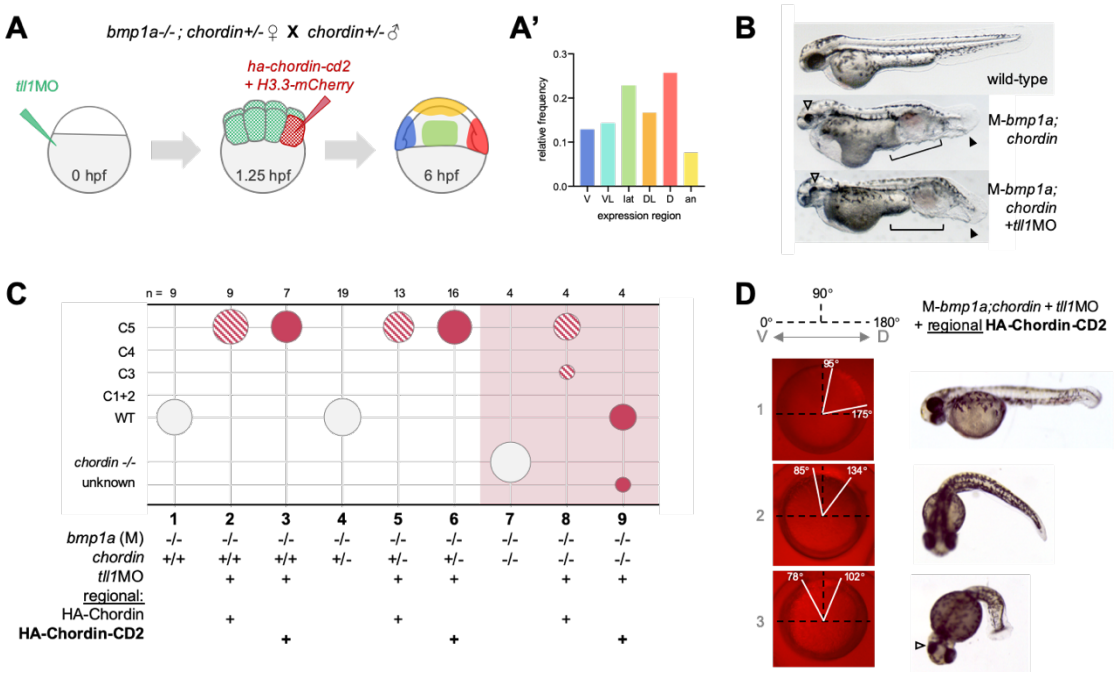

Figure 2.7 Chordin mobility is dispensable for DV patterning *in vivo*

(**A**) Schematic of the cross (*bmp1a*^{t31169}*; chordin/+* female crossed to a *chordin/+* male) and injection conditions (3ng *tll1*MO and 250-500pg *HA-chordin-cd2*) used to generate regional expression of membrane-tethered HA-Chordin-CD2. (**A'**) Relative frequency of expression in each region (n=210 from 5 replicates). V: ventral, VL: ventrolateral, lat: lateral, DL: dorsolateral, D: dorsal, an: animal. VL and DL positions classified as intermediate or overlapping expression of V/lat or D/lat, respectively. (**B**) The *chordin* mutant phenotype is characterized by a reduced eye (open arrowhead), expansion of posterior somites, yolk extension, and blood island (bracket), and duplication of the ventral tail fin (black arrowhead). This is observed in M-*bmp1a*^{t31169};*chordin*-/- siblings with and without the *tll1*MO, quantified in **Figure 6F** at 1 dpf and shown here at 2 dpf. (**C**) Phenotypes of M-*bmp1a*^{t31169} embryos injected in (**A**) separated by *chordin* genotype. Regional expression of HA-Chordin-CD2 (column 9), but not HA-Chordin (column 8), rescued the *chordin* mutant phenotype. Expression regions of HA-Chordin-CD2 shown in (**D**). HA-Chordin was expressed in dorsal, lateral, and ventral regions. Ubiquitous expression controls performed in parallel are shown in **Figures 6F and S7F-G**. (**D**) Regional expression at 6 hpf and 2 dpf phenotypes of the three rescued *chordin* mutants (**C, column 9**). White lines define the size and position of H3.3-mCherry fluorescence marking the HA-Chordin-CD2 expression region. The region for each embryo is also marked in Fig 6A' with gray arrowheads and the respective embryo number. When compared to the un-injected controls described in (**B**), nearly all characteristics of *chordin* mutants have been rescued.

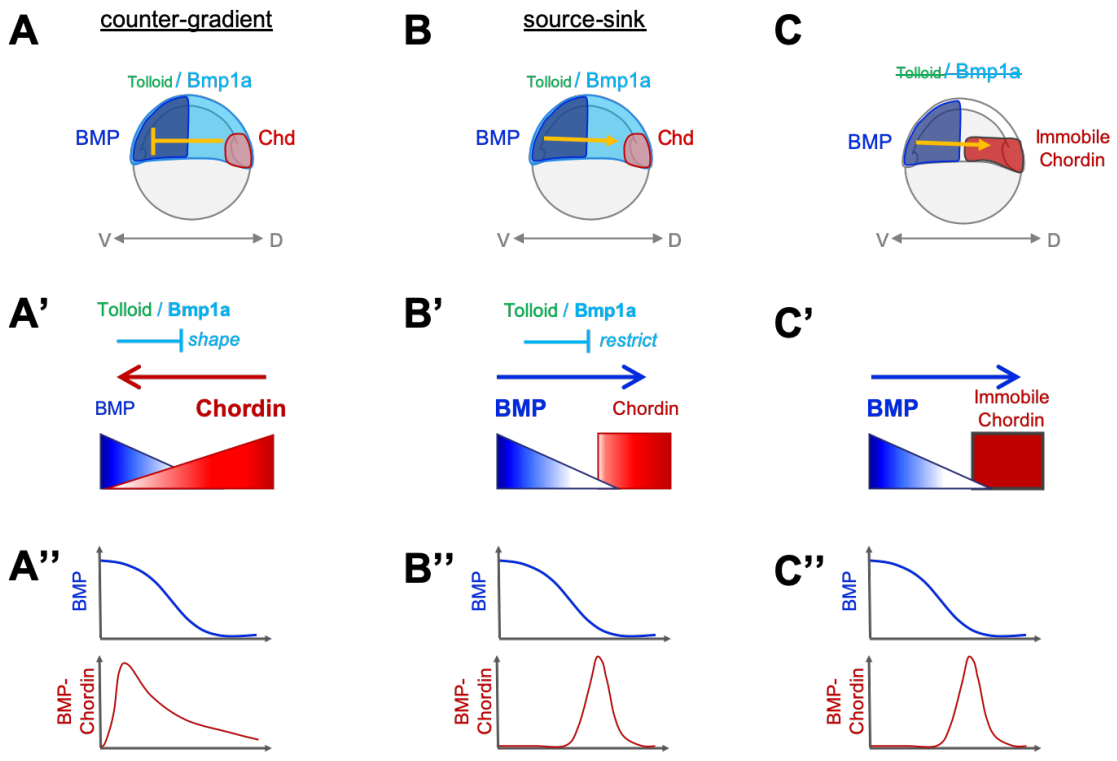

Figure 2.8 Distinguishing mechanisms of BMP gradient formation.

Mechanistic characteristics of the counter-gradient model (**A-A''**), the source-sink (**B-B''**) model, and the membrane-tethered Chordin experiment (**C-C''**). (**A,B,C**) Embryo schematics depicting mRNA expression domains and predominant mechanism of action (yellow lines). (**A',B',C'**) Simplified schematic of BMP and Chordin protein distribution. (**A'**) In the counter-gradient model, Chordin diffuses ventrally (red arrow), resulting in Chordin's range spanning the entire embryo (red triangle) that generates a reciprocal BMP gradient. Tolloid/Bmp1a shape the distribution of embryo-wide Chordin. (**B'**) In the source-sink model, Chordin's range is limited (red rectangle) by Tolloid/Bmp1a, resulting in BMP flux (blue arrow) driving gradient formation. (**C'**) Expression of membrane-immobilized Chordin recapitulates the limited Chordin range and proposed function of Tolloid/Bmp1a in the source-sink model. (**A'',B'',C''**) 1D profiles of free BMP (blue) or BMP bound to Chordin (red). The BMP gradient profile (wild-type) remains the same, but the distribution of BMP-Chordin differs. (**A''**) In the counter-gradient model BMP binds Chordin ventrally, while in (**B'',C''**) the source-sink model and membrane-tethered Chordin experiment, BMP binds Chordin in the dorsal/lateral regions.

Parameter	Units	Symbol	Value	
Time (3.5-5.7hpf)	min	t	130	
Length of Embryo (1D)	μm	–	700	
Length of Chordin Domain (from dorsal)	μm	–	145	
Length of Noggin Domain (from dorsal)	μm	–	78	
Length of Bmp1a Domain	μm	–	700	
Dissociation Constant BMP-Chd	nM	–	1	
Dissociation Constant BMP-Nog	nM	–	0.1	
BMP Diffusivity	$\mu m^2/s$	D_B	4.4	
Chordin Diffusivity	$\mu m^2/s$	D_C	7	
Sizzled Diffusivity	$\mu m^2/s$	D_S	10	
BMP Decay Rate	1/s	dec_B	$8.9 * 10^{-5}$	
Chordin Decay Rate	1/s	dec_C	$9.6 * 10^{-5}$	
			Upper bound	Lower bound
BMP Production Rate	nM/s	$\emptyset_B$	10^{-2}	10^{2}
Chordin Production Rate	nM/s	$\emptyset_C$	10^{-2}	10^{2}
Noggin Production Rate	nM/s	$\emptyset_N$	10^{-2}	10^{2}
Noggin Decay Rate	1/s	dec_N	10^{-5}	10^{-1}
Sizzled Decay Rate	1/s	dec_S	10^{-5}	10^{-1}
Noggin Diffusivity	$\mu m^2/s$	D_N	10^{-2}	10^{2}
BMP-Chordin Diffusivity	$\mu m^2/s$	D_{BC}	10^{-2}	10^{2}
BMP-Noggin Diffusivity	$\mu m^2/s$	D_{BN}	10^{-2}	10^{2}
Binding Rate for BMP and Chordin	1/nM*1/S	k_{onC}	10^{-4}	10^{0}
Unbinding Rate for BMP and Chordin	1/S	k_{offC}	10^{-4}	10^{0}
Binding Rate for BMP and Noggin	1/nM*1/S	k_{onN}	10^{-4}	10^{0}
Unbinding Rate for BMP and Noggin	1/S	k_{offN}	10^{-5}	10^{-1}
BMP-Chordin Degradation by Tolloid	1/s	λ_{tBC}	10^{-4}	10^{0}
Chordin Degradation by Tolloid	1/s	λ_{tC}	10^{-4}	10^{0}
BMP-Chordin Degradation by Bmp1a	1/s	λ_{aBC}	10^{-4}	10^{0}
Chordin Degradation by Bmp1a	1/s	λ_{aC}	10^{-4}	10^{0}
Michaelis Constant of Tolloid	nM	k_{mt}	10^{0}	10^{2}
Michaelis Constant of Bmp1a	nM	k_{ma}	10^{0}	10^{2}
Sizzled Inhibitor Constant with Tolloid	nM	k_{it}	$10^{-1} * S_{max}$	$10 * S_{max}$
Sizzled Inhibitor Constant with Bmp1a	nM	k_{ia}	$10^{-1} * S_{max}$	$10 * S_{max}$

Table 1 Dynamic Bmp1a/Tolloid expression screen parameters

Related to Figures 2.5 and Supplemental 2.6, and Table 2. Model parameters used for the differential Bmp1a/Tolloid expression condition screens. Fixed parameters at indicated value. Varied parameters between indicated upper and lower bounds. Results in **Table 2**.

	Tolloid Distribution		Tolloid Onset		Bmp1a Dynamics		# of solutions (out of 100,000) fit to:							
	uniform	gradient	3.5 hpf	5.3 hpf	decrease	constant	wt	*tolloid* wt	M-*bmp1a* wt	M-*bmp1a;tolloid* wt	*tolloid* M-*bmp1a* M-*bmp1a;tolloid* wt	*chordin* wt	*sizzled* wt	*noggin* wt
1	X		X		X		12,647	9,431	45	538	12	6,165	8,097	8,852
2		X	X			X	12,926	9,920	67	592	20	6,401	8,096	9,115
3	X		X			X	10,851	7,725	57	890	18	5,147	9,606	7,040
4	X			X		X	12,782	10,445	127	447	30	6,215	8,424	8,997
5	X			X	X		12,869	10,543	87	287	14	6,286	8,780	9,143
6		X		X		X	12,855	10,507	123	449	33	6,299	8,527	9,087

Table 2 Number of solutions for dynamic Bmp1a/Tolloid expression screens

Related to Figures 2.5 and Supplemental 2.6, and Table 1. Six groups of indicated differential Bmp1a/Tolloid expression conditions and the corresponding number of solutions (out of 100,000 simulations each) fit to the indicated P-Smad5 profiles (NRMSD<0.12). Parameter input in **Table 1** and number of solutions that fit wild-type, *tolloid*, M-*bmp1a*, and M-*bmp1a;tolloid* P-Smad5 profiles is plotted in **Supplemental Figure 2.5F**.

Parameter	Units	Symbol	Value	
Time (3.5-5.7hpf)	min	t	130	
Length of Embryo (1D)	μm	–	700	
Length of Chordin Domain (from dorsal)	μm	–	145	
Length of Noggin Domain (from dorsal)	μm	–	78	
Length of Bmp1a Domain	μm	–	700	
Dissociation Constant BMP-Chd	nM	–	1	
Dissociation Constant BMP-Nog	nM	–	0.1	
BMP Diffusivity	$\mu m^2/s$	D_B	4.4	
Chordin Diffusivity	$\mu m^2/s$	D_C	7	
Sizzled Diffusivity	$\mu m^2/s$	D_S	10	
BMP Decay Rate	1/s	dec_B	$8.9 * 10^{-5}$	
Chordin Decay Rate	1/s	dec_C	$9.6 * 10^{-5}$	
			Upper bound	Lower bound
BMP Production Rate	nM/s	$\emptyset_B$	10^{-2}	10^{2}
Chordin Production Rate	nM/s	$\emptyset_C$	10^{-2}	10^{2}
Noggin Production Rate	nM/s	$\emptyset_N$	10^{-2}	10^{2}
Noggin Decay Rate	1/s	dec_N	10^{-5}	10^{-1}
Sizzled Decay Rate	1/s	dec_S	10^{-5}	10^{-1}
BMP-Chordin Decay Rate	1/s	dec_{BC}	10^{-5}	10^{-3}
BMP-Noggin Decay Rate	1/s	dec_{BN}	10^{-5}	10^{-3}
Noggin Diffusivity	$\mu m^2/s$	D_N	10^{-2}	10^{2}
BMP-Chordin Diffusivity	$\mu m^2/s$	D_{BC}	10^{-2}	10^{2}
BMP-Noggin Diffusivity	$\mu m^2/s$	D_{BN}	10^{-2}	10^{2}
Binding Rate for BMP and Chordin	1/nM*1/S	k_{onC}	10^{-4}	10^{0}
Unbinding Rate for BMP and Chordin	1/S	k_{offC}	10^{-4}	10^{0}
Binding Rate for BMP and Noggin	1/nM*1/S	k_{onN}	10^{-4}	10^{0}
Unbinding Rate for BMP and Noggin	1/S	k_{offN}	10^{-5}	10^{-1}
BMP-Chordin Degradation by Tolloid	1/s	λ_{tBC}	10^{-4}	10^{0}
Chordin Degradation by Tolloid	1/s	λ_{tC}	10^{-4}	10^{0}
BMP-Chordin Degradation by Bmp1a	1/s	λ_{aBC}	10^{-4}	10^{0}
Chordin Degradation by Bmp1a	1/s	λ_{aC}	10^{-4}	10^{0}
Michaelis Constant of Tolloid	nM	k_{mt}	10^{0}	10^{2}
Michaelis Constant of Bmp1a	nM	k_{ma}	10^{0}	10^{2}
Sizzled Inhibitor Constant with Tolloid	nM	k_{it}	$10^{-1} * S_{max}$	$10 * S_{max}$
Sizzled Inhibitor Constant with Bmp1a	nM	k_{ia}	$10^{-1} * S_{max}$	$10 * S_{max}$

Table 3 Initial parameter conditions for large-scale screen with model

Related to Figure 2.5 and Table 6. Starting model parameters for 1 million simulations of BMP gradient formation. Fixed parameters at indicated value. Varied parameters between indicated upper and lower bounds. Results in **Table 6**.

Parameter	Units	Symbol	Value	
Time (3.5-5.7hpf)	min	t	130	
Length of Embryo (1D)	μm	–	700	
Length of Chordin Domain (from dorsal)	μm	–	145	
Length of Noggin Domain (from dorsal)	μm	–	78	
Length of Bmp1a Domain	μm	–	700	
Dissociation Constant BMP-Chd	nM	–	1	
Dissociation Constant BMP-Nog	nM	–	0.1	
BMP Diffusivity	$\mu m^2/s$	D_B	4.4	
Sizzled Diffusivity	$\mu m^2/s$	D_S	10	
BMP Decay Rate	1/s	dec_B	$8.9 * 10^{-5}$	
Chordin Decay Rate	1/s	dec_C	$9.6 * 10^{-5}$	
			Upper bound	Lower bound
BMP Production Rate	nM/s	$\emptyset_B$	10^{-2}	10^2
Chordin Production Rate	nM/s	$\emptyset_C$	10^{-2}	10^2
Noggin Production Rate	nM/s	$\emptyset_N$	10^{-2}	10^2
Noggin Decay Rate	1/s	dec_N	10^{-5}	10^{-1}
Sizzled Decay Rate	1/s	dec_S	10^{-5}	10^{-1}
BMP-Chordin Decay Rate	1/s	dec_{BC}	10^{-5}	10^{-3}
BMP-Noggin Decay Rate	1/s	dec_{BN}	10^{-5}	10^{-3}
Chordin Diffusivity	$\boldsymbol{\mu m^2/s}$	$\boldsymbol{D_C}$	$\mathbf{0.5 * 10^0}$	$\mathbf{0.5 * 10^2}$
Noggin Diffusivity	$\mu m^2/s$	D_N	10^{-2}	10^2
BMP-Chordin Diffusivity	$\mu m^2/s$	D_{BC}	10^{-2}	10^2
BMP-Noggin Diffusivity	$\mu m^2/s$	D_{BN}	10^{-2}	10^2
Binding Rate for BMP and Chordin	1/nM*1/S	k_{onC}	10^{-4}	10^0
Unbinding Rate for BMP and Chordin	1/S	k_{offC}	10^{-4}	10^0
Binding Rate for BMP and Noggin	1/nM*1/S	k_{onN}	10^{-4}	10^0
Unbinding Rate for BMP and Noggin	1/S	k_{offN}	10^{-5}	10^{-1}
BMP-Chordin Degradation by Tolloid	1/s	λ_{tBC}	10^{-4}	10^0
Chordin Degradation by Tolloid	1/s	λ_{tC}	10^{-4}	10^0
BMP-Chordin Degradation by Bmp1a	1/s	λ_{aBC}	10^{-4}	10^0
Chordin Degradation by Bmp1a	1/s	λ_{aC}	10^{-4}	10^0
Michaelis Constant of Tolloid	nM	k_{mt}	10^0	10^2
Michaelis Constant of Bmp1a	nM	k_{ma}	10^0	10^2
Sizzled Inhibitor Constant with Tolloid	nM	k_{it}	$10^{-1} * S_{max}$	$10 * S_{max}$
Sizzled Inhibitor Constant with Bmp1a	nM	k_{ia}	$10^{-1} * S_{max}$	$10 * S_{max}$

Table 4 Model optimization I - varied Chordin diffusion

Related to Figure 2.5 and Table 6. Change from initial conditions (**Table 3**) is indicated with bold text: Chordin diffusion (D_C) was varied up to 50 $\mu m^2/s$ instead of being fixed at 7 $\mu m^2/s$, the published effective Chordin diffusion rate (Pomreinke et al., 2017). Results in **Table 6**.

Parameter	Units	Symbol	Value	
Time (3.5-5.7hpf)	min	t	130	
Length of Embryo (1D)	μm	–	700	
Length of Chordin Domain (from dorsal)	μm	–	145	
Length of Noggin Domain (from dorsal)	μm	–	78	
Length of Bmp1a Domain	μm	–	700	
Dissociation Constant BMP-Chd	nM	–	1	
Dissociation Constant BMP-Nog	nM	–	0.1	
BMP Diffusivity	$\mu m^2/s$	D_B	4.4	
Sizzled Diffusivity	$\mu m^2/s$	D_S	10	
BMP Decay Rate	1/s	dec_B	$8.9 * 10^{-5}$	
Chordin Decay Rate	1/s	dec_C	$9.6 * 10^{-5}$	
BMP Production < Chordin Production Rate	**nM/s**	$\emptyset_B, \emptyset_C$	–	
			Upper bound	Lower bound
BMP Production Rate	**nM/s**	$\emptyset_B$	$\mathbf{10^{-2}}$	$\mathbf{10^{0}}$
Chordin Production Rate	**nM/s**	$\emptyset_C$	$\mathbf{10^{-1}}$	$\mathbf{10^{1}}$
Noggin Production Rate	nM/s	$\emptyset_N$	10^{-2}	10^{2}
Noggin Decay Rate	1/s	dec_N	10^{-5}	10^{-1}
Sizzled Decay Rate	1/s	dec_S	10^{-5}	10^{-1}
BMP-Chordin Decay Rate	1/s	dec_{BC}	10^{-5}	10^{-3}
BMP-Noggin Decay Rate	1/s	dec_{BN}	10^{-5}	10^{-3}
Chordin Diffusivity	$\boldsymbol{\mu m^2/s}$	$\boldsymbol{D_C}$	$\mathbf{0.5 * 10^{0}}$	$\mathbf{0.5 * 10^{2}}$
Noggin Diffusivity	$\mu m^2/s$	D_N	10^{-2}	10^{2}
BMP-Chordin Diffusivity	$\mu m^2/s$	D_{BC}	10^{-2}	10^{2}
BMP-Noggin Diffusivity	$\mu m^2/s$	D_{BN}	10^{-2}	10^{2}
Binding Rate for BMP and Chordin	1/nM*1/S	k_{onC}	10^{-4}	10^{0}
Unbinding Rate for BMP and Chordin	1/S	k_{offC}	10^{-4}	10^{0}
Binding Rate for BMP and Noggin	1/nM*1/S	k_{onN}	10^{-4}	10^{0}
Unbinding Rate for BMP and Noggin	1/S	k_{offN}	10^{-5}	10^{-1}
BMP-Chordin Degradation by Tolloid	1/s	λ_{tBC}	10^{-4}	10^{0}
Chordin Degradation by Tolloid	1/s	λ_{tC}	10^{-4}	10^{0}
BMP-Chordin Degradation by Bmp1a	1/s	λ_{aBC}	10^{-4}	10^{0}
Chordin Degradation by Bmp1a	1/s	λ_{aC}	10^{-4}	10^{0}
Michaelis Constant of Tolloid	nM	k_{mt}	10^{0}	10^{2}
Michaelis Constant of Bmp1a	nM	k_{ma}	10^{0}	10^{2}
Sizzled Inhibitor Constant with Tolloid	nM	k_{it}	$10^{-1} * S_{max}$	$10 * S_{max}$
Sizzled Inhibitor Constant with Bmp1a	nM	k_{ia}	$10^{-1} * S_{max}$	$10 * S_{max}$

Table 5 Model optimization II - limiting BMP and Chordin production

Related to Figure 2.5 and Table 6. Changes from initial conditions (**Table 3**) are indicated with bold text: Chordin diffusion (D_C) was varied up to 50 $\mu m^2/s$ instead of being fixed at 7 $\mu m^2/s$, the published effective Chordin diffusion rate (Pomreinke et al., 2017). The bounds for BMP (ϕ_B) and Chordin (ϕ_C) production rates were decreased from 10^{-2}–10^{2} nM/s to 10^{-2}–10^{0} and 10^{-1}–10^{1}, respectively. BMP production was also constrained to be less than Chordin production. Results in **Table 6**.

Supp. Table	Chordin Diffusivity (Dc, um2/s)	BMP Production ($\emptyset_B$, nM/s)	Chordin Production ($\emptyset_C$, nM/s)	Relative Production Restraints	# of solutions (out of 1,000,000) fit to:							
					wt	*tolloid* wt	M-*bmp1a* wt	M-*bmp1a;tolloid* wt	*tolloid* M-*bmp1a* M-*bmp1a;tolloid* wt	*chordin* wt	*sizzled* wt	**All**
3	7	0.01 - 100	0.01 - 100	–	126908	98904	101	587	6	82174	84447	0
4	0.5 – 50	0.01 - 100	0.01 - 100	–	162826	113975	424	1508	25	84408	90945	1
5	0.5 – 50	0.01 - 1	0.1 - 10	$\emptyset_B < \emptyset_C$	200416	129605	860	3457	77	78574	174321	16

Table 6 Number of solutions for initial and optimized models

Related to Figure 2.5 and Tables 3-5. The corresponding number of solutions (out of 1 million simulations each) for the model parameters listed in **Tables 3-5** fit to the indicated P-Smad5 profiles (NRMSD<0.11 for wt, *tolloid*, *chordin*, and *sizzled*; <0.06 for M-*bmp1a* and M-*bmp1a;tolloid*).

Parameter	Units	Symbol	Value	
Time (3.5-5.7hpf)	min	t	130	
Length of Embryo (1D)	μm	–	700	
Length of Noggin Domain (from dorsal)	μm	–	78	
Length of Bmp1a Domain	μm	–	700	
Dissociation Constant BMP-Chd	nM	–	1	
Dissociation Constant BMP-Nog	nM	–	0.1	
BMP Diffusivity	$\mu m^2/s$	D_B	4.4	
Chordin Diffusivity	$\boldsymbol{\mu m^2/s}$	$\boldsymbol{D_C}$	**0**	
Sizzled Diffusivity	$\mu m^2/s$	D_S	10	
BMP Decay Rate	1/s	dec_B	$8.9 * 10^{-5}$	
Chordin Decay Rate	1/s	dec_C	$9.6 * 10^{-5}$	
BMP-Chordin Degradation by Tolloid	**1/s**	$\boldsymbol{\lambda_{tBC}}$	**0**	
Chordin Degradation by Tolloid	**1/s**	$\boldsymbol{\lambda_{tC}}$	**0**	
BMP-Chordin Degradation by Bmp1a	**1/s**	$\boldsymbol{\lambda_{aBC}}$	**0**	
Chordin Degradation by Bmp1a	**1/s**	$\boldsymbol{\lambda_{aC}}$	**0**	
			Upper bound	Lower bound
Start of Chordin Domain (from dorsal)	$\boldsymbol{\mu m}$	–	**0**	**700**
End of Chordin Domain (from dorsal)	$\boldsymbol{\mu m}$	–	**0**	**700**
BMP Production Rate	nM/s	$\emptyset_B$	10^{-2}	10^2
Chordin Production Rate	nM/s	$\emptyset_C$	10^{-2}	10^2
Noggin Production Rate	nM/s	$\emptyset_N$	10^{-2}	10^2
Noggin Decay Rate	1/s	dec_N	10^{-5}	10^{-1}
Sizzled Decay Rate	1/s	dec_S	10^{-5}	10^{-1}
Noggin Diffusivity	$\mu m^2/s$	D_N	10^{-2}	10^2
BMP-Chordin Diffusivity	$\mu m^2/s$	D_{BC}	10^{-2}	10^2
BMP-Noggin Diffusivity	$\mu m^2/s$	D_{BN}	10^{-2}	10^2
Binding Rate for BMP and Chordin	1/nM*1/S	k_{onC}	10^{-4}	10^0
Unbinding Rate for BMP and Chordin	1/S	k_{offC}	10^{-4}	10^0
Binding Rate for BMP and Noggin	1/nM*1/S	k_{onN}	10^{-4}	10^0
Unbinding Rate for BMP and Noggin	1/S	k_{offN}	10^{-5}	10^{-1}
Michaelis Constant of Tolloid	nM	k_{mt}	10^0	10^2
Michaelis Constant of Bmp1a	nM	k_{ma}	10^0	10^2
Sizzled Inhibitor Constant with Tolloid	nM	k_{it}	$10^{-1} * S_{max}$	$10 * S_{max}$
Sizzled Inhibitor Constant with Bmp1a	nM	k_{ia}	$10^{-1} * S_{max}$	$10 * S_{max}$

Table 7 Immobile Chordin screen

Related to Figure 2.6. Changes from initial conditions (**Table 3**) are indicated with bold text: Chordin diffusion (D_C) was set to 0 to model immobile, non-diffusing Chordin. λ_t and λ_a were set to 0 to model a M-*bmp1a;tolloid* mutant background. The initial and final positions of the immobile Chordin domain varied by 5-degree intervals from 0-700μm. Results (NRMSD<0.08) in **Figure 2.6A-A'**.

CHAPTER 3. Tolloid and Sizzled distinctly shape the BMP morphogen gradient during gastrulation

Contributions: This chapter contains figures and direct quotes from a manuscript being prepared by Tuazon and Mullins.

Summary

A fundamental question in developmental biology is how morphogens, such as Bone Morphogenetic Protein (BMP), form precise signaling gradients to impart positional and functional identity to the cells of the early embryo. Though embryonic patterning spans the process of gastrulation, whereby dramatic cell movements rapidly reorganize the embryo, it remains unknown how the BMP gradient accounts for gastrulation cell movements to faithfully specify DV tissues over time. We performed quantitative immunofluorescence and determined that the wild-type BMP signaling gradient changes shape, steepening, by the end of gastrulation. We discovered that Tolloid and Sizzled, extracellular regulators of the BMP antagonist Chordin, play distinct spatiotemporal roles in shaping the BMP gradient during gastrulation: they act at different stages and impact different aspects of the steepening BMP gradient. These results suggest that gastrulation represents a new signaling environment, distinct from when the BMP signaling gradient is established, that requires additional regulation by Tolloid and Sizzled. Thus, Tolloid and Sizzled are key to correctly shaping a steeper BMP morphogen gradient to properly pattern the tail.

3.1 Introduction

As detailed in Sections 1.4 and 1.5, the BMP morphogen gradient must be tightly regulated in space and time to correctly pattern all DV tissues. Briefly, DV tissues are progressively patterned from anterior to posterior throughout gastrulation (Hashiguchi and Mullins, 2013; Tucker et al., 2008) **(Figure 3.1A-B)**. This means that the BMP signaling gradient must maintain a correct shape during the dynamic cell rearrangements of gastrulation to properly pattern all tissues, from head to tail. Additionally, during gastrulation epiboly movements rapidly bring the ventral- and dorsal-most cells, which

have opposite levels of BMP signaling, in increasingly close proximity until they eventually directly abut **(Figure 3.1C)**. Given these morphogenetic changes, it was unknown whether the BMP morphogen gradient maintained the same shape during gastrulation or if it adapted a new shape in its changing environment. Furthermore, the roles of the various extracellular BMP regulators in maintaining or reshaping the gradient during gastrulation is not known.

3.2 Results

3.2.1 Establishing a reliable staging method based on relative nuclei density

Understanding how the BMP signaling gradient is regulated over time relies first on being able to clearly distinguish distinct developmental stages. Previous staging methods relied either solely on time, measured in hours post fertilization (hpf) (Kimmel et al., 1995; Zinski et al., 2017; Zinski et al., 2019), or percent epiboly, the extent to which the blastoderm covers the yolk cell, which can be difficult to precisely ascertain (Kimmel et al., 1995). Moreover, differences in temperature can affect the speed of development (Kimmel et al., 1995) and injection of translation-blocking morpholinos can cause a developmental delay. Since the BMP signaling gradient is highly dynamic (Zinski et al., 2017), any variability in staging could impact our quantitation of BMP gradient shape. To conduct a precise time-course of the wild-type BMP signaling gradient, and to characterize mutant and/or morpholino-mediated loss of function phenotypes over time, we developed a methodology that differentiates key stages of development by relative nuclei density **(Figure 3.2)**.

Our approach utilizes quantitative immunofluorescence of individual nuclei, which were stained by Sytox dye simultaneously with P-Smad5 immunostaining (Section 6.4.1). Close attention was paid to limit variability in the timing of developmental progression. First, parent fish remained separated overnight and, after being mixed in the morning, were only allowed to mate for 10 minutes after the first eggs dropped. Embryos were then promptly sorted into no more than 30 embryos per petri dish and multiple incubators (31°C and 28°C) utilized to ensure that the morphological stage and percent epiboly matched the hours-post-fertilization stage (Kimmel et al., 1995) prior to fixation. Second, embryos were immunostained, imaged, segmented, and registered, as previously described (Zinski et al., 2017; Zinski et al., 2019) (summarized in Section 6.4). Finally, all nuclei were projected on a sphere divided into 4800 equilateral triangles and nuclei within each triangle averaged together. Though this approach was used to generate the 3-D embryo-wide displays of mean P-Smad5 (with the P-Smad5 intensity of each nuclei within a triangle averaged together), it was similarly applied to visualize relative nuclei density (with the proportion of nuclei within each triangle relative to total number of nuclei in the embryo calculated), depicted as a heatmap **(Figure 3.2)**.

Importantly, we found that we could clearly distinguish developmental stages that were 25-35 minutes apart **(Figure 3.2)**. Embryos at 50% epiboly, or 5.3 hpf, were defined by their highest nuclei density being at the animal pole, consistent with the start of the blastoderm spreading vegetally **(Figure 3.2A,E,I)**. Embryos at germ stage, or 5.7 hpf, displayed their highest nuclei density in a clear ring around the margin, consistent with the onset of gastrulation **(Figure 3.2B,F,J)**. Embryos at shield stage, or 6.3 hpf, had their highest nuclei density localized in a circle dorsally, indicative of involution, and a broader band of high cell density at the margin as gastrulation proceeds **(Figure 3.2C,G,K)**.

Notably, we can clearly distinguish germ stage (5.7 hpf), our readout for BMP gradient formation used in Chapter 2 (Zinski et al., 2017), from 50% epiboly (5.3 hpf) and shield (6.3 hpf) stages, which are only 25-35 minutes apart. Finally, embryos at 65% epiboly, or 7 hpf, were characterized by their lowest nuclei density being ventral-animal and the anterior spreading of the high-nuclear-density dorsal shield **(Figure 3.2D,H,L)**. The anteroposterior height of embryos at each stage also progressively increased, consistent with epiboly **(Figure 3.2I-L)**.

This precise staging method employs qualitative analysis of quantitative imaging data to confirm that each embryo within an imaging dataset is stage matched. It also establishes a staging framework for other studies that gather imaging data with single-cell resolution, such as the visualization of other morphogen gradients, fluorescent *in situ* hybridization (FISH), or single molecule fluorescence *in situ* hybridization (smFISH) and RNAscope, to ensure staging consistency during zebrafish gastrulation.

3.2.2 The shape of the wild-type BMP signaling gradient changes during gastrulation

Prior to the development of the above staging paradigm, we performed quantitative immunofluorescence of nuclear P-Smad5 in wild-type embryos during gastrulation, specifically at 6, 8, 9.5, and 10 hpf. Unfortunately, embryos 8 hpf and older were too large to be imaged in full by the objective we use, but we were able to capture half of the BMP signaling gradient at these stages and the gradient it is presumed to be symmetric at these stages, as it is at earlier stages (Zinski et al., 2017). Beautifully, we observed an embryo-wide P-Smad5 gradient at all stages of gastrulation **(Figure 3.3)**. Since embryo morphology is changing due to dorsal-convergence and other gastrulation movements, we limited our analysis to the margin and vegetal-most region of the embryo **(Figure 3.3B'-**

D'), where peak P-Smad5 levels were observed and DV patterning occurs (Figure 3.1A) (Tucker et al., 2008; Zinski et al., 2017),

Interestingly, we observed that the shape of the BMP signaling gradient changed during gastrulation. Primarily, the distance between cells with the highest P-Smad5 levels and those of lowest P-Smad5 levels decreased dramatically (Figure 3.3A'-D'). This distance was measured in approximate nuclei number. At the onset of gastrulation, this distance was 58 nuclei, or approximately 50% of the total embryo (assuming a nucleus diameter of 6μm and an embryo diameter of 700μm) (Figure 3.3A'). Though this distance decreased modestly to 47 nuclei (41% of total embryo diameter) by mid-gastrulation (Figure 3.3B'), the most dramatic decrease was at late- and the end of gastrulation, when this distance decreased to 24 (21% of total embryo diameter) and 18 nuclei (16% of total embryo diameter), respectively (Figure 3.3C',D'). This decrease in distance between the highest and lowest P-Smad5 intensities reveals a steeper P-Smad5 gradient (Figure 3.3E,F). Essentially, this distance represents all intermediate P-Smad5 levels, or the slope of the gradient. The smaller DV distance that these intermediate levels occupy, the steeper the P-Smad5 slope (Figure 3.3E,F).

3.2.3 Tolloid and Sizzled are required at discrete stages of gastrulation

Considering the steeper P-Smad5 gradient at the end of gastrulation and that the tail is patterned during these stages (Figure 3.1) (Connors et al., 2006; Kanki and Ho, 1997; Tucker et al., 2008), the late BMP signaling gradient may require additional regulators to generate its steeper shape and thus correctly pattern the tail. Interestingly, Tolloid and Sizzled were identified as opposing regulators of tail DV patterning because of their opposite phenotypic effects on the tail (Figure 3.4A,B) (Hammerschmidt et al., 1996a; Mullins et al., 1996). Specifically, *tolloid* mutants display a loss of the ventral tail

fin while *sizzled* mutants display a duplication of the ventral tail fin **(Figure 3.4B)**. Furthermore, not only do cells of highest and lowest BMP signaling levels increase in proximity during gastrulation **(Figure 3.1)**, but the localization of *tolloid*, *sizzled*, *chordin*, and *bmp* also all concentrate in the tailbud **(Figure 3.4D,E)**. Double *in situ* hybridization has shown that *tolloid* directly abuts the *chordin* domain while *bmp4* does not **(Figure 3.4D)** (Connors et al., 1999). Thus, Tolloid and Sizzled may be key to shaping the steeper BMP signaling gradient during gastrulation.

A role for Tolloid and Sizzled in shaping the BMP signaling gradient later during gastrulation, as opposed to establishing it early in gastrulation, is supported by neither mutant displaying a P-Smad5 phenotype at 5.7 hpf **(Figure 3.5)**. Instead, we found that *tolloid* and *sizzled* mutants first display P-Smad5 defects during different stages of gastrulation **(Figures 3.6-3.9)**. While *tolloid* mutants displayed no change at 6.3 hpf **(Figure 3.6)**, *sizzled* mutants had a clear and significant expansion of the marginal P-Smad5 gradient into the lateral regions **(Figure 3.7)**. This phenotype remained consistent whether we analyzed the P-Smad5 gradient shape around the margin or over the top of the embryo **(Figure 3.7C,D)**. However, as we compared the P-Smad5 gradient shape between *sizzled* mutants and wild-type controls at progressively more anterior positions, we saw an additional increase in P-Smad5 levels ventrally and dorsally **(Figure 3.8)**. Thus, while the maximal P-Smad5 level embryo-wide does not change, the relative maximum at more anterior positions in *sizzled* mutants does increase significantly.

Tolloid mutants exhibited a P-Smad5 phenotype by 7 hpf, displaying a significantly reduced gradient **(Figure 3.9)**. Around the margin and over the top of the embryo, the P-Smad5 gradient is lower ventrally and also shallower compared to controls **(Figure 3.9E,F)**. One caveat, though, is that heterozygous siblings were used as controls but their

P-Smad5 gradient at 7 hpf was slightly different from other wild-type controls used in previous experiments **(Figure 2.3 and Supplemental Figure 2.4)**. Namely, the P-Smad5 gradient appears more narrowly confined ventrally, as opposed to being broadly distributed, and there is a dip in P-Smad5 intensity in the anterior **(Figure 3.9F)**, both of which persist in mutants and controls. It is unlikely to be an imaging artifact since it has not been observed before, so this experiment will have to be repeated with in-tube wild-type controls.

3.2.4 Gradient shaping roles of Tolloid and Sizzled persist at the end of gastrulation

After identifying the earliest timepoint when Tolloid and Sizzled shape the BMP signaling gradient (7 hpf and 6.3 hpf, respectively), we analyzed their effects on the steeper gradient apparent at the end of gastrulation **(Figure 3.10)**. Interestingly, though we focused our analysis on the vegetal-most region of the embryos, as we did with the wild-type timecourse **(Figure 3.3)**, we observed changes embryo-wide. We found that their respective P-Smad5 phenotypes persisted at the end of gastrulation (10 hpf). Specifically, that *tolloid* mutants displayed a lower and shallower gradient while *sizzled* mutants displayed a laterally-expanded gradient **(Figure 3.10E,F)**.

Again, we characterized the steepness of each mutant gradient by measuring the approximate distance between the cells of highest and lowest P-Smad5 levels, which was 18 nuclei in wild-type **(Figure 3.10A')**. That distance significantly increased to 50 nuclei in *tolloid* mutants, while it remained similar to wild-type at 16 nuclei in *sizzled* mutants **(Figure 3.10B',C')**. This indicates that the *tolloid* mutant P-Smad5 gradient is shallower than wild-type **(Figure 3.10E)**, suggesting that Tolloid plays a role in maintaining the steepness of the late wild-type BMP signaling gradient. Notably, the distance between the cells of highest and lowest P-Smad5 levels in *tolloid* mutants at the end of gastrulation

(Figure 3.10B') is similar to wild-type embryos at the onset of gastrulation **(Figure 3.3A')**, 50 nuclei compared to 58 nuclei, respectively. This similarity is consistent with a role for Tolloid in steepening the BMP signaling gradient since Tolloid does not play an individual role at the onset of gastrulation **(Figure 3.5A-C)**, when the gradient is broader.

In contrast, though *sizzled* mutants displayed no significant change in the steepness of the P-Smad5 gradient, they instead showed a lateral expansion of the highest P-Smad5 levels **(Figure 3.10F)**. The lateral extent of maximal P-Smad5 levels was characterized as an angle (71° in wild-type) and we observed that, while it moderately decreased in *tolloid* mutants (to 51°), it significantly increased in *sizzled* mutants (to 114°) **(Figure 3.10A'-C')**. This indicates that the *sizzled* mutant P-Smad5 gradient is broader than wild-type **(Figure 3.10F)**, suggesting that Sizzled plays a key role in regulating the extent of the highest BMP signaling levels laterally. Together, this indicates that at the end of gastrulation Tolloid shapes the steepness of the BMP signaling gradient while Sizzled limits the lateral extent of maximum BMP levels.

3.3 Discussion and Future Directions

3.3.1 Additional considerations for quantitative P-Smad5 analysis during gastrulation

Though we clearly observe a change in the P-Smad5 gradient shape during gastrulation, further quantitation would strengthen this observation. First, as previously mentioned, the wild-type timecourse analysis was performed prior to the development of our staging paradigm. Second, it was also performed without utilizing a calibration bead during image acquisition, which controls for variations in laser intensity (Section 6.4.1) (Zinski et al., 2019). Repeating the wild-type timecourse with these considerations would

improve the precision of our measurements. Specifically, it would enable us to reliably determine if the ventral maximum intensity increases in wild-type embryos during gastrulation, which has been observed during blastula and early gastrula stages (4.7 hpf to 6.7 hpf) (Zinski et al., 2017), and compare that in *tolloid* and *sizzled* mutants.

A third aspect of our gastrulation timecourse analysis of wild-type and *tolloid* and *sizzled* mutants that can be improved is that we can only image half of the BMP signaling gradient **(Figures 3.3 and 3.10)**. Due to the shape of late-gastrula embryos, it is not possible to accurately register these halves together for population analyses. To circumvent this difficulty, we have begun preliminary imaging and post-acquisition analysis tests of late gastrula (95-100% epiboly) embryos with their anterior halves removed. Remarkably, fixed embryos are quite resilient and removing the anterior region is possible while maintaining the structural integrity and morphology of the remaining vegetal embryo half. These vegetal 'bottoms' closely resemble early gastrula in size and shape, so it is possible to both image them in full and integrate them into our existing post-acquisition analysis pipeline. This enables population mean analyses as well as analysis in multiple spatial dimensions, including scale invariance (Umulis and Othmer, 2013).

A complimentary approach to imaging these vegetal embryo 'bottoms' is to use Light Sheet Fluorescence Microscopy to capture P-Smad5 intensities across the entire late gastrula embryo. Though we are hesitant to use Light Sheet for quantitation, due to its nonuniform sample illumination, we could still use it to collect qualitative data to answer remaining questions. First, it is unclear whether the number of cells with intermediate P-Smad5 levels (represented by the distance between the highest and lowest signal cells) changes during gastrulation. The steepening of the wild-type gradient could be due to these cells either converging into a narrow band or encountering different BMP signaling

levels and converting to high or low signal cells. As long as we can capture the embryo in full, cell counting based on P-Smad5 intensity thresholds can directly answer this question. Second, *tolloid* and *sizzled* mutants also display mild convergence and extension defects (Connors et al., 1999; Hammerschmidt et al., 1996a; Mullins et al., 1996). Light Sheet Microscopy offers the potential for volumetric and cell density analyses to quantify and contextualize these defects with the BMP signaling gradient.

3.3.2 Tolloid and Sizzled shape distinct aspects of the late BMP signaling gradient

We show that Tolloid and Sizzled play distinct spatiotemporal roles in shaping the BMP signaling gradient. Sizzled is first required by 6.3 hpf to limit maximal BMP signaling laterally, while Tolloid is required by 7 hpf to protect the steepness of the BMP signaling gradient. Interestingly, the earliest changes in DV marker expression in *sizzled* and *tolloid* mutants are not observed until 70% epiboly (7.5 hpf) (Miller-Bertoglio et al., 1999) and 100% epiboly (10 hpf) (Connors et al., 1999), respectively. Higher resolution analysis of gene expression may reveal earlier DV patterning defects, or it is possible that there is a delay in the mutant P-Smad5 gradients causing gene expression changes.

It remains to be determined why Tolloid and Sizzled are first required at distinct developmental time points. However, the *tolloi*d mutant P-Smad5 phenotype emerging at 7 hpf is consistent with our work suggesting that *tolloid* expression reaches functional levels after the onset of gastrulation (Section 2.2.6) **(Figure 2.5A-B, Supplemental Figure 2.5F-H, Table 2)** and that *tolloid* mediates the recovery of the phenotype during gastrulation (Section 2.2.4) **(Figure 2.3 and Supplemental Figure 2.4)**. Future studies can test this mechanism of M-*bmp1a* P-Smad5 recovery by characterizing the P-Smad5 gradient in zygotic *bmp1a;tolloid* double mutants. Sizzled, on the other hand, has been implicated to play an important role in feedback regulation of BMP signaling (Inomata et

al., 2013). Autoregulatory feedback loops (discussed in detail in Section 5.4.1) initiate in the early gastrula at 6.3 hpf, which is the same stage that the *sizzled* P-Smad5 phenotype emerges. Future studies can determine if Sizzled is required at 6.3 hpf because of a role in BMP feedback regulation.

Given that *tolloid* and *sizzled* mutant P-Smad5 phenotypes are consistent from when each is first observed through the end of gastrulation **(Figures 3.7, 3.9, 3.10)**, we postulate that Tolloid and Sizzled play distinct roles in shaping the BMP signaling gradient during gastrulation **(Figure 3.11)**. In this model, at the end of gastrulation a steep BMP gradient is maintained by Tolloid and Chordin directly abutting in the tailbud **(Figure 3.11A)**, recapitulating their mRNA expression domains **(Figure 3.4D)**. Sizzled prevents Tolloid-mediated promotion of BMP signaling in the lateral regions **(Figure 3.11A)**. In *tolloid* mutants, Chordin is unrestricted in the tailbud and aberrantly inhibits BMP, resulting in a shallower and lower BMP signaling gradient **(Figure 3.11B)**. In *sizzled* mutants, the steepness of the gradient is maintained since Tolloid is present to combat Chordin in the tailbud. However, without Sizzled inhibition, Tolloid aberrantly promotes BMP signaling, to its highest levels, in the lateral regions of the embryo **(Figure 3.11C)**.

3.3.3 Examining the mechanism and functional consequences of a steep BMP gradient

Integrating our findings with our model of BMP gradient formation (Chapter 2), it is possible that the steep BMP gradient at the end of gastrulation is generated by a source-sink mechanism, similar to how the BMP gradient is established at the onset of gastrulation **(Figure 2.8)**. In this model, the distance between the source and sink is greatly compressed, resulting in a steeper gradient. We plan to address this through a mathematical model with closer *bmp*, *chordin*, *tolloid* and *sizzled* initial expression domains, as schematized in **Figure 3.4D-E**. Another fascinating question for future studies

is whether a steeper BMP signaling gradient is required to pattern tail tissues. In the steeper gradient characterized here, significantly fewer cells across the DV axis see intermediate levels of BMP signaling **(Figure 3.3)**. Instead, the gradient may become almost binary and switch-like. It remains unknown whether this is a consequence of the margin constricting during epiboly or whether it is required to correctly specify the DV tissues of the tail.

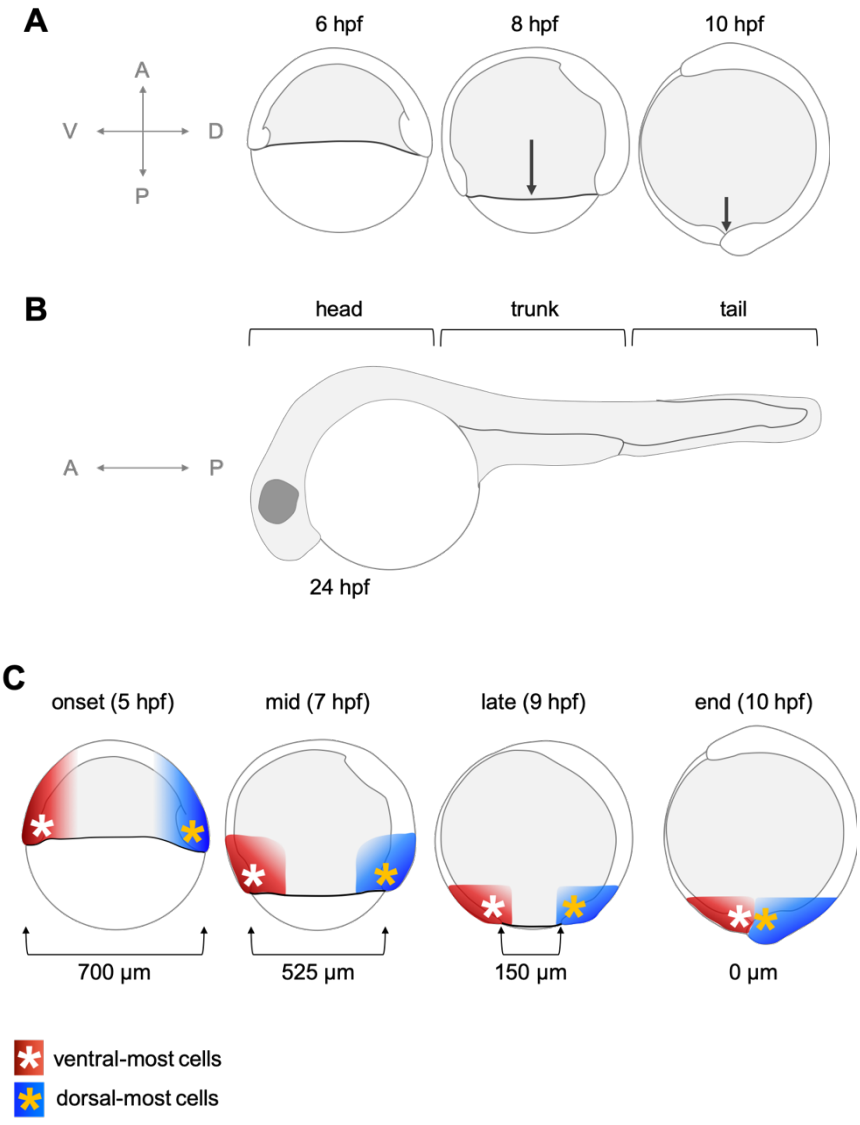

Figure 3.1 Correct DV patterning must account for time

Similar concepts depicted in Figures 1.3 and 1.7. (**A,B**) Schematics depicting the progressive patterning of DV tissues from anterior to posterior during gastrulation. From late blastula to early gastrula stages, the most anterior (head) tissues, are patterned. At mid-gastrula stages, trunk tissues are patterned. From late gastrula to early somitogenesis, the most posterior (tail) tissues are patterned. (**A**) Zebrafish embryos during the stages of DV patterning. As gastrulation proceeds, the region of active patterning progresses posteriorly, indicated by bold line and arrow at the margin. (**B**) Corresponding portion of the body plan represented by the larval zebrafish. (**C**) During gastrulation, there is a dramatic decrease in distance between the ventral- and dorsal-most cells. By the end of epiboly, the ventral- and dorsal-most cells are in direct contact.

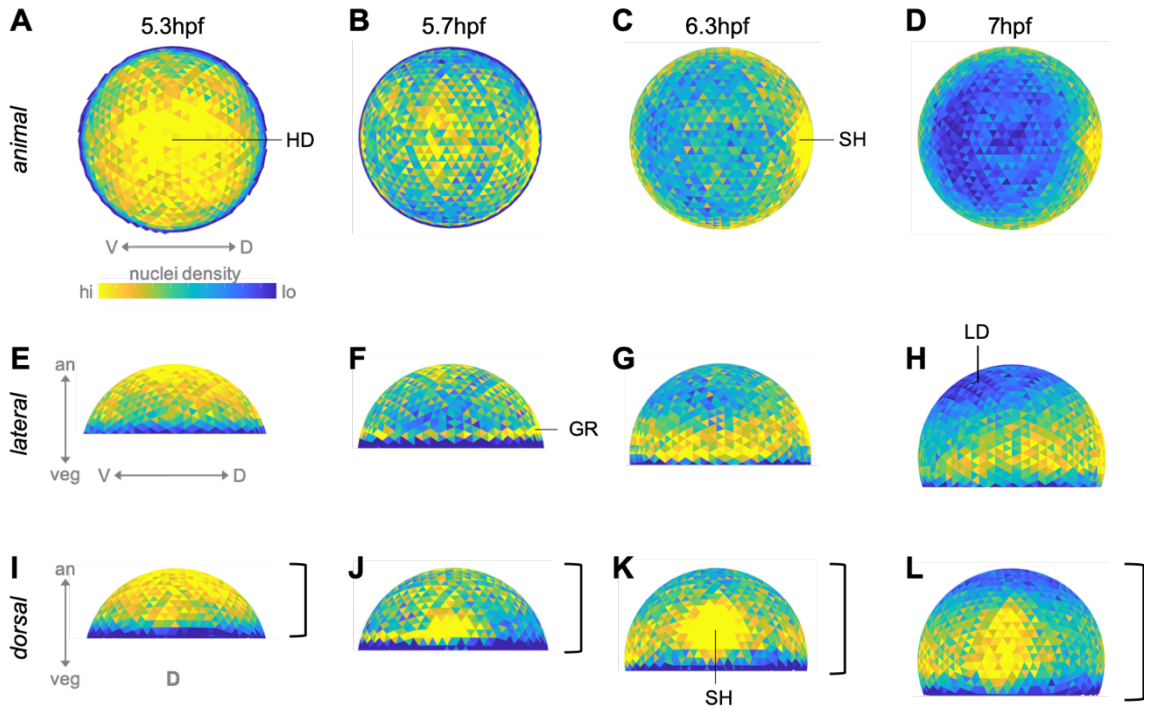

Figure 3.2 Nuclei density reveals distinct morphological features to confirm group staging

(**A-D**) Animal pole, (**E-H**) lateral, and (**I-L**) dorsal views of average nuclei density in sets of wild-type embryos. We confirmed that the nuclei density of each individual embryo matched the qualitative features of the stage being investigated, detailed here, with the ability to distinguish stages that are less than 25 minutes apart. (**A, E , I**) At 5.3 hpf (n=14), or 50% epiboly, the highest density (HD) of nuclei remains at the animal pole as cells of the blastoderm begin epiboly and spread vegetally. (**B, F, J**) At 5.7 hpf (n=14), or germ stage, there is a high concentration of nuclei at the margin, demarcating the stage's characteristic germ ring (GR) and thickening at the margin as gastrulation begins. (**C, G, K**) At 6.3 hpf (n=8), or shield stage, the highest concentration of nuclei is dorsal, indicates the presence of the dorsal shield (SH), and spread along the margin as gastrulation and involution proceeds. (**D, H, L**) At 7 hpf (n=11), or 65% epiboly, the highest density of nuclei remains at the dorsal shield, thought it has spread animally (**L**). There is an emergent low density (LD) region of nuclei that is ventral animal due to dorsal convergence. (**I-L**) From 5.3-7 hpf, there is also a progressive increase in animal-vegetal height of the embryo (brackets).

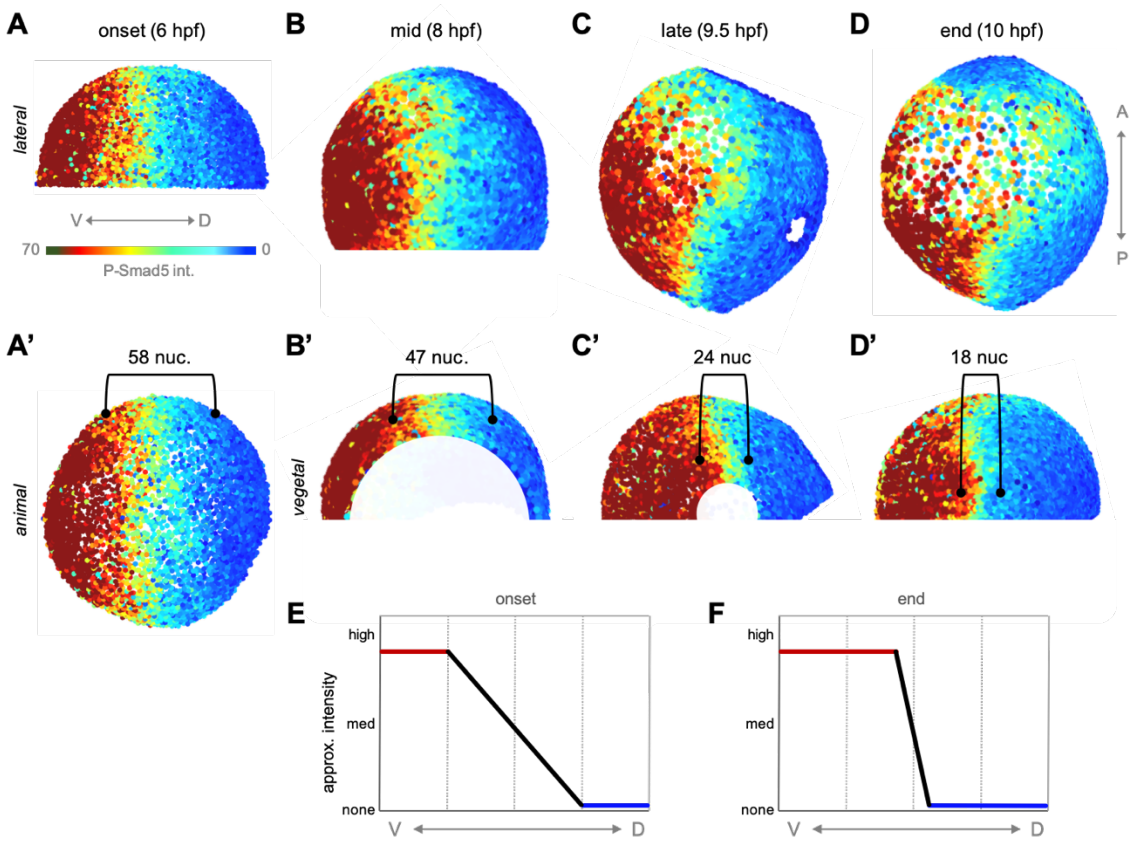

Figure 3.3 Steepening of the wild-type P-Smad5 gradient during gastrulation

(**A-D**) Lateral, (**A'**) animal, and (**B'-D'**) vegetal views of P-Smad5 intensities of individual wild-type embryos at indicated stages. (**A'-D'**) Mean distance, in approximate nuclei diameters, between the highest and lowest P-Smad5 levels of multiple embryos at each stage: (**A'**) 6.3 hpf (n = 7), (**B'**) 8 hpf (n = 4), (**C'**) 9.5 hpf (n = 7), (**D'**) 10 hpf (n = 8). (**E,F**) Schematics of the approximate P-Smad5 gradient shape at the onset © and end (**F**) of gastrulation. Red and blue lines represent the highest and lowest levels of P-Smad5 respectively. Black lines represent the intermediate levels of P-Smad5. By the end of gastrulation, intermediate P-Smad5 levels extend across a significantly shorter distance along the DV axis, with a concomitant expansion of the domains of highest and lowest P-Smad5 levels (compare **F** to **E**), indicating a steepening of the P-Smad5 gradient.

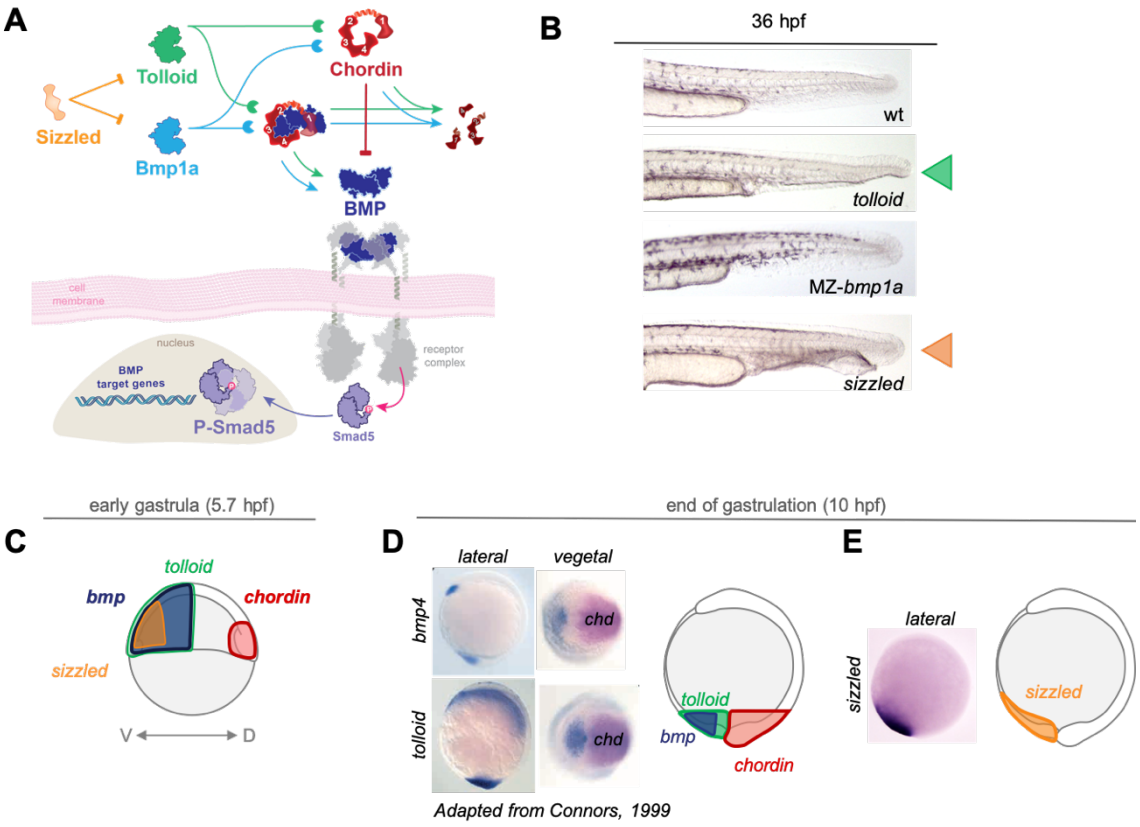

Figure 3.4 Tolloid and Sizzled likely play a key role in regulating BMP signaling during tail patterning

(**A**) Schematic of the extracellular BMP regulators explored in this section, adapted from (Dutko and Mullins, 2011), and also shown in **Figures 1.1 and 2.1**. (**B**) 36 hpf tail phenotypes of wild-type and *tolloid*, *sizzled*, and MZ-*bmp1a*^{t31169} mutants. Open arrow: loss of ventral tail fin in *tolloid* mutants. Solid arrow: duplication of ventral tail fin in *sizzled* mutants. (**C-E**) Published mRNA expression domains in the (**C**) early gastrula (6.3 hpf) and at (**D-E**) the end of gastrulation (10 hpf).

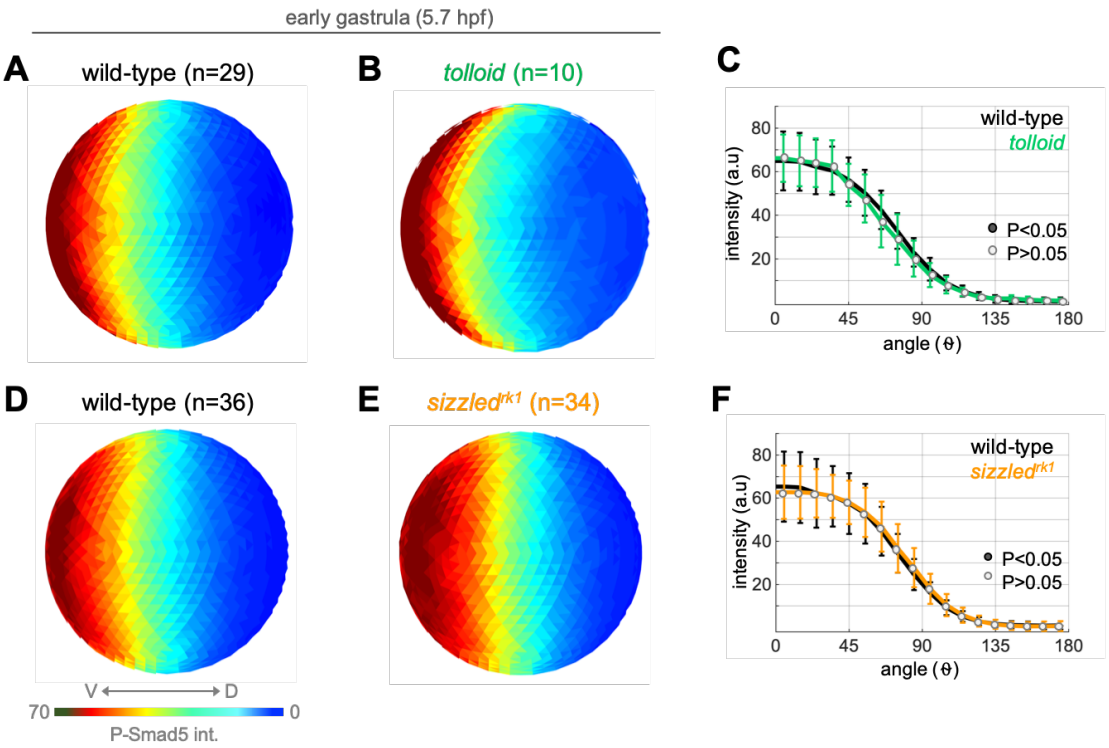

Figure 3.5 *tolloid* and *sizzled* mutants display no P-Smad5 defects at 5.7 hpf

Re-print of panels from Figures 2.2.2 and 2.2.4. (**A,B,D,E**) Animal view of mean P-Smad5 intensities at early gastrula stage (5.7 hpf) in: (**A**) wild-type controls (n=29) for (**B**) *tolloid* mutants (n=10, 3 replicates), (**D**) wild-type controls (n=36) for © *sizzled*^{rk1} mutants (n=34 from 3 replicates). (**C,F)** Average marginal P-Smad5 intensities of **A,B,D,E**. Wild-type controls are shown in black. Error bars indicate standard deviation. Filled circles indicate a significant (P<0.05) difference at each position compared to wild-type, unless a bracket indicates another comparison.

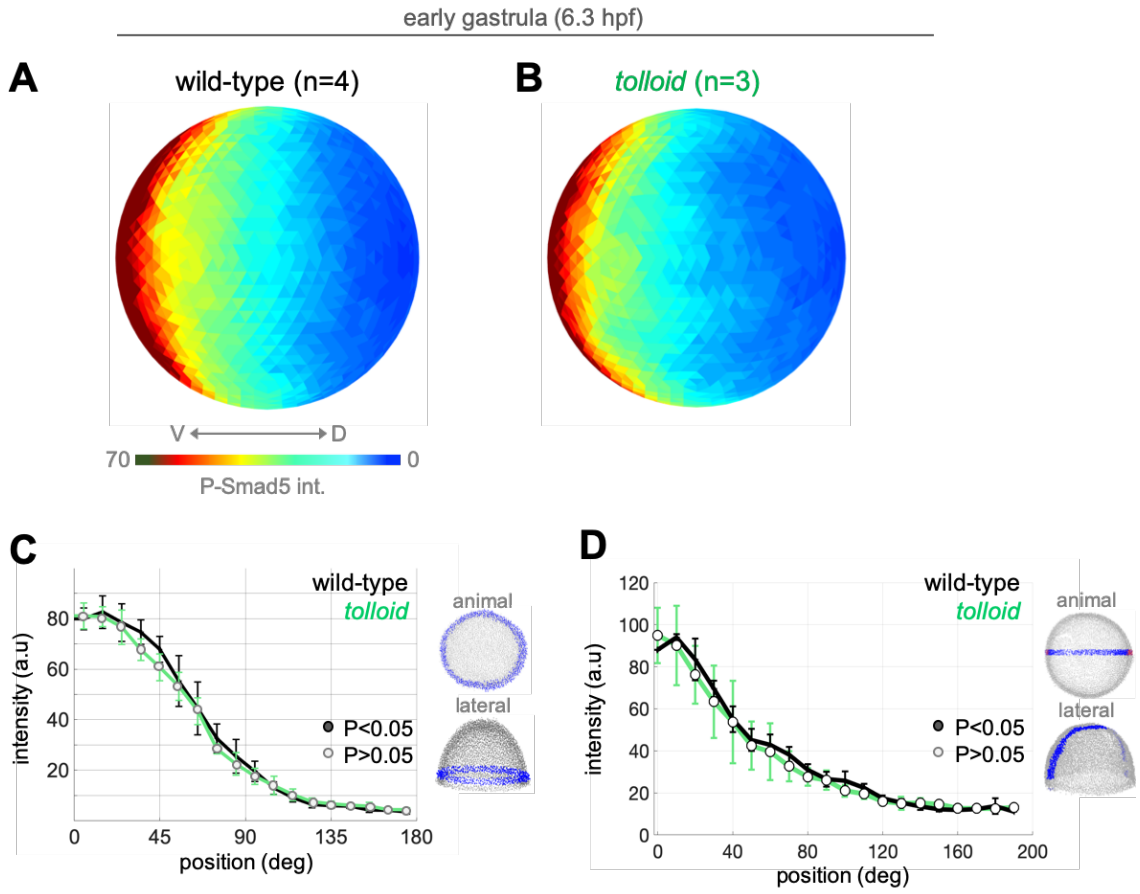

Figure 3.6 *tolloid* mutants display no P-Smad5 defects at 6.3 hpf

(**A,B**) Animal view of mean P-Smad5 intensities at gastrula stage (6.3 hpf) in: (**A**) wild-type controls for (**B**) *tolloid* mutants. (**C,D**) Average P-Smad5 intensities of a 30μm band of cells in **A,B**. Wild-type controls are shown in black. Error bars indicate standard deviation. Filled circles indicate a significant (P<0.05) difference at each position compared to wild-type. (**C**) Marginal mean P-Smad5 intensities, cell location indicated in blue on the right. (**D**) Mean P-Smad5 intensities over the top of the embryo, cell location indicated in blue on the right.

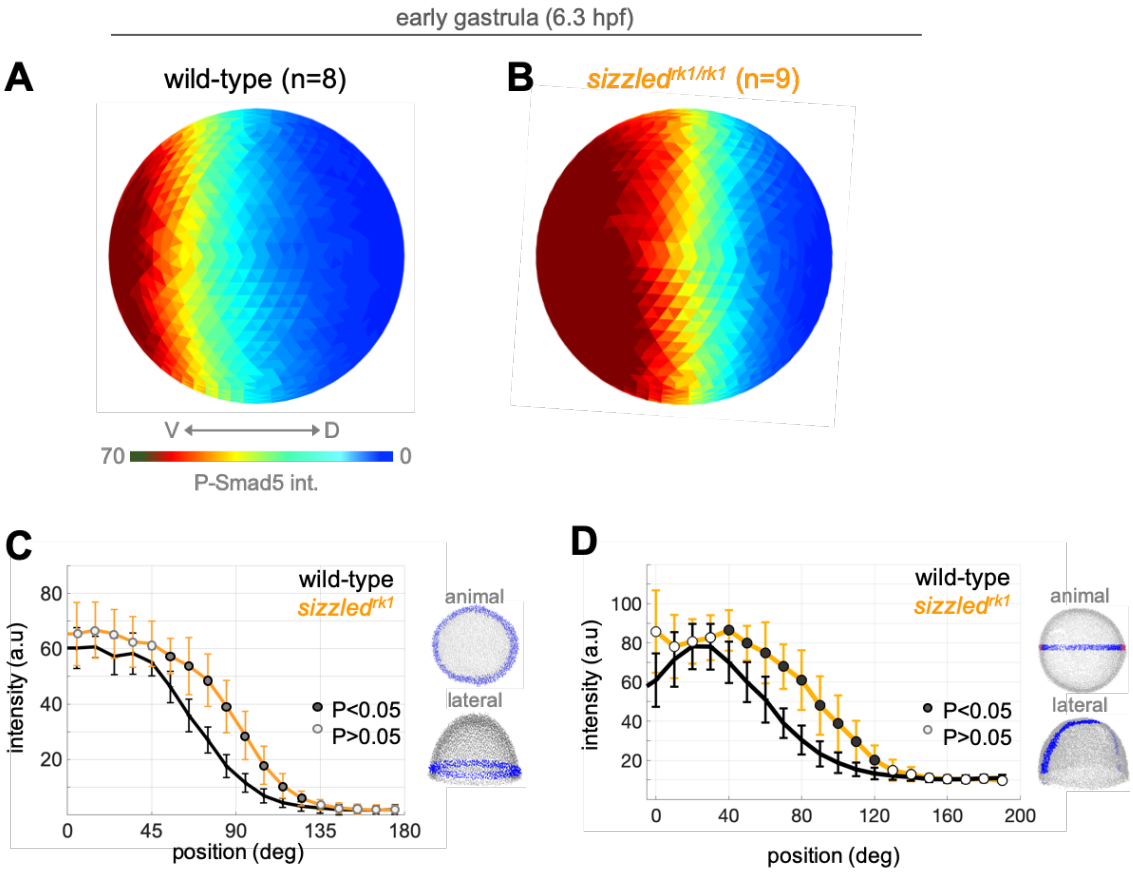

Figure 3.7 *sizzled* mutants first display P-Smad5 defects at 6.3 hpf

(**A,B**) Animal view of mean P-Smad5 intensities at gastrula stage (6.3 hpf) in: (**A**) wild-type controls for (**B**) *sizzled*^{rk1} mutants. (**C,D**) Average P-Smad5 intensities of a 30μm band of cells in **A,B**. Wild-type controls are shown in black. Error bars indicate standard deviation. Filled circles indicate a significant (P<0.05) difference at each position compared to wild-type. (**C**) Marginal mean P-Smad5 intensities, cell location indicated in blue on the right. (**D**) Mean P-Smad5 intensities over the top of the embryo, cell location indicated in blue on the right.

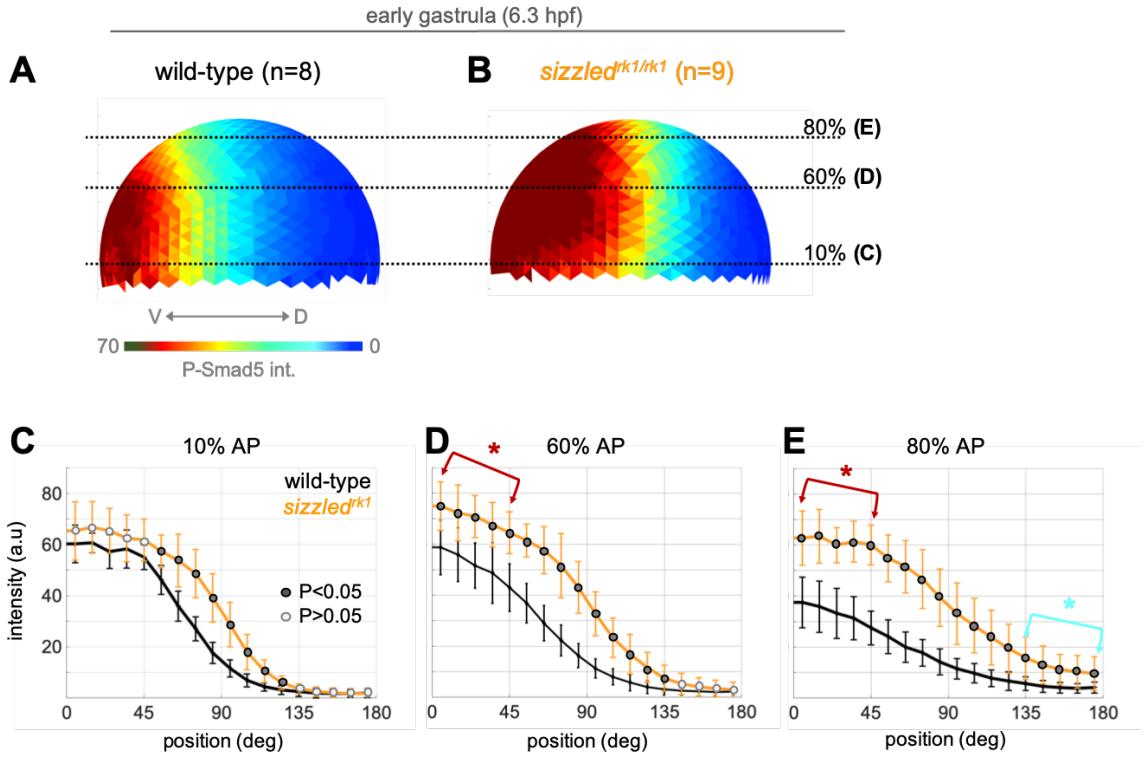

Figure 3.8 *sizzled* mutants display increased P-Smad5 at relative AP positions

(**A**,**B**) Lateral view of mean P-Smad5 intensities at gastrula stage (6.3 hpf) in: (**A**) wild-type controls for (**B**) *sizzled*^{trk1} mutants. Dashed lines indicate location of 30μm band of cells used to generate **C-E**, respectively. (**C-E**) Average P-Smad5 intensities in **A**,**B**. Wild-type controls are shown in black. Error bars indicate standard deviation. Filled circles indicate a significant (P<0.05) difference at each position compared to wild-type. (**C**) Marginal mean P-Smad5 intensities, located at 10% of total embryo anteroposterior (AP) height. Reprinted from **Figure 3.2.6C**. (**D**) Mean P-Smad5 intensities, located at 60% of total embryo AP height, show a significant increase ventrally (red bracket and asterisk) in *sizzled*^{trk1} mutants compared to controls. © Mean P-Smad5 intensities, located at 80% of total embryo AP height, show a significant increase ventrally (red bracket and asterisk) and dorsally (teal bracket at asterisk) in *sizzled*^{trk1} mutants compared to controls.

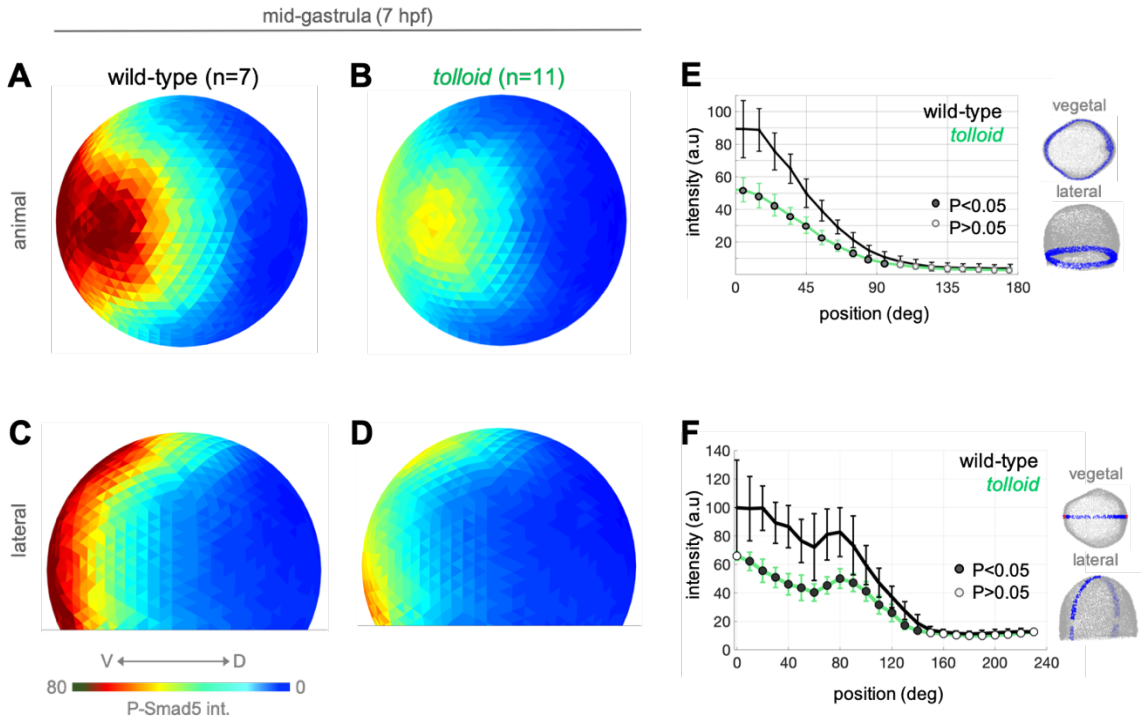

Figure 3.9 *tolloid* mutants first display P-Smad5 defects at 7 hpf

(**A,B**) Animal and (**C,D**) lateral views of mean P-Smad5 intensities at mid-gastrula stage (7 hpf) in: (**A**) wild-type controls for (**B**) *tolloid* mutants. (**E,F**) Average P-Smad5 intensities of a 30μm band of cells in **A,B,C,D**. Wild-type controls are shown in black. Error bars indicate standard deviation. Filled circles indicate a significant (P<0.05) difference at each position compared to wild-type. © Marginal mean P-Smad5 intensities, cell location indicated in blue on the right. (**F**) Mean P-Smad5 intensities over the top of the embryo, cell location indicated in blue on the right.

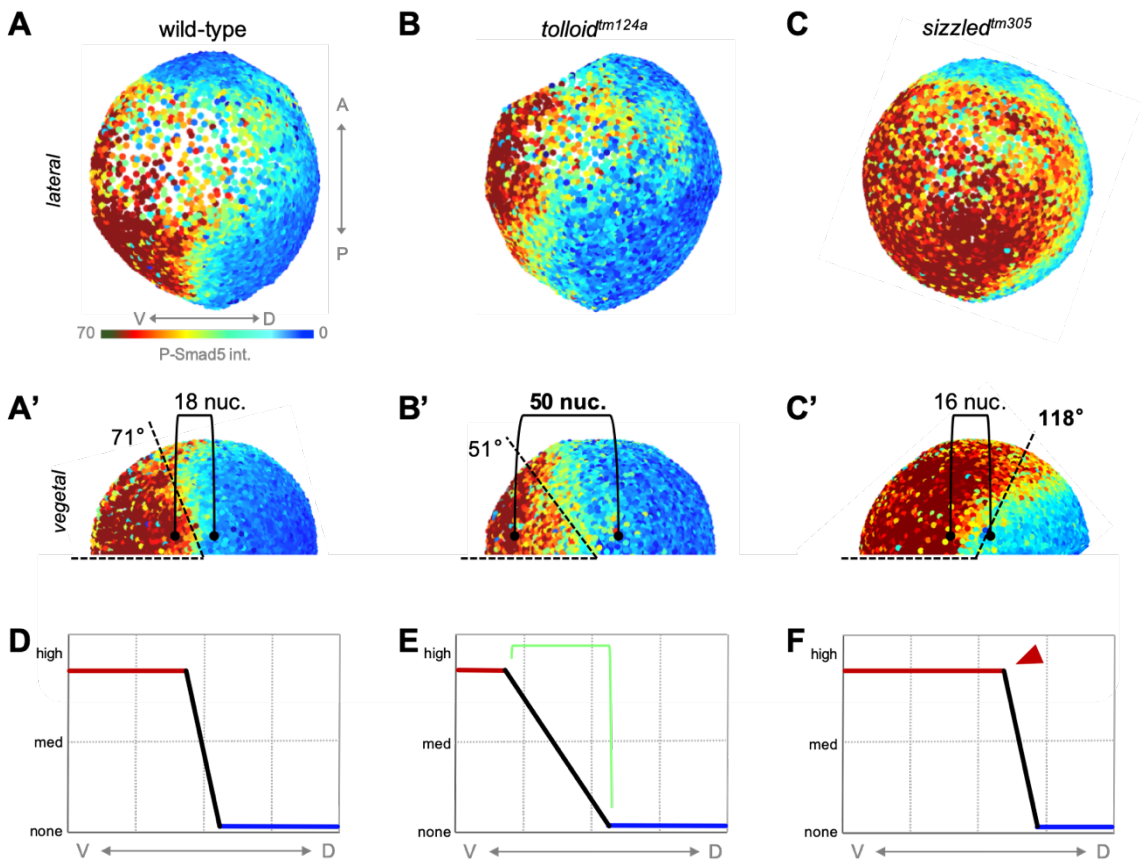

Figure 3.10 *tolloid* and *sizzled* mutants display defects in distinct aspects of the P-Smad5 gradient at the end of gastrulation

(**A-C**) Lateral and (**A'-C'**) vegetal views of P-Smad5 intensities of individual (**A,A'**) wild-type, (**B,B'**) *tolloid*^{tm124a} mutant, and (**C,C'**) *sizzled*^{rk1} mutant embryos at the end of gastrulation. (**A'-C'**) Mean distance, in approximate nuclei diameters, between the highest and lowest P-Smad5 levels and mean angle of extension of the highest levels of P-Smad5 in multiple embryos of each genotype: (**A'**) wild-type (n = 9), (**B'**) *tolloid* (n = 4), and (**C'**) *sizzled* (n = 7). (**D-F**) Schematics of the approximate P-Smad5 gradient shape of each genotype. Red and blue lines represent the highest and lowest levels of P-Smad5 respectively. Black lines represent the intermediate levels of P-Smad5. (**D**) The steep wild-type gradient at the end of gastrulation. © In *tolloid* mutants, the approximate P-Smad5 gradient is shallower (green bracket) while (**F**) in *sizzled* mutants, there is a lateral extension of the highest levels of P-Smad5 (red arrow).

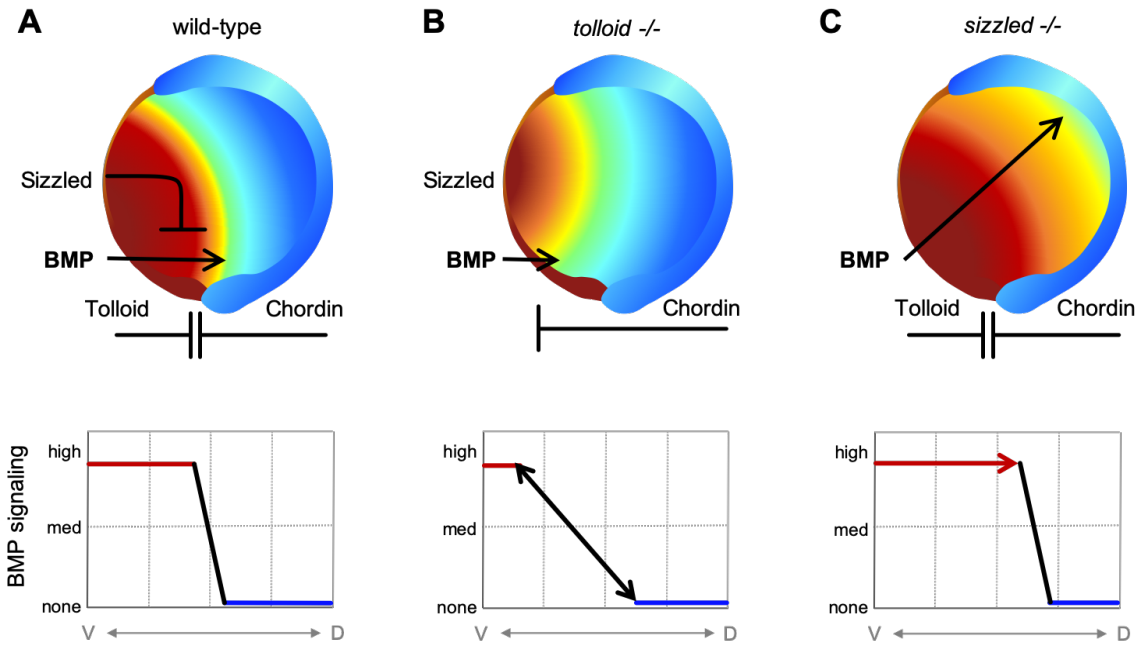

Figure 3.11 Model of how Tolloid and Sizzled shape distinct aspects of the steep BMP signaling gradient

(**A**) In wild-type embryos at the end of gastrulation, a steep gradient is maintained by Tolloid and Chordin directly abutting in the tailbud while Sizzled prevents Tolloid-mediated promotion of BMP signaling in the lateral regions. (**B**) In *tolloid* mutants, Chordin is unrestricted in the tailbud and aberrantly inhibits BMP, resulting in a shallower and lower BMP signaling gradient. (**C**) In *sizzled* mutants, the steepness of the gradient is maintained since Tolloid is present to combat Chordin in the tailbud. However, without Sizzled inhibition, Tolloid aberrantly promotes BMP signaling, to its highest levels, in the lateral regions of the embryo.

CHAPTER 4. Bmper promotes BMP signaling during otic vesicle development

Contributions: This chapter contains select figures and direct quotes from a manuscript being prepared in collaboration with Sarah Baxendale and Tanya Whitfield (University of Sheffield, UK) and uses the *bmper*$^{\Delta 12}$ allele, which was generated by Joseph Zinski (unpublished).

4.1 Introduction

Another context that presents spatial and temporal challenges for BMP regulation is the boundary of neural and nonneural ectoderm. Distinct intermediate levels of BMP signaling pattern the preplacodal ectoderm (PPE), which gives rise to sensory organs like the inner ear and olfactory epithelium **(Figure 4.1A-C)** (Nguyen et al., 1998; Nguyen et al., 2000; Wawersik et al., 2005). BMP signaling must be tightly regulated to generate such a distinct signaling level in this very narrow region **(Figure 4.1A)**. PPE patterning also requires two contrary phases of BMP signaling: at late blastula stages BMP signaling is required to specify PPE precursors, while at late gastrula stages BMP antagonists must block BMP signaling for further PPE development (Kwon et al., 2010). Finally, as the PPE develops into the inner ear, it is dramatically remodeled from a simple band of cells to a hollow ball of epithelial cells **(Figure 4.1B)**, and finally a complex labyrinthine structure **(Figure 4.1C)**. The correct development of the semicircular canal ducts of the mature inner **(Figure 4.1C)**, in turn, require BMP signaling. Thus, patterning of the PPE and its subsequent development into the inner ear presents a unique environment to study the spatial and temporal mechanisms that regulate BMP signaling and BMP antagonist activity.

Bmper (BMP-binding endothelial regulator), introduced in Section 1.2.4, may play a key role in this process (Reichert et al., 2013). Bmper is known to both promote and inhibit BMP function in different contexts. Bmper can both bind the BMP ligand and the BMP antagonist Chordin **(Figure 4.1D)** (Ambrosio et al., 2008; Rentzsch et al., 2006; Serpe et al., 2008), and in zebrafish enhances BMP signaling when Chordin is present while inhibiting BMP signaling when Chordin is absent (Zhang et al., 2010). Previous studies utilizing morpholino-mediated knockdown of Bmper suggested that Bmper is

required to promote BMP signaling during DV patterning (Ambrosio et al., 2008; Rentzsch et al., 2006; Zhang et al., 2010). However, multiple zebrafish mutant alleles generated by our lab (*bmper*$^{\Delta 2}$ and *bmper*$^{\Delta 5}$) and the Sanger Zebrafish Mutation Project (*bmper*^{sa0108}) (Kettleborough et al., 2013) do not show any overt DV patterning defects at 1-2 dpf. Instead, at 5 dpf all *bmper* mutants display defects in the dorsal inner ear, resulting from the truncation of the anterior and posterior semicircular canal ducts **(Figure 4.1E-F)**.

4.2 Results

4.2.1 Bmper is dispensable for BMP signaling during gastrulation

Though the semicircular canal ducts defect indicates that Bmper is required for correct inner ear development **(Figure 4.1E-F)**, it remained unclear whether these morphogenesis defects were caused by earlier alterations in PPE specification. To determine if Bmper plays a role in shaping the distinct BMP signaling domain that gives rise to the PPE **(Figure 4.1A)**, we performed quantitative immunofluorescence of nuclear P-Smad5 in 7 hpf (mid-gastrulation) embryos **(Figure 4.2)**. We generated maternal-zygotic (MZ) loss of *bmper* by crossing a *bmper*$^{\Delta 2/\Delta 2}$ female to a *bmper*$^{\Delta 2}$ heterozygous male. All embryos were genotyped after imaging and MZ-*bmper*$^{\Delta 2/\Delta 2}$ embryos were compared to their *bmper*$^{\Delta 2/+}$ siblings, which served as wild-type controls **(Figure 4.2A-B)**. There was no significant difference in mean P-Smad5 profiles at the margin **(Figure 4.2C)** or over the anterior of the embryo **(Figure 4.2C')** between MZ-*bmper* homozygotes and their heterozygous siblings, indicating that Bmper is likely not required for initial PPE specification.

4.2.2 Bmper promotes BMP signaling in the developing otic vesicle

To determine how loss of Bmper affect BMP signaling in the otic vesicle, we applied our quantitative immunofluorescence protocol, including confocal microscopy, to 32-48 hpf embryos (see Methods). Analysis of the otic vesicle in 32 hpf embryos revealed a decrease in P-Smad5 intensity in MZ-*bmper*$^{\Delta 2/\Delta 2}$ embryos compared to heterozygous siblings used as wild-type controls **(Figure 4.3)**. Though the nuclear staining precluded analysis of P-Smad5 intensity in individual nuclei, we were still able to characterize effects on BMP signaling through analysis of maximum projections and segmentation of the P-Smad5 signal (performed in Imaris). Interestingly, we observed the highest levels of P-Smad5 in the anterior and posterior poles of the vesicle, relative to the ventral and dorsal sides **(Figure 4.3)**. By 48 hpf, low levels of P-Smad5 were apparent around the outer cell layer of the otic vesicle in wild-type controls **(Figure 4.4A-C)**. In comparison, MZ-*bmper*$^{\Delta 2/\Delta 2}$ embryos displayed a total loss of dorsal P-Smad5 and a gap in ventral P-Smad5 **(Figure 4.4D-F)**. Interestingly, the highest P-Smad5 levels at this stage were observed in the presumptive hair cells and at the site of the lateral projection, where no appreciable difference in intensity was evident between MZ-*bmper*$^{\Delta 2/\Delta 2}$ embryos and wild-type controls **(Figure 4.4A-B, D-E)**.

4.3 Future Directions

4.3.1 Determining the earliest requirement for Bmper

We have determined that Bmper is not required for the earliest PPE specification by 7 hpf **(Figure 4.2)** but does promote BMP signaling in the otic vesicle by 32 hpf **(Figure 4.3)**. However, the role of Bmper between these two timepoints remains unknown.

Specifically, from 10-24 hpf the PPE transitions from a swath of cells (10 hpf), to an unorganized ball of cells (14 hpf), to a hollow epithelial structure with apicobasal polarity (24 hpf) **(Figure 4.1B)**. Since Bmper may still play a role in regulating BMP signaling during these remodeling stages, additional P-Smad5 analysis is required to determine the earliest function for Bmper. Furthermore, Bmper appears to regulate BMP signaling in different regions of the otic vesicle as it develops from 32 to 48 hpf: Bmper promotes BMP signaling in the anterior and posterior poles at 32 hpf **(Figure 4.3)**, while additionally at 48 hpf it promotes BMP signaling in the ventral and dorsal outer cell layers of the otic vesicle **(Figure 4.4)**. The functional consequences of these differences remain to be characterized.

4.3.2 Further characterization of *bmper* mutants

Though *bmper* mutants have a specific defect in the dorsal region of the inner ear **(Figure 4.1F)**, the role of Bmper in the morphogenetic mechanisms that shape the inner ear is a continuing area of study for Dr. Whitfield and colleagues. The mature ear remarkably develops from a simple ball of epithelial cells into a complex labyrinthine structure that is able to detect sound, gravity, linear acceleration and rotational movement **(Figure 4.1B-C)**. This process requires a highly orchestrated integration of different signaling pathways to specify the many different cell types and structures in the mature ear (Alsina and Whitfield, 2017; Whitfield and Hammond, 2007). Ongoing studies from the Whitfield lab show that *bmper* mutants display subtle changes in the expression of *dlx5a*, *hmx3a* and some BMP pathway genes in the dorsal otic epithelium and periotic mesenchyme. They are also using light-sheet microscopy of a *Tg(smad6b:GFP)* transgenic line to characterize cell number, shape and movements in both wild-type and *bmper* mutant zebrafish. Finally, analysis of adult *bmper* mutants has identified a

behavioral signature consistent with the structural defects observed in the semicircular canals.

4.3.3 Integrating Bmper and Twisted-gastrulation function

Though Bmper alone does not appear to play a role in DV patterning, it may function in conjunction with Twisted-gastrulation (Tsg, Section 1.2.4). In zebrafish, *tsg* morphants are dorsalized (Little and Mullins, 2004), with Tsg's proposed role being to enhance the degradation of Chordin by Tolloid (Xie and Fisher, 2005), thus promoting BMP signaling. It has been proposed that Bmper also promotes BMP signaling by directly binding Chordin, though the mechanism is still unclear (Rentzsch et al., 2006; Zhang et al., 2010). Finally, in Xenopus, Bmper binds Tsg and forms a ternary complex with Tsg and BMP, though this results in the inhibition of BMP signaling (Ambrosio et al., 2008). Overall, since both Bmper and Tsg promote BMP signaling in zebrafish, and may do so through Chordin and/or binding each other, Bmper and Tsg may act redundantly. Future studies can evaluate the *bmper;tsg* double mutant phenotype to determine if they play a redundant role, if any, in DV patterning.

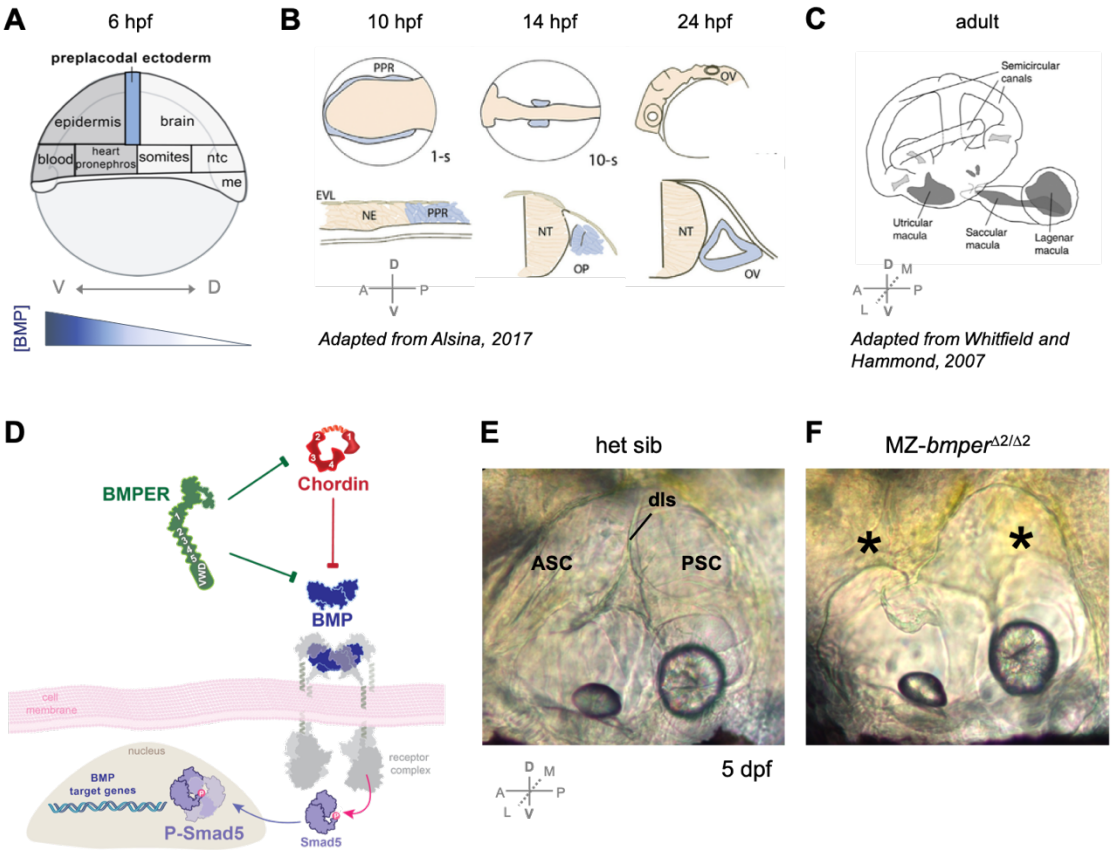

Figure 4.1 Bmper regulates BMP signaling to correctly pattern the inner ear.

(A-C) Schematics of zebrafish inner ear development. **(A)** Location of the PPE relative to the embryo-wide BMP signaling gradient in the early gastrula. **(B)** Development of the preplacodal region (PPR) into the otic placode (OP), which subsequently undergoes epithelialization and hollowing to generate the otic vesicle (OV), all during somitogenesis. Adapted from (Alsina and Whitfield, 2017). **(C)** The mature ear, adapted from (Whitfield and Hammond, 2007). **(D)** Bmper has been reported to play dual roles, either promoting or inhibiting BMP signaling. Schematic adapted from (Dutko and Mullins, 2011). **(E-F)** DIC images of MZ-*bmper*$^{\Delta 2/\Delta 2}$ **(F)** and heterozygous sibling **(E)** at 5 dpf. Asterisks indicate truncation of the anterior and posterior semicircular canal ducts (ASC and PSC, respectively); dls: dorsolateral septum.

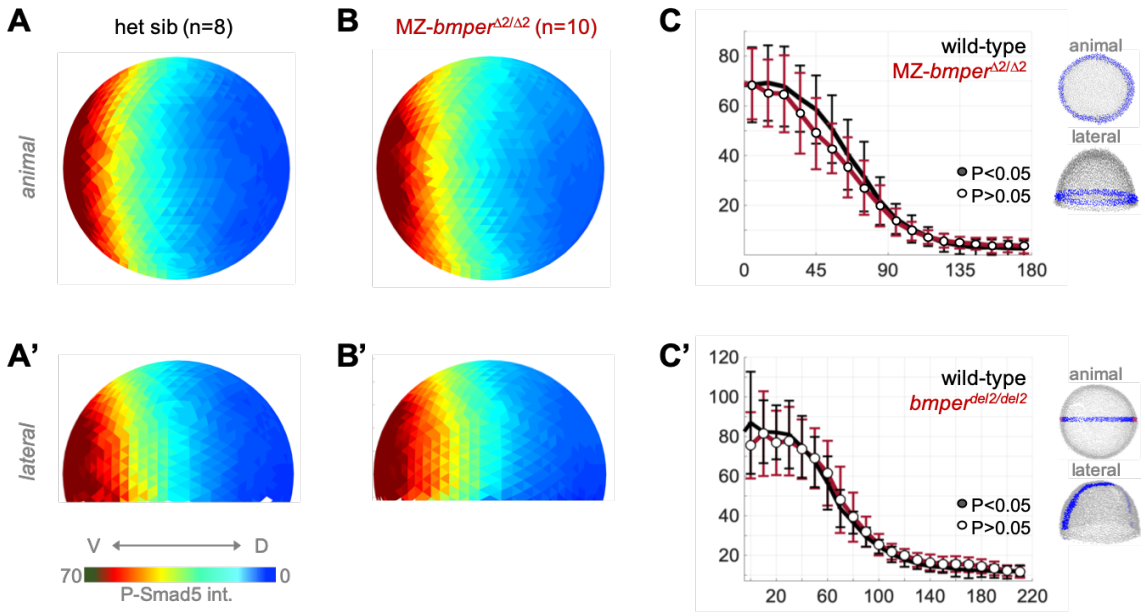

Figure 4.2 MZ-*bmper* gastrulae show no alteration in the P-Smad5 gradient

(**A-B**) Animal and (**A'-B'**) lateral views of mean P-Smad5 intensities at mid-gastrula stage (7 hpf) in: (**A-A'**) heterozygous siblings, which serve as wild-type controls (n=8, 2 replicates) and (**B-B'**) *MZ-bmper*$^{\Delta 2/\Delta 2}$ mutants (n=10, 2 replicates). (**C-C'**) Mean marginal P-Smad5 intensities of **A-B**, calculated from nuclei binned in 10° intervals around the embryo and displayed from ventral (0°) to dorsal (180° or 220°). Error bars indicate standard deviation; filled circles indicate a significant (P<0.05) difference at each position compared to wild-type (shown in black). (**C**) Comparison of the mean marginal P-Smad5 profiles, with the location of the 30µm band of cells used shown in blue on the right. (**C'**) Comparison of the mean P-Smad5 profiles over the anterior of the embryos, with the location of 30µm band of cells used shown in blue on the right.

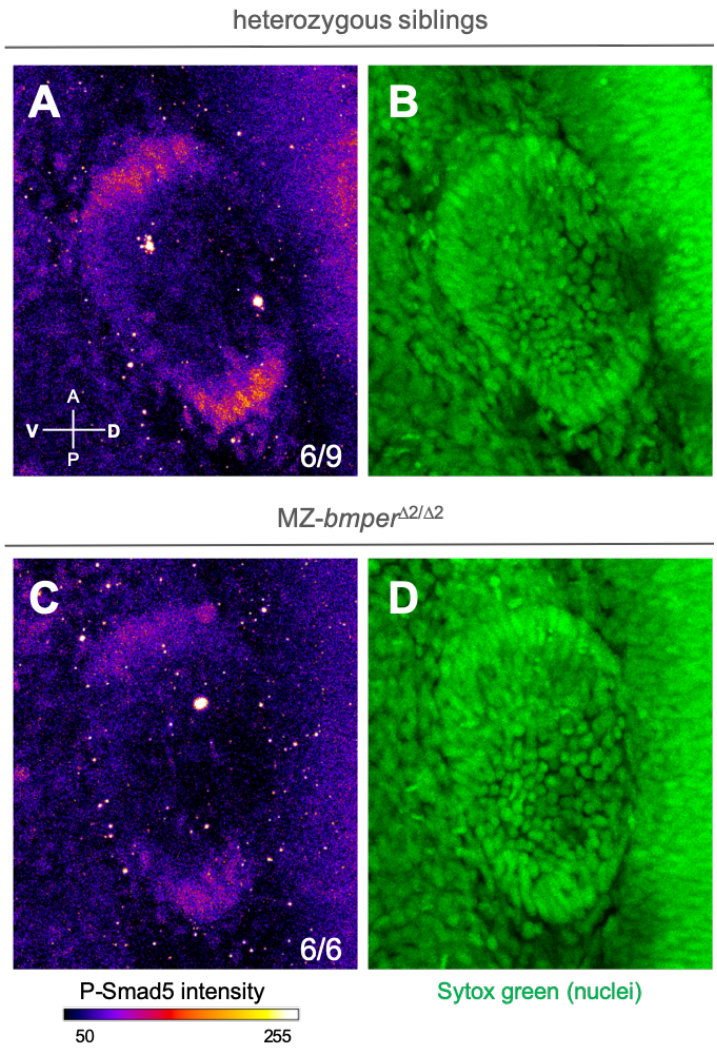

Figure 4.3 Bmper promotes BMP signaling in the otic vesicle by 32 hpf

Maximum projections in wild-type controls (**A-B**) and MZ-*bmper*$^{\Delta 2/\Delta 2}$ (**C-D**) otic vesicles at 32 hpf. (**A,C**) Heatmap display of relative P-Smad5 intensity shows that P-Smad5 signal is significantly decreased in MZ-*bmper*$^{\Delta 2/\Delta 2}$ otic vesicles. (**B,D**) Individual cell nuclei, visualized by sytox green, used to identify the otic vesicle.

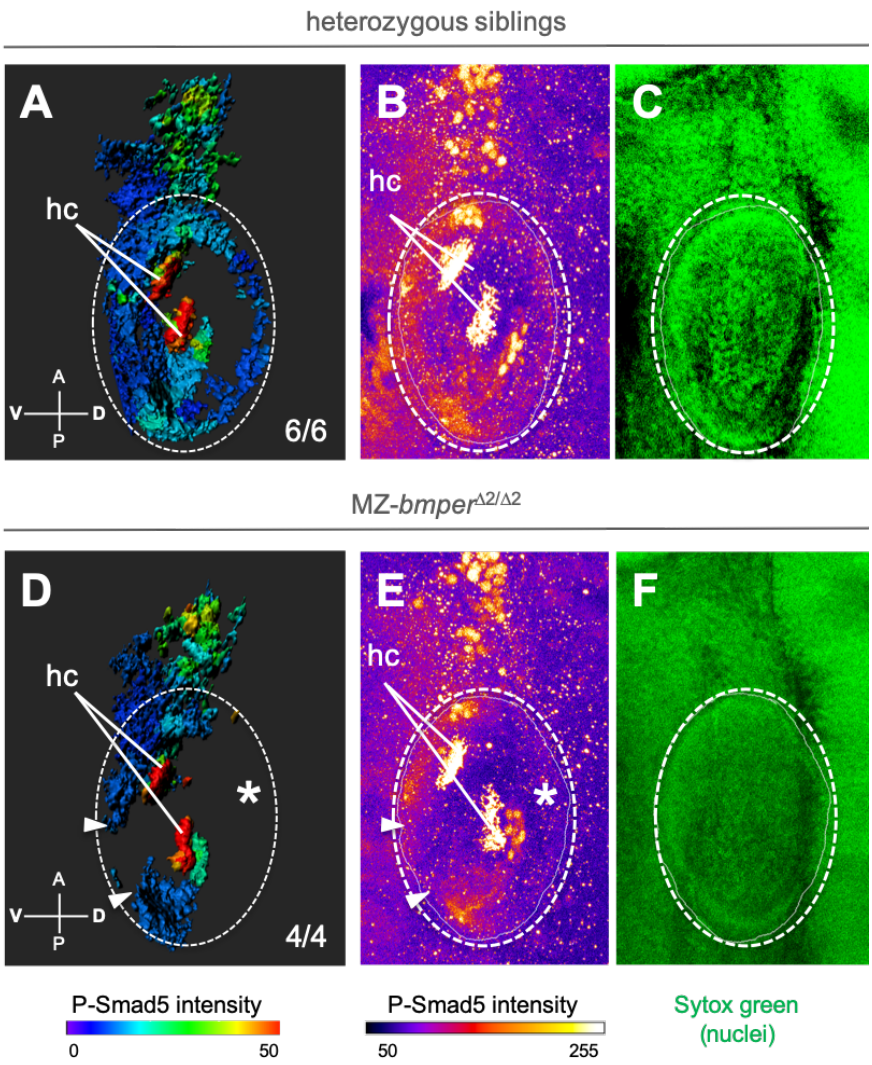

Figure 4.4 Bmper is required for BMP signaling at the edge of otic vesical at 48 hpf

Analysis of P-Smad5 fluorescence Otic vesicle is outlined (dashed white line) and hair cells (hc) are indicated. (**A,D**) 3D surface heatmap display of relative mean P-Smad5 intensity, generated in Imaris by segmenting the P-Smad5 signal. MZ-*bmper*$^{\Delta 2/\Delta 2}$ display a loss of P-Smad5 at the outer cell layer of the otic vesicle. At the ventral side, there is a gap in P-Smad5 expression (arrowheads), while at the the dorsal side there is a complete loss of P-Smad5 (asterisk). (**B,C,E,F**) Maximum projections of P-Smad5 (**B,E**) and Sytox (**C,F**) in wild-type controls (**B-C**) and MZ-*bmper*$^{\Delta 2/\Delta 2}$ (**E-F**) otic vesicles at 48 hpf. (**B,E**) Heatmap display of relative P-Smad5 intensity otic vesicles. (**C,F**) Individual cell nuclei, visualized by sytox green, used to identify the otic vesicle.

CHAPTER 5. Perspective and Future Directions

Contributions: This chapter contains direct quotes from Tuazon and Mullins published in 2015 in *Seminars in Cell and Developmental Biology* (Tuazon and Mullins, 2015).

5.1 Summary of major conclusions

This project elucidated the underlying mechanisms that shape the BMP morphogen gradient in space and time to correctly pattern the DV axis of the developing zebrafish embryo. The primary focus was to uncover the role of metalloprotease-related extracellular regulation (Section 1.2.4) in both establishing and then shaping the BMP signaling gradient. Specifically, we investigated the roles of Bmp1a and Tolloid, metalloproteases that promote BMP signaling by cleaving the critical BMP antagonist Chordin, and their competitive inhibitor Sizzled, at both the onset of gastrulation (Chapter 2) and then during and at the end of gastrulation (Chapter 3).

In Chapter 2, we combined rigorous mutant analyses with quantitative immunofluorescence to determine that Bmp1a and Tolloid are partially redundant and serve to spatially restrict Chordin's range in the early gastrula. We discovered that maternally-deposited Bmp1a plays an unexpected and non-redundant role in establishing the BMP gradient, while Sizzled is surprisingly dispensable. Combining mathematical models and *in vivo* analyses with an immobile Chordin construct, we demonstrate that Chordin diffusion is dispensable for BMP gradient formation and DV patterning. These results exclude a counter-gradient of Chordin and instead favor a Chordin sink, established by Bmp1a and Tolloid, as the primary mechanism that generated the BMP signaling gradient.

In Chapter 3, we applied quantitative immunofluorescence to wild-type embryos during gastrulation and determined that the BMP signaling gradient changes shape, steepening in fact, by the end of gastrulation. We discovered that Tolloid and Sizzled play distinct spatiotemporal roles in shaping the BMP gradient during gastrulation: they are required first at different stages and then impact different aspects of the steepening BMP

gradient. These results suggest that gastrulation represents a new signaling environment, distinct from when the BMP signaling gradient is established, that requires Tolloid and Sizzled. Moreover, since defects in both *tolloid* and *sizzled* mutants are confined to the tail, this supports that how Tolloid and Sizzled shape the BMP gradient at the end of gastrulation is key to correctly patterning the tail.

In Chapter 4, we explored how tissue-specific regulation of BMP signaling patterns the otic vesicle, or presumptive inner ear, of *bmper* mutants, which display defective inner ear development. We applied quantitative immunofluorescence to characterize the role of Bmper, which can promote or inhibit BMP function in different contexts. We found that while Bmper is not required during the initial specification of the preplacodal ectoderm, Bmper is later required to promote BMP signaling in the otic vesicle. Finally, Bmper may play distinct spatiotemporal roles, first promoting BMP signaling in the anterior and posterior poles of the otic vesicle at 32 hpf and then in the dorsal and ventral outer cell layers at 48 hpf.

5.2 Applying the distinct spatiotemporal roles of BMP regulation across contexts

The central question that inspired this project was: why does the embryo need so many layers of BMP inhibition (Section 1.7)? Why is the BMP antagonist, Chordin, not sufficient for all DV patterning? Why does Chordin need to be inhibited by Bmp1a and Tolloid, which are in turn inhibited by Sizzled? When does Bmper fit in? Excitingly, we have defined distinct spatiotemporal roles for each of these layers of extracellular BMP regulation. Taken together, we see that the purpose of each regulator is context dependent. First, Bmp1a and Tolloid work together to generate a Chordin sink to set-up the BMP signaling gradient in the early gastrula, with Bmp1a playing the predominant role

in this process. Then, Tolloid and Sizzled become the dominant factors during gastrulation to correctly shape a steeper BMP gradient in a highly dynamic environment. Finally, Bmper has a tissue-specific role in the otic vesicle to promote BMP signaling. Defining these contexts in which each regulator functions provides the larger BMP signaling field with the opportunity to compare systems and delve into the underlying reasons why each context has its own unique requirement.

One approach to understanding these mechanistic differences is from an evolutionary perspective. BMP, Chordin, and Tolloid are highly conserved in DV patterning across invertebrates and vertebrates. In fact, vertebrate Chordin and the *Drosophila* ortholog, known as Sog, are remarkably interchangeable: expressing *sog* can pattern the DV axis in *Xenopus* and vice versa, *chordin* can pattern the DV axis in *Drosophila* (Holley et al., 1995). However, the mechanisms underlying Chordin and Sog function are almost completely opposite. As we show in zebrafish, Chordin must be critically restricted by Bmp1a/Tolloid to function as a sink (Chapter 2). In contrast, in *Drosophila* Sog must be highly mobile and cleavage by Tolloid actually concentrates the highest levels of BMP (Ashe and Levine, 1999; Marques et al., 1997). A potential reason for these divergent mechanisms is that the *Drosophila* BMP signaling gradient is much steeper than the BMP signaling gradient in the early zebrafish gastrula (Zinski et al., 2017). Future studies are needed to address why these gradient shapes and mechanisms diverged. For example, it could be due to embryo size or cell number, the speed of development, or even the presence of the additional regulators Bmp1a and Sizzled in vertebrates.

Another perspective on understanding regulatory differences between BMP signaling contexts is to consider the predominant BMP antagonists in each context. Although Chordin is the primary BMP antagonist in zebrafish DV patterning, and the focus

of this dissertation project, additional antagonists exist. During DV patterning, Noggin and Follistatin are partially redundant to Chordin, with loss of all three antagonists resulting in radial ventralization (Dal-Pra et al., 2006; Khokha et al., 2005). However, Noggin plays a later role as a critical BMP antagonist in the neural tube (McMahon et al., 1998; Selleck et al., 1998). An additional BMP antagonist, Gremlin, also plays functionally distinct roles from Chordin, Noggin, and Follistatin in digit patterning (Merino et al., 1999). After characterizing distinct functional requirements for each antagonist in these contexts, future studies may be aimed at uncovering why each system relies more heavily on specific BMP antagonists. Is it simply based on which antagonist is expressed? If so, what controls or differentiates which antagonists are expressed when and where? Or, are there intrinsic biochemical differences that distinguish each antagonist, such as target BMP binding specificity, additional binding partners, and/or diffusion coefficients? If there are differences, do they make an antagonist the optimal choice for its respective context?

Notably, these mechanistic insights into the spatiotemporal regulation of BMP signaling all occur extracellularly, essentially modulating BMP ligand availability. Just as there is the potential to discover or delineate additional layers of extracellular regulation, these opportunities also exist for understanding the intracellular transduction of BMP signaling. Though P-Smad5 is the known downstream effector of BMP signaling, there is a gap in our mechanistic understanding of how the Smad5 transcription factor is phosphorylated by the BMP receptor complex and the identity of potential Smad5 co-factors in the nucleus remains unknown. These intracellular and intranuclear aspects of BMP signal transduction must also be addressed to fully understand context-dependent regulation of BMP signaling.

5.3 New avenues for exploring cell competency in the early embryo

Through this project we unexpectedly discovered exciting new contexts to address the question of cell competency. As mentioned in the Introduction (Section 1.1), to achieve proper embryo patterning not only must morphogen levels be maintained throughout the patterning process, but cells must also be competent, or able to respond, to morphogen signals at exact timepoints to correctly adopt their fate. This dissertation primarily focused on the first issue, determining how the correct distribution of BMP morphogen levels is established, and then maintained, during DV patterning. However, through that work we uncovered multiple exciting arenas for future studies of target cell competency in response to BMP signaling.

5.3.1 Understanding plasticity: M-*bmp1a* homozygous and heterozygous mutants

The first context is M-*bmp1a* mutants, which offer a unique opportunity to study the endogenous recovery of BMP signaling. We found that although M-*bmp1a-/-* embryos have a significantly diminished P-Smad5 gradient at the onset of gastrulation **(Figure 2.2)**, the P-Smad5 gradient recovers by mid-gastrulation **(Figure 2.3)**, consistent with their apparently normal body plan at 24 hpf. However, anterior dorsal markers still remain expanded at mid-gastrulation in M-*bmp1a*-/- embryos **(Figure 2.4)**. While this persistent expansion of dorsal markers supports our model that the anterior of the embryo is patterned by the BMP gradient at the onset of gastrulation **(Figures 1.3 and 3.1)** (Section 1.4), the extent to which the patterning defects persist warrants further investigation. Some fascinating questions include: do these neural patterning defects endure through later CNS development? If so, does the embryo compensate for expanded neural specification (such as by limiting cell division)? Are all aspects of M-*bmp1a*-/- embryos wild-type at 24 hpf or are there additional defects not visible morphologically?

Though previous work from our lab has determined when BMP is required to progressively pattern the DV axis, these studies did so by inhibiting BMP signaling (Sections 1.4) (Hashiguchi and Mullins, 2013; Tucker et al., 2008). It is difficult to compare the findings here to that work since BMP signing is reintroduced in the M-*bmp1a-/-* embryo. For example, the persistence of dorsal marker expansion in M-*bmp1a-/-* embryos at mid-gastrula stages (7 hpf) may be independent of the M-*bmp1a-/-* P-Smad5 phenotype at the onset of gastrulation (5.7 hpf). Instead, it is entirely possible that dorsal markers remain expanded due to the shape of the M-*bmp1a-/-* BMP signaling gradient. By 7 hpf in M-*bmp1a-/-* embryos, ventral P-Smad5 levels were fully rescued to wild-type levels, while lateral P-Smad5 levels, though they approach wild-type levels, are still significantly lower **(Figure 2.4)**. This remaining lateral reduction in P-Smad5 may account for dorsal marker expansion in M-*bmp1a-/-* mid-gastrula embryos. Future studies can resolve this through careful characterization of the timing of patterning defects in M-*bmp1a-/-* embryos, as well as an understanding of the minimum thresholds of P-Smad5 that inhibit dorsal gene activation.

Interestingly, similar P-Smad5 phenotypes and rescue dynamics are observed in M-*bmp1a+/-* embryos **(Supplemental Figure 2.4)**, yet the mechanism underlying the M-*bmp1a-/-* and M-*bmp1a+/-* similarity remains to be fully described. Though we were able to determine that *bmp1a* transcript in M-*bmp1a+/-* embryos is reduced to a similar extent as in M-*bmp1a-/-* embryos by *in situ* hybridization **(Supplemental Figure 2.3)**, future studies utilizing quantitative-PCR and/or FISH are needed. Furthermore, since *bmp1a* is not a target of miR-430, which targets maternal transcripts for degradation, the mechanism that reduces *bmp1a* transcript in M-*bmp1a+/-* embryos remains entirely unknown. In sum, the P-Smad5 and DV patterning phenotypes in M-*bmp1a-/-* and M-*bmp1a+/-* embryos

provide a powerful context to investigate the recovery of BMP signaling, the plasticity of the early gastrula, and how the embryo may compensate for an early expansion of neural tissues later during development.

5.3.2 Understanding loss of competency: *sizzled* and *tolloid* mutants

The second new context for studying cell competency to BMP signaling is in *sizzled* mutants at the onset of gastrulation. While *sizzled* mutants display no significant P-Smad5 phenotype at the onset of gastrulation (5.7 hpf), shortly after there is a striking expansion of P-Smad5 levels laterally during early gastrulation (6.3 hpf) **(Figures 3.5 and 3.7)**. Despite significant changes in P-Smad5 levels across the DV axis, especially in the anterior **(Figure 3.7-8)**, the earliest DV patterning defects have been reported is during mid-gastrulation (7.5 hpf), over an hour later (Miller-Bertoglio et al., 1999). Furthermore, the patterning of anterior neurectoderm markers appears normal (Miller-Bertoglio et al., 1999). Normal neural patterning is consistent with our model that anterior regions are patterned at the onset of gastrulation (5.7 hpf) **(Figures 1.3 and 3.1)** (Section 1.4), however it also implies that anterior regions must be refractory to P-Smad5 changes by early gastrulation (6.3 hpf), less than an hour later, when *sizzled* mutants first display a significant phenotype.

Cells losing the ability to respond to BMP signaling is also readily apparent in both *sizzled* and *tolloid* mutants at the end of gastrulation (10 hpf), the third and final new context for studying cell competency. Surprisingly, although the mutant phenotypes are restricted to the tail **(Figure 3.4)**, the P-Smad5 phenotypes are embryo-wide **(Figure 3.10)**. Still, there are no reports of anterior patterning defects in *sizzled* and *tolloid* mutants despite dramatic changes in anterior P-Smad5 intensity (Connors et al., 1999; Miller-Bertoglio et al., 1999). Taken together, these results beg the question: how do cells stop

responding to BMP signaling? Moreover, is the mechanism responsible in *sizzled* mutants at 6.3 hpf the same as what's acting at 10 hpf?

To address how cells become refractory to BMP signaling, earlier reports of normal DV marker expression in *sizzled* and *tolloid* mutants must first be confirmed. This requires combining careful quantitation of DV patterning markers by higher resolution methods, such as FISH, with our rigorous staging method **(Figure 3.2)**. If anterior DV marker expression is in fact normal, then these mutants become a powerful system to dissect the loss of BMP competency in both space and time. Potential approaches may include RNA-seq (to address transcriptional mechanisms) and ATAC-seq (to address epigenetic mechanisms), though a significant challenge will be distinguishing cells in anterior regions from cells at the margin. A complementary approach is the development of 3-D mathematical models incorporating the spatial and temporal complexity of these P-Smad5 phenotypes, which can determine if there is differential BMP signaling regulation in the anterior regions of the embryo versus at the margin. This approach is being developed by our collaborators at Purdue University, Linlin Li and David Umulis. Notably, since *sizzled* and *tolloid* phenotypes emerge during gastrulation, autoregulatory feedback loops (discussed in the next section) may contribute to a loss of competency.

5.4 Understanding autoregulatory feedback loops during embryonic patterning

5.4.1 Determining the role of feedback in DV patterning

A remaining aspect of BMP regulation that was not addressed in this project is the role of autoregulatory feedback. Interestingly, BMP signaling in *Xenopus* and zebrafish is regulated by multiple feedback mechanisms. First, high levels of BMP signaling ventrally

promote *bmp*, *tolloid*, *tsg*, and *bmper* expression, all BMP-promoting factors (Connors et al., 1999; Little and Mullins, 2004; Rentzsch et al., 2006; Schmid et al., 2000) **(Figure 5.1)**. However, high BMP signaling also induces *sizzled*, which antagonizes BMP signaling by inhibiting Tolloid/Bmp1a cleavage of Chordin (Collavin and Kirschner, 2003; Yabe et al., 2003) **(Figure 5.1)**. High levels of BMP signaling also repress *chordin* expression, restricting it to dorsal regions (Miller-Bertoglio et al., 1999) **(Figure 5.1)**. Additionally, there is a recent report in zebrafish that factors in extraembryonic tissues can initiate a positive feedback loop on BMP signaling (Sun et al., 2014) **(Figure 5.1)**. BMP signaling also induces the expression of *bambi* **(Figure 5.1)**, which encodes a transmembrane protein implicated in attenuating BMP signaling (Grotewold et al., 2001; Onichtchouk et al., 1999; Reichert et al., 2013; Tsang et al., 2000), although loss-of-function studies have yet to determine a role for *bambi* in DV patterning (O'Connor et al., 2009).

Importantly, all of these feedback loops are active after the onset of gastrulation (Hild et al., 1999; Kramer et al., 2002; Nguyen et al., 1998; Reversade and De Robertis, 2005; Schmid et al., 2000) and, therefore, do not contribute to establishing the BMP signaling gradient. However, these feedback mechanisms likely contribute to regulating BMP signaling during gastrulation, when we have described a steepening of the BMP signaling gradient and the prominent roles of Tolloid and Sizzled in this process (Chapter 3). A strategic first step in dissecting this complex network of BMP autoregulatory feedback during gastrulation is applying large-scale, non-biased computational screens. This is being addressed by our collaborators at Purdue University, Xu Wang and David Umulis, who are extending our existing mathematical model of the BMP signaling gradient (Sections 2.2.6-7 and 6.8). After incorporating all of the known feedback mechanisms **(Figure 5.1)** (though the existing model already includes BMP-induced *sizzled*

expression), that model will be fit to wild-type and mutant P-Smad5 profiles progressively during gastrulation. This will identify critically limiting parameters, which can then be directly tested *in vivo*.

5.4.2 Does feedback coordinate DV and AP patterning?

Another aspect of DV patterning that remains to be fully characterized is the role of, and crosstalk between, the autoregulatory transcriptional feedback mechanisms that are activated by both DV and AP signaling. Across zebrafish, *Xenopus*, and mouse, there are known feedback mechanisms that regulate FGF, Nodal, and BMP signaling. FGF and Nodal signaling transcriptionally activate their respective inhibitors. FGF signaling induces the expression of *sprouty* (*spry*) and Spry proteins comprise a major class of FGF/RTK inhibitors (Furthauer et al., 2001; Mason et al., 2006). Nodal signaling induces the expression of Antivin/Lefty proteins, which antagonize Nodal signaling (Bisgrove et al., 1999; Cheng et al., 2000; Meno et al., 1999; Thisse and Thisse, 1999). BMP signaling similarly activates its inhibitor *sizzled*, though BMP signaling also promotes itself through various feedback loops, detailed in the previous section **(Figure 5.1)**.

Transcriptional feedback may be integral to regulate and/or shape FGF, Nodal and BMP signaling gradients. Indeed, studies applying mathematical models support a key role for both activating and inhibitory feedback loops in stabilizing and refining morphogen gradients for pattern formation (Barkai and Shilo, 2009; Inomata et al., 2013; Lee et al., 2009; Meinhardt, 2015b; Muller et al., 2012; Rogers and Schier, 2011; Xue et al., 2014). However, the requirement for these feedback loops and whether they primarily confer robustness to the morphogen gradient or serve to refine the DV and AP pattern remain unknown. In addition to direct *in vivo* experiments addressing feedback mechanisms within each signaling pathway, crosstalk of feedback mechanisms between signaling

pathways remains to be addressed. Though complex, the coordination of multi-pathway feedback mechanisms could represent an important mechanism that links DV and AP patterning, contributes to defining cell competency, and bolsters robust patterning in the highly dynamic environment of the developing embryo.

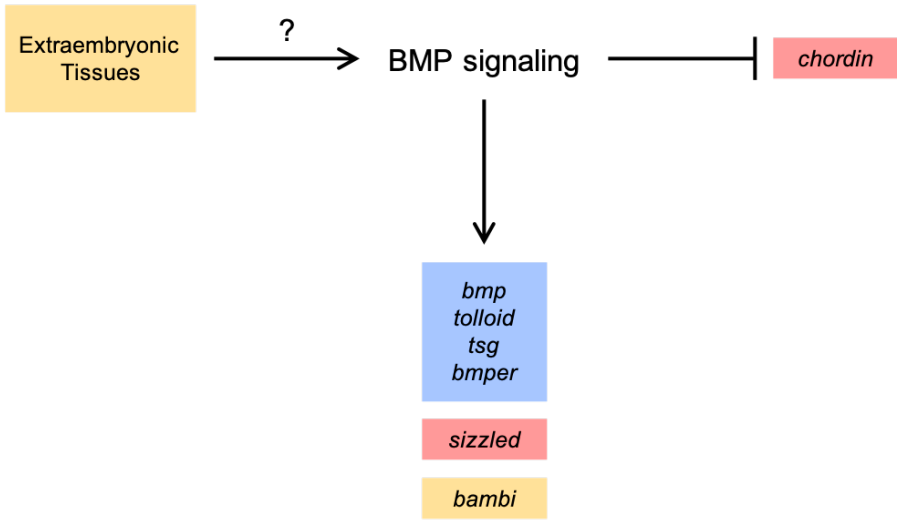

Figure 5.1 BMP signaling autoregulatory feedback loops

Schematic of the known feedback mechanisms affecting BMP signaling. Gene expression shown in italics. Effect of each gene product represented by colored box: blue indicates BMP-promoting, red indicates BMP-inhibiting, and yellow indicates a role yet to be characterized.

CHAPTER 6. Materials and methods

Contributions: This chapter includes methods developed in Zinkski, Tuazon, et al. published in 2019 in *Methods in Molecular Biology* (Zinski et al., 2019) and direct quotes from Tuazon, et al., under revision at *Cell Reports*.

6.1 Zebrafish wild-type and mutant lines

6.1.1 Organism details

Adult zebrafish were kept at 28°C in a 12-hr light/12-hr dark cycle. Most embryos used for experiments were between 0-12 hours post fertilization, with some phenotypes tracked from 1-5 days post fertilization. These were collected and raised at 28°C in E3 solution. In this study, sex/gender is not relevant since zebrafish sex determination takes place after 25 days post fertilization (Santos et al., 2017).

Wild-type (TU)	RRID: ZIRC_ ZL57
chordin^{tt250}	RRID: ZDB-ALT-980413-523, ZIRC_ZL61
tolloid^{tm124a}	RRID: ZDB-ALT-001220-2, ZIRC_ZL464
bmp1a^{t31169}	RRID: ZDB-ALT-061101-360, EZRC_9002
bmp1a^{sa2416}	RRID: ZDB-ALT-120411-333
sizzled^{rk1}	RRID: ZDB-ALT-030530-2
sizzled^{tm305}	RRID: ZDB-ALT-980203-1563, ZIRC_ ZL830, EZRC_750

6.1.2 Genotyping of mutant alleles

Genotyping of adults and embryos for the following alleles was performed using KASPar genotyping (Smith and Maughan, 2015). Primers were designed and generated by LGC Bioscience Technologies (previously KBioscience) to the following sequences flanking the [WT/mutant] nucleotide:

chordin^{tt250}	GTTTGGTGTGATGCACTGCGTTATGTGTCATTGTGAGCCG[G/A] TGAGTTGTGCACAGTTCAGTTTGAAATCCATATTGAATCT

tolloid^{tm124a}	TGGAGGAGTCATCCCTTACGTCATAGGAGGCAACTTCACC[G/T] GTAAGAGGACTAAGTGTTTGCCTTTTCAGCATCAATGTGT
bmp1a^{t31169}	GCACACGCGACCCGACAGAGACGAACACGTCAGTATCATA[C/T] GAGACAACATTCAGCCAGGTAGGAGAAAAAAACTGTAGGG
bmp1a^{sa2416}	CGAGAGGCATGATAACTGTGCGTACGACTACCTGGAGGTT[C/T] GAGACGGGAACTCRGAAAGCAGCCCGCTTTTGGGCAGGTT
sizzled^{rk1}	CCTTCGTCTGCTCGCTCATCGCCCCTGTATGCCTCGACAG[G/A] TACGTGTTGAGACACCTAAAATATTATGAGAAATACACAT

sizzled^{tm305} was genotyped as described in (Yabe et al., 2003) by using the primer pair 5'-CCTCGATCTGACGACTTGAGGA-3' and 5'-GCCAGTTCTAAATCATGAGCTACAC-3'. The amplified PCR product was digested with *Taq*α*-1*, which cleaves the wild-type allele but not the mutant.

6.1.3 Mutant embryo pictures

All embryos were photographed using a Leica IC80HD at 12-48 hpf, as indicated. Brightness, contrast, and color balance were adjusted in the whole image in Photoshop.

6.1.4 Maintenance of *bmp1a* mutants

bmp1a^{t31169} fish were a gift from M. Harris. As previously reported, *bmp1a*^{t31169} homozygous females would not lay (Bowen et al., 2012). Despite these females being gravid with mature oocytes, attempts at isolating eggs for *in vitro* fertilization were also

unsuccessful. However, by outcrossing *bmp1a*^{t31169} to the AB wild-type background, we were able to generate homozygous females that laid over multiple generations.

6.1.5 Generation of *bmp1a* in-tube controls

Since M-*bmp1a* embryos are generated by crossing a *bmp1a*$^{t31169/t31169}$ or *bmp1a*$^{sa2416/sa2416}$ female to a wild-type (Tu) male, all progeny are M-*bmp1a* mutants. As such, there is no possibility for wild-type sibling controls for P-Smad5 and *in situ* DV marker analysis. The same is true for MZ-*bmp1a* mutants, whose siblings are M-*bmp1a*. To circumvent this, we added stage-matched wild-type embryos to the same Eppendorf tube as M- or MZ-*bmp1a* embryos prior to fixation and then fixed, stained, imaged, and processed both genotypes together. These in-tube wild-type controls (indicated by an asterisk in all figures) were identified by genotyping after imaging, ensuring that the M-*bmp1a* phenotype is not an artifact and analysis was blinded. In-tube controls were pooled with *tolloid/+* or *sizzled/+* sibling controls when appropriate.

6.2 *in situ* hybridization and domain size measurement

Whole-mount *in situ* hybridizations were performed using DIG-labeled anti-sense RNA probes (made with labeling kit: Roche 11277073910) to *pax2.1, krox20, bmp1a* and *sizzled* (gifts from M. Hibi), *chordin*, *gata2, foxb1a* (also known as *fkd3* and *foxb1.2*)*, otx2,* and *gbx1*. Probes were visualized with anti-DIG-Alkaline Phosphatase (Roche 11093274910) developed with BM Purple (Roche 11442074001). Embryos were photographed using a Leica IC80HD either in PBS or cleared in BABB, a 1:2 ratio of benzyl alcohol (Sigma B-1042) and benzyl benzoate (Sigma B-6630). Images were processed

using ImageJ and animal view domain sizes determined by fitting a circle to each embryo and measuring the domain size angle at the circle center-point.

6.3 Fluorescent *in situ* hybridization of *tolloid*

Embryos were fixed with 4% PFA at room temperature for 4 hours, gradually dehydrated in methanol, and then incubated with Pretreat 3 (ACD #320045) at room temperature for 15 minutes to permeate the embryos. RNAscope probes *chordin-C1* (ACD #440081) and *tolloid-C2* (ACD #475501-C2) were hybridized at 40°C for 16 hours. RNAscope Fluorescent multiplex detection reagents (ACD #320851) were used to stain the probes, specifically AltC was used for Amp4 in the staining kit, and DAPI was used to stain the nuclei.

6.3.1 Imaging

Whole embryos were mounted with the animal region on the top and imaged with a 20×/1.0 Plan-Apochromat water immersion lens (D = 0.17 M27 75 mm). *tolloid* and *chordin* mRNA signals were imaged by 647nm and 555nm excitation wavelengths, respectively. XY pixels were 0.312 μm and Z pixels were 3 μm. The bottom 10% of each embryo (excluding the YSL) was extracted as the marginal layer and converted to a maximum projection image.

6.3.2 Quantification

tolloid signal was segmented using a Gaussian filter to remove background and normalize each pixel from 0 to 1. All pixels above 0.08 and lower than 0.3 were extracted and the bwlabeln MATLAB function used to find all mRNA spots. The mRNA distribution was

extracted by arranging each spot on a coordinate system. First, the center of the mRNA circle was moved to the (0,0) position in an x,y plane. Then, mRNA spot position was rotated based on the *chordin* expression, which defines dorsal. Finally, the mRNA spot number was calculated every 10 degrees and the two sides of the margin averaged to generate the ventral to dorsal profile of *tolloid* distribution.

6.4 Quantitative P-Smad5 assay

P-Smad5 immunostaining, imaging, and quantification were performed as previous described (Zinski et al., 2017), with the protocol and methodology thoroughly described in Zinski et al. (2019).

6.4.1 Immunostaining and image acquisition

Briefly, embryos were fixed in 4% paraformaldehyde at 4°C, blocked in NCS-PBST, and probed overnight with a 1:100 dilution of anti-phosphoSmad1/5/8 antibody (Cell Signaling Technology Cat# 13820, RRID:AB_2493181), followed by a 1:500 dilution of goat anti-rabbit Alexa Fluor 647 (Molecular Probes Cat# A-21244, RRID:AB_141663) and a 1:2000 dilution of Sytox Green (ThermoFisher Scientific Cat# S7020). For timepoints 24 hpf and later, embryos were additionally permeabilized in acetone after fixation.

Embryos were cleared and mounted in BABB, a 1:2 ratio of benzyl alcohol (Sigma B-1042) and benzyl benzoate (Sigma B-6630). Mounted embryos were imaged on a Zeiss LSM710 or LSM880 confocal microscope with an LD LCI Plan-Achromat 25X/0.8 Imm Corr DIC M27 multi-immersion lens in the oil-immersion setting. A single bead from a calibration slide (ThermoFisher Scientific Cat#F369009, well A1) was imaged between embryos to account for any fluctuations in laser power.

6.4.2 Gradient quantification

Post-acquisition P-Smad5 analysis utilized a custom MATLAB algorithm to identify individual nuclei center-points and extract P-Smad5 intensities in each nucleus (Zinski et al., 2017; Zinski et al., 2019), which were normalized based on a standard calibration bead intensity. Resulting embryos were aligned across the DV axis and conformed using Coherent Point Drift. Population means were generated after genotyping for in-tube/heterozygous sibling controls since all imaging and analysis was performed blinded. Mean profiles were generated by averaging P-Smad5 intensities of cells in a 30μm band either at the margin or more animal positions. 3-D embryo-wide displays of mean P-Smad5 were generated by projecting all nuclei on a sphere divided into 4800 equilateral triangles and nuclei within each triangle averaged together. Nuclei density was similarly displayed, with a heatmap depicting nuclei number within each triangle relative to the total number of nuclei. We confirmed that the nuclei density of each individual embryo matched the qualitative features of the stage being investigated, detailed in **Figure 3.2**. MATLAB algorithms used for analysis have been previously published (Zinski et al., 2017; Zinski et al., 2019).

It was not possible to generate population means for embryos 7 hpf and later. Embryos at these later stages were too large to be imaged in full by the 25X objective used and these irregularly incomplete embryos could not be registered together. Qualitative P-Smad5 gradient shape analysis was performed by thresholding the maximum and minimum P-Smad5 signal populations and quantifying the distance by assuming a nuclei diameter of 6μm and total embryo diameter 700μm.

For stages 24 hpf and later, relative P-Smad5 intensities were analyzed qualitatively, either by maximum projection analysis in ImageJ or segmentation of the P-Smad5 signal in Imaris.

6.5 Generating Immobile Chordin

Membrane-tethered Chordin was generated by by inserting the rat *CD2* cDNA fragment from the *sog-CD2* construct (a gift from H. Ashe) used for similar experiments in *Drosophila* (Ashe and Levine, 1999). The *CD2* fragment (which lacks the signal sequence) was amplified by PCR with an additional N-terminal *ClaI* site and inserted in-frame at the *ClaI* site in zebrafish *chordin*-PCS2, which is upstream of the *stop* codon. An N-terminal HA epitope tag was also inserted downstream of the *chordin* signal sequence.

6.6 Embryo microinjection

Embryos were injected with 2-3ng of *tll1* MO1 (GCAGAGTAAAGGTAGTCCATCTGAG) at the 1-cell stage. mRNA for *HA-Chordin* and *HA-Chordin-CD2* were generated using the SP6 MMessage Machine kit (ThermoFisher Science AM1340) and *H3.3-mCherry* mRNA was a gift from AJ Lucy. 800pg of *HA-Chordin* and *HA-Chordin-CD2* were injected at the 1-cell stage for HA-immunostaining and localization analysis. For regional expression, 250-900pg of *HA-Chordin-CD2* with 500pg of *H3.3-mCherry* was injected into a single blastomere at the 16-32-cell stage (total injection volume was no more than 0.5nl).

6.7 HA immunostaining and imaging

Embryos injected with 800pg of *HA-Chordin* or *HA-Chordin-CD2* at the 1-cell stage were fixed in 4% paraformaldehyde at 4°C, blocked in NCS-PBST, and probed overnight with a 1:500 dilution of rabbit anti-HA (Thermo Fisher Scientific Cat# 71-5500, RRID:AB_2533988) and 1:1000 dilution of mouse anti-β-catenin (BD Biosciences Cat# 610153, RRID:AB_397554). This was followed by incubation in a 1:500 dilution of goat anti-rabbit Alexa Fluor 594 (Thermo Fisher Scientific Cat# A-11037, RRID:AB_2534095), a 1:500 dilution of goat anti-mouse Alexa Fluor 633 (Thermo Fisher Scientific Cat# A-21126, RRID:AB_2535768), and a 1:2000 dilution of Sytox Green (ThermoFisher Scientific Cat# S7020). Embryos were imaged on a Zeiss LSM880 confocal microscope with a C-Apochromat 40X/1.2 NA W Corr objective.

6.8 Mathematical modeling

6.8.1 Reaction-diffusion equations

The system of partial differential equations (PDE) listed below, and in **Supplemental Figure 2.5A**, describes zebrafish development from blastula to early gastrula stages (3.5 hpf to 5.7 hpf). BMP ligand, Chordin, Noggin and Sizzled are denoted by *B*, *C*, *N* and *S*, and the complexes of BMP-Chordin and BMP-Noggin are denoted by *BC* and *BN*, respectively. The embryo is divided into 36 nodes from ventral (x=0) to dorsal (x=700μm). PDE were solved as before (Zinski et al., 2017), with either 100,000 or 1 million groups of known and randomly varied parameters **(Tables 1, 3-5, and 7)** and proteins symmetrically distributed. For each parameter matrix, the model was solved in

wild-type and 6 loss of function conditions: for *chordin, noggin,* and *sizzled* loss of function, the production rate was set to zero; for M-*bmp1a* and *tolloid* single mutants and M-*bmp1a;tolloid* double mutants, the λ (maximum degradation velocity) of the corresponding protein was set to zero. The normalized root-mean-square deviation (NRMSD) between each model and the corresponding P-Smad5 profile was calculated to find the best fit models (see Quantification and Statistical Analysis section for more detail).

1) $\frac{\partial B}{\partial t} = D_B \frac{\partial^2 B}{\partial x^2} + \phi_B(x) + \lambda_{tBC} \cdot \frac{1}{1+S/kit+(C+BC)/kmt} \cdot BC + \lambda_{aBC} \cdot \frac{1}{1+S/kia+(C+BC)/kma} \cdot BC - k_{onC} B \cdot C + k_{offC} BC - k_{onN} B \cdot N + k_{offN} BN - dec_B B$

2) $\frac{\partial C}{\partial t} = D_C \frac{\partial^2 C}{\partial x^2} + \phi_C(x) - \lambda_{tC} \cdot \frac{1}{1+S/kit+(C+BC)/kmt} \cdot C - \lambda_{aC} \cdot \frac{1}{1+S/kia+(C+BC)/kma} \cdot C - k_{onC} B \cdot C + k_{offC} BC - dec_C C$

3) $\frac{\partial N}{\partial t} = D_N \frac{\partial^2 N}{\partial x^2} + \phi_N(x) - k_{onN} B \cdot N + k_{offN} BN - dec_N N$

4) $\frac{\partial BC}{\partial t} = D_{BC} \frac{\partial^2 BC}{\partial x^2} - \lambda_{tBC} \cdot \frac{1}{1+S/kit+(C+BC)/kmt} \cdot BC - \lambda_{aBC} \cdot \frac{1}{1+S/kia+(C+BC)/kma} \cdot BC + k_{onC} B \cdot C - k_{offC} BC - dec_{BC} BC$

5) $\frac{\partial BN}{\partial t} = D_{BN} \frac{\partial^2 BN}{\partial x^2} + k_{onN} B \cdot N - k_{offN} BN - dec_{BN} BN$

6) $\frac{\partial S}{\partial t} = D_S \frac{\partial^2 S}{\partial x^2} + \frac{Vs \cdot B^n}{K^n + B^n} - dec_S S$

7) $\frac{etaS}{Vs} = \frac{p * b^n}{\frac{K}{B0}^n + b^n}$

6.8.2 Model Input

Production regions of BMP, Chordin and Noggin **(Figure 2.5D)** were previously determined (Zinski et al., 2017). Production rates (ϕ) of BMP, Chordin and Noggin are not known and were screened as varied parameters Chordin and BMP decay rates and BMP diffusion were fixed based on recent measurements (Pomreinke et al., 2017; Zinski et al., 2017). The production region of Tolloid was determined by RNAscope **(Figure 2.5A-D and Supplemental Figure 2.6)** and Bmp1a by alkaline phosphatase *in situ* **(Figures 2.5D and 2.1B)**. The λ term represents the maximum degradation velocity of Chordin or BMP-

Chordin by the proteinase Tolloid (λ_t) or Bmp1a (λ_a), as indicated. These, as well as the Michaelis constants of Tolloid (*kmt*) and Bmp1a (*kma*), were screened as varied parameters.

Since *sizzled* expression is induced by BMP signaling **(Figure 2.4A)** (Yabe et al., 2003), Sizzled was considered a target of BMP signaling that could be described by the Hill equation (the second term in Equation 6), which was transformed to Equation 7 to compress parameters. *etaS* represents the production of Sizzled and *Vs* is the maximum of Sizzled expression, so *etaS*/*Vs* (Equation 7) describes the shape of Sizzled expression from ventral to dorsal. B0 is the maximum of BMP and *b* is B/B0, which can be described by the pSmad distribution. Following the Hill equation, *p* is the scaled parameter, *K* is concentration of BMP at half-maximum, and *n* is the gene-control cooperativity parameter.

To determine the fixed values of *p*, *n*, and K/B0 we measured the distribution of *sizzled* mRNA (*etaS*/*Vs*) and compared it directly to the stage-matched distribution of P-Smad5 (*b*) **(Supplemental Figure 2.5C-E)**. Interestingly, the *sizzled* expression profile is narrower overall than the P-Smad5 profile, which presumably drives *sizzled* expression. Using the Lsqnonlin nonlinear data-fitting function in MATLAB, we fit the distributions **(Supplemental Figure 2.5C-D)**:

$etaS/V_s$= exp(-(x-23.19)/50)/(0.02+exp(-(x-23.19)/50))

b = exp(-(x-1828000)/714400)/(0.2+exp((x-427.7)/61.26))

Combining these expressions in Equation 7, we solved for *p* (=164), *n* (=4), and K/B0 **(Supplemental Figure 2.5E)**, which became fixed values in all of our simulations as we calculate saturation and production kinetics. A previous model of Sizzled in zebrafish used an *n* value of 20 (Pomreinke et al., 2017), which is essentially a switch-like behavior. This would theoretically require 20 P-Smad5 binding sites on the *sizzled* promoter, while our

analysis of the putative regulatory region suggests only 4 binding sites (Farre et al., 2003; Messeguer et al., 2002).

Cooperative Parameter/ Hill Coefficient	*n*	4
Scaled Parameter	*p*	164
K/B0		4.1

Initially, we generated B0 in 1 million parameter simulations. We ran the model with only BMP, Chordin and Noggin and B0 was the maximum of BMP in Chordin-/-. These B0 values were used to determine Sizzled expression and the *ki* range. *ki* is the dissociation constant of Tolloid (*kit*) or Bmp1a (*kia*) with Sizzled, which is described as a competitive inhibitor (Lee et al., 2006). To determine the *ki* range for our parameter screen, we calculated the maximum of Sizzled based on B0 and the corresponding *ki* was assigned a random value between 1/10 and 10 times the maximum of Sizzled.

6.8.3 Screens of Tolloid and Bmp1a expression dynamics

The inputs and expression dynamics conditions tested are listed in **Tables 1-2**. For each group, we ran 100,000 simulations as described above, though BN and BC decay terms (Equations 4 and 5) were not included. The number of solutions that fit measured WT, M-*bmp1a* and *tolloid* single mutant, and M-*bmp1a;tolloid* double mutant P-Smad5 profiles (NRMSD <0.12) was compared to determine the optimal combination of expression conditions **(Supplemental Figure 2.5F and Table 2)**. To determine the optimal onset time of Tolloid expression, we ran eleven screens (100,000 simulations each) with the onset time for each screen set at distinct 12-minute intervals **(Supplemental Figure 2.5G)**. Again, the number of solutions that fit measured WT, M-*bmp1a* and *tolloid* single mutant,

and M-*bmp1a;tolloid* double mutant P-Smad5 profiles (NRMSD<0.12) was compared to determine the optimal onset time **(Supplemental Figure 2.5H-I)**.

6.8.4 Large-scale screens

After determining optimal Bmp1a/Tolloid input conditions **(Figure 2.5D-E)**, as described above, we performed 1 million simulations with the inputs listed in **Tables 3-5**. Initially, when we fixed D_C at the published value of 7 um^2/s (Pomreinke et al., 2017), there were no solutions that adequately fit all our mutant profiles **(Tables 3 and 6)**. When we varied D_C up to 50 um^2/s we almost tripled the number of solutions fitting the M-*bmp1a;tolloid* profile, but M-*bmp1a* remained constraining **(Tables 4 and 6)**. This was not due to Tolloid onset time since 5.3 hpf was still optimal for fitting the M-*bmp1a* profile alone with wild-type **(Supplemental Figure 2.5I)**. Instead, in these solutions we found that production rates ϕ_B and ϕ_C were restricted to much lower ranges (0.01–1 nM/s and 0.1–10 nM/s, respectively) and ϕ_B was consistently less than ϕ_C. By repeating the model under these conditions, we doubled the number of M-*bmp1a* fitting solutions and were able to generate 16 good-fitting solutions (NRMSD<0.11 for wt, *tolloid*, *chordin*, and *sizzled*; <0.06 for M-*bmp1a* and M-*bmp1a;tolloid*) **(Tables 5 and 6)**.

6.8.5 Immobile Chordin Simulations

1 million simulations were performed with immobile Chordin (D_C = 0) in a M-*bmp1a;tolloid* double mutant background (λ_t=0, λ_a =0) and the initial and final positions the immobile Chordin domain varied by 5° intervals from 0-180°, or ~19μm intervals from 0-700μm **(Table 7)**, though BN and BC decay terms (Equations 4 and 5) were not included. Solutions were fit with the wild-type P-Smad5 profiles (NRMSD < 0.08), giving 62,047 total solutions. Since BMP production (ϕ_B) was varied over a larger range (0.01–100 nM/s) than

what we found to be relevant **(Figure 2.5F)**, we excluded solutions with ϕ_B greater than 1nM/s, giving 40615 total solutions. Solutions were classified in **Figure 2.6A-A'** as dorsal, lateral, or ventral based on the dorsal-most site of the region: ventral as 0-60°, lateral as60-120°, and dorsal as 120-180°.

6.9 Quantification and statistical analyses

6.9.1 Bmp1a and Tolloid Comparison

Amino acid sequences of zebrafish Bmp1a and Tolloid were compared using LALIGN Pairwise Sequence Alignment (Chojnacki et al., 2017).

6.9.2 Comparing P-Smad5 profiles

To determine if two P-Smad5 profiles were significantly different, two-tailed T-Tests were performed with a 5% significance level. Profiles shown represent the mean with errors bars indicating standard deviation. Exact values of n and number of replicates can be found in the figure legends.

6.9.3 Comparing DV marker expression domains

To determine if domain sizes of DV markers were significantly different, angle measurements were input into GraphPad Prism and two-tailed T-Tests were performed with a 5% significance level. Exact values of n and number of replicates can be found in the figure legends.

6.9.4 Defining best-fit model solutions

Best-fit model solutions were determined by normalized root-mean-square deviation (NRMSD) error thresholds. Relative threshold NRMSD values were calculated based on the standard deviation observed in each P-Smad5 profile.

BIBLIOGRAPHY

Agathon, A., Thisse, C., and Thisse, B. (2003). The molecular nature of the zebrafish tail organizer. Nature *424*, 448-452.

Agius, E., Oelgeschlager, M., Wessely, O., Kemp, C., and De Robertis, E.M. (2000). Endodermal Nodal-related signals and mesoderm induction in Xenopus. Development *127*, 1173-1183.

Alsina, B., and Whitfield, T.T. (2017). Sculpting the labyrinth: Morphogenesis of the developing inner ear. Semin Cell Dev Biol *65*, 47-59.

Amaya, E., Musci, T.J., and Kirschner, M.W. (1991). Expression of a dominant negative mutant of the FGF receptor disrupts mesoderm formation in Xenopus embryos. Cell *66*, 257-270.

Ambrosio, A.L., Taelman, V.F., Lee, H.X., Metzinger, C.A., Coffinier, C., and De Robertis, E.M. (2008). Crossveinless-2 Is a BMP feedback inhibitor that binds Chordin/BMP to regulate Xenopus embryonic patterning. Dev Cell *15*, 248-260.

Angerer, L., Hussain, S., Wei, Z., and Livingston, B.T. (2006). Sea urchin metalloproteases: a genomic survey of the BMP-1/tolloid-like, MMP and ADAM families. Dev Biol *300*, 267-281.

Armes, N.A., and Smith, J.C. (1997). The ALK-2 and ALK-4 activin receptors transduce distinct mesoderm-inducing signals during early Xenopus development but do not co-operate to establish thresholds. Development *124*, 3797-3804.

Asharani, P.V., Keupp, K., Semler, O., Wang, W., Li, Y., Thiele, H., Yigit, G., Pohl, E., Becker, J., Frommolt, P.*, et al.* (2012). Attenuated BMP1 function compromises osteogenesis, leading to bone fragility in humans and zebrafish. Am J Hum Genet *90*, 661-674.

Ashe, H.L., and Briscoe, J. (2006). The interpretation of morphogen gradients. Development *133*, 385-394.

Ashe, H.L., and Levine, M. (1999). Local inhibition and long-range enhancement of Dpp signal transduction by Sog. Nature *398*, 427-431.

Balaskas, N., Ribeiro, A., Panovska, J., Dessaud, E., Sasai, N., Page, K.M., Briscoe, J., and Ribes, V. (2012). Gene regulatory logic for reading the Sonic Hedgehog signaling gradient in the vertebrate neural tube. Cell *148*, 273-284.

Bang, A.G., Papalopulu, N., Goulding, M.D., and Kintner, C. (1999). Expression of Pax-3 in the lateral neural plate is dependent on a Wnt-mediated signal from posterior nonaxial mesoderm. Dev Biol *212*, 366-380.

Barkai, N., and Shilo, B.Z. (2009). Robust generation and decoding of morphogen gradients. Cold Spring Harb Perspect Biol *1*, a001990.

Bazzini, A.A., Lee, M.T., and Giraldez, A.J. (2012). Ribosome profiling shows that miR-430 reduces translation before causing mRNA decay in zebrafish. Science *336*, 233-237.

Beck, C.W., Whitman, M., and Slack, J.M. (2001). The role of BMP signaling in outgrowth and patterning of the Xenopus tail bud. Dev Biol *238*, 303-314.

Begemann, G., Marx, M., Mebus, K., Meyer, A., and Bastmeyer, M. (2004). Beyond the neckless phenotype: influence of reduced retinoic acid signaling on motor neuron development in the zebrafish hindbrain. Dev Biol *271*, 119-129.

Bellipanni, G., Varga, M., Maegawa, S., Imai, Y., Kelly, C., Myers, A.P., Chu, F., Talbot, W.S., and Weinberg, E.S. (2006). Essential and opposing roles of zebrafish beta-catenins in the formation of dorsal axial structures and neurectoderm. Development *133*, 1299-1309.

Bhat, N., Kwon, H.J., and Riley, B.B. (2013). A gene network that coordinates preplacodal competence and neural crest specification in zebrafish. Dev Biol *373*, 107-117.

Bier, E., and De Robertis, E.M. (2015). EMBRYO DEVELOPMENT. BMP gradients: A paradigm for morphogen-mediated developmental patterning. Science *348*, aaa5838.

Bisgrove, B.W., Essner, J.J., and Yost, H.J. (1999). Regulation of midline development by antagonism of lefty and nodal signaling. Development *126*, 3253-3262.

Blader, P., Rastegar, S., Fischer, N., and Strahle, U. (1997). Cleavage of the BMP-4 antagonist chordin by zebrafish tolloid. Science *278*, 1937-1940.

Bowen, M.E., Henke, K., Siegfried, K.R., Warman, M.L., and Harris, M.P. (2012). Efficient mapping and cloning of mutations in zebrafish by low-coverage whole-genome sequencing. Genetics *190*, 1017-1024.

Branam, A.M., Hoffman, G.G., Pelegri, F., and Greenspan, D.S. (2010). Zebrafish chordin-like and chordin are functionally redundant in regulating patterning of the dorsoventral axis. Dev Biol *341*, 444-458.

Brennan, J., Lu, C.C., Norris, D.P., Rodriguez, T.A., Beddington, R.S., and Robertson, E.J. (2001). Nodal signalling in the epiblast patterns the early mouse embryo. Nature *411*, 965-969.

Briscoe, J., and Small, S. (2015). Morphogen rules: design principles of gradient-mediated embryo patterning. Development *142*, 3996-4009.

Cabrita, M.A., and Christofori, G. (2008). Sprouty proteins, masterminds of receptor tyrosine kinase signaling. Angiogenesis *11*, 53-62.

Cai, A.Q., Radtke, K., Linville, A., Lander, A.D., Nie, Q., and Schilling, T.F. (2012). Cellular retinoic acid-binding proteins are essential for hindbrain patterning and signal robustness in zebrafish. Development *139*, 2150-2155.

Chen, C., and Shen, M.M. (2004). Two modes by which Lefty proteins inhibit nodal signaling. Curr Biol *14*, 618-624.

Chen, Y., and Schier, A.F. (2001). The zebrafish Nodal signal Squint functions as a morphogen. Nature *411*, 607-610.

Chen, Y., and Schier, A.F. (2002). Lefty proteins are long-range inhibitors of squint-mediated nodal signaling. Curr Biol *12*, 2124-2128.

Cheng, A.M., Thisse, B., Thisse, C., and Wright, C.V. (2000). The lefty-related factor Xatv acts as a feedback inhibitor of nodal signaling in mesoderm induction and L-R axis development in xenopus. Development *127*, 1049-1061.

Cho, G.S., Choi, S.C., and Han, J.K. (2013). BMP signal attenuates FGF pathway in anteroposterior neural patterning. Biochem Biophys Res Commun *434*, 509-515.

Chojnacki, S., Cowley, A., Lee, J., Foix, A., and Lopez, R. (2017). Programmatic access to bioinformatics tools from EMBL-EBI update: 2017. Nucleic Acids Res *45*, W550-W553.

Christen, B., and Slack, J.M. (1997). FGF-8 is associated with anteroposterior patterning and limb regeneration in Xenopus. Dev Biol *192*, 455-466.

Christian, J.L., and Moon, R.T. (1993). Interactions between Xwnt-8 and Spemann organizer signaling pathways generate dorsoventral pattern in the embryonic mesoderm of Xenopus. Genes Dev *7*, 13-28.

Collavin, L., and Kirschner, M.W. (2003). The secreted Frizzled-related protein Sizzled functions as a negative feedback regulator of extreme ventral mesoderm. Development *130*, 805-816.

Collery, R.F., and Link, B.A. (2011). Dynamic smad-mediated BMP signaling revealed through transgenic zebrafish. Dev Dyn *240*, 712-722.

Cong, L., Ran, F.A., Cox, D., Lin, S., Barretto, R., Habib, N., Hsu, P.D., Wu, X., Jiang, W., Marraffini, L.A*., et al.* (2013). Multiplex genome engineering using CRISPR/Cas systems. Science *339*, 819-823.

Connors, S.A., Trout, J., Ekker, M., and Mullins, M.C. (1999). The role of tolloid/mini fin in dorsoventral pattern formation of the zebrafish embryo. Development *126*, 3119-3130.

Connors, S.A., Tucker, J.A., and Mullins, M.C. (2006). Temporal and spatial action of tolloid (mini fin) and chordin to pattern tail tissues. Dev Biol *293*, 191-202.

Cox, W.G., and Hemmati-Brivanlou, A. (1995). Caudalization of neural fate by tissue recombination and bFGF. Development *121*, 4349-4358.

Dal-Pra, S., Furthauer, M., Van-Celst, J., Thisse, B., and Thisse, C. (2006). Noggin1 and Follistatin-like2 function redundantly to Chordin to antagonize BMP activity. Dev Biol *298*, 514-526.

Dale, L., Howes, G., Price, B.M., and Smith, J.C. (1992). Bone morphogenetic protein 4: a ventralizing factor in early Xenopus development. Development *115*, 573-585.

Darnell, D.K., Stark, M.R., and Schoenwolf, G.C. (1999). Timing and cell interactions underlying neural induction in the chick embryo. Development *126*, 2505-2514.

De Robertis, E.M. (2006). Spemann's organizer and self-regulation in amphibian embryos. Nat Rev Mol Cell Biol *7*, 296-302.

De Robertis, E.M., and Moriyama, Y. (2016). The Chordin Morphogenetic Pathway. Curr Top Dev Biol *116*, 231-245.

De Robertis, E.M., and Sasai, Y. (1996). A common plan for dorsoventral patterning in Bilateria. Nature *380*, 37-40.

Dick, A., Hild, M., Bauer, H., Imai, Y., Maifeld, H., Schier, A.F., Talbot, W.S., Bouwmeester, T., and Hammerschmidt, M. (2000). Essential role of Bmp7 (snailhouse) and its prodomain in dorsoventral patterning of the zebrafish embryo. Development *127*, 343-354.

Dick, A., Meier, A., and Hammerschmidt, M. (1999). Smad1 and Smad5 have distinct roles during dorsoventral patterning of the zebrafish embryo. Dev Dyn *216*, 285-298.

Dixon Fox, M., and Bruce, A.E. (2009). Short- and long-range functions of Goosecoid in zebrafish axis formation are independent of Chordin, Noggin 1 and Follistatin-like 1b. Development *136*, 1675-1685.

Doniach, T. (1995). Basic FGF as an inducer of anteroposterior neural pattern. Cell *83*, 1067-1070.

Dorey, K., and Amaya, E. (2010). FGF signalling: diverse roles during early vertebrate embryogenesis. Development *137*, 3731-3742.

Dorsky, R.I., Itoh, M., Moon, R.T., and Chitnis, A. (2003). Two tcf3 genes cooperate to pattern the zebrafish brain. Development *130*, 1937-1947.

Dorsky, R.I., Sheldahl, L.C., and Moon, R.T. (2002). A transgenic Lef1/beta-catenin-dependent reporter is expressed in spatially restricted domains throughout zebrafish development. Dev Biol *241*, 229-237.

Draper, B.W., Stock, D.W., and Kimmel, C.B. (2003). Zebrafish fgf24 functions with fgf8 to promote posterior mesodermal development. Development *130*, 4639-4654.

Dubrulle, J., Jordan, B.M., Akhmetova, L., Farrell, J.A., Kim, S.H., Solnica-Krezel, L., and Schier, A.F. (2015). Response to Nodal morphogen gradient is determined by the kinetics of target gene induction. Elife *4*.

Durston, A.J., Timmermans, J.P., Hage, W.J., Hendriks, H.F., de Vries, N.J., Heideveld, M., and Nieuwkoop, P.D. (1989). Retinoic acid causes an anteroposterior transformation in the developing central nervous system. Nature *340*, 140-144.

Dutko, J.A., and Mullins, M.C. (2011). SnapShot: BMP signaling in development. Cell *145*, 636, 636 e631-632.

Dyer, C., Blanc, E., Hanisch, A., Roehl, H., Otto, G.W., Yu, T., Basson, M.A., and Knight, R. (2014). A bi-modal function of Wnt signalling directs an FGF activity gradient to spatially regulate neuronal differentiation in the midbrain. Development *141*, 63-72.

Eivers, E., Fuentealba, L.C., and De Robertis, E.M. (2008). Integrating positional information at the level of Smad1/5/8. Curr Opin Genet Dev *18*, 304-310.

Erter, C.E., Solnica-Krezel, L., and Wright, C.V. (1998). Zebrafish nodal-related 2 encodes an early mesendodermal inducer signaling from the extraembryonic yolk syncytial layer. Dev Biol *204*, 361-372.

Erter, C.E., Wilm, T.P., Basler, N., Wright, C.V., and Solnica-Krezel, L. (2001). Wnt8 is required in lateral mesendodermal precursors for neural posteriorization in vivo. Development *128*, 3571-3583.

Fainsod, A., Deissler, K., Yelin, R., Marom, K., Epstein, M., Pillemer, G., Steinbeisser, H., and Blum, M. (1997). The dorsalizing and neural inducing gene follistatin is an antagonist of BMP-4. Mech Dev *63*, 39-50.

Farre, D., Roset, R., Huerta, M., Adsuara, J.E., Rosello, L., Alba, M.M., and Messeguer, X. (2003). Identification of patterns in biological sequences at the ALGGEN server: PROMO and MALGEN. Nucleic Acids Res *31*, 3651-3653.

Fauny, J.D., Thisse, B., and Thisse, C. (2009). The entire zebrafish blastula-gastrula margin acts as an organizer dependent on the ratio of Nodal to BMP activity. Development *136*, 3811-3819.

Faure, S., Lee, M.A., Keller, T., ten Dijke, P., and Whitman, M. (2000). Endogenous patterns of TGFbeta superfamily signaling during early Xenopus development. Development *127*, 2917-2931.

Fekany-Lee, K., Gonzalez, E., Miller-Bertoglio, V., and Solnica-Krezel, L. (2000). The homeobox gene bozozok promotes anterior neuroectoderm formation in zebrafish through negative regulation of BMP2/4 and Wnt pathways. Development *127*, 2333-2345.

Feldman, B., Concha, M.L., Saude, L., Parsons, M.J., Adams, R.J., Wilson, S.W., and Stemple, D.L. (2002). Lefty antagonism of Squint is essential for normal gastrulation. Curr Biol *12*, 2129-2135.

Feldman, B., Gates, M.A., Egan, E.S., Dougan, S.T., Rennebeck, G., Sirotkin, H.I., Schier, A.F., and Talbot, W.S. (1998). Zebrafish organizer development and germ-layer formation require nodal-related signals. Nature *395*, 181-185.

Feng, X.H., and Derynck, R. (2005). Specificity and versatility in tgf-beta signaling through Smads. Annu Rev Cell Dev Biol *21*, 659-693.

Fisher, S., Amacher, S.L., and Halpern, M.E. (1997). Loss of cerebum function ventralizes the zebrafish embryo. Development *124*, 1301-1311.

Fisher, S., and Halpern, M.E. (1999). Patterning the zebrafish axial skeleton requires early chordin function. Nat Genet *23*, 442-446.

Flores, M.V., Lam, E.Y., Crosier, K.E., and Crosier, P.S. (2008). Osteogenic transcription factor Runx2 is a maternal determinant of dorsoventral patterning in zebrafish. Nat Cell Biol *10*, 346-352.

Fuentealba, L.C., Eivers, E., Ikeda, A., Hurtado, C., Kuroda, H., Pera, E.M., and De Robertis, E.M. (2007). Integrating patterning signals: Wnt/GSK3 regulates the duration of the BMP/Smad1 signal. Cell *131*, 980-993.

Furthauer, M., Reifers, F., Brand, M., Thisse, B., and Thisse, C. (2001). sprouty4 acts in vivo as a feedback-induced antagonist of FGF signaling in zebrafish. Development *128*, 2175-2186.

Furthauer, M., Thisse, C., and Thisse, B. (1997). A role for FGF-8 in the dorsoventral patterning of the zebrafish gastrula. Development *124*, 4253-4264.

Furthauer, M., Van Celst, J., Thisse, C., and Thisse, B. (2004). Fgf signalling controls the dorsoventral patterning of the zebrafish embryo. Development *131*, 2853-2864.

Gamse, J., and Sive, H. (2000). Vertebrate anteroposterior patterning: the Xenopus neurectoderm as a paradigm. Bioessays *22*, 976-986.

Gawantka, V., Pollet, N., Delius, H., Vingron, M., Pfister, R., Nitsch, R., Blumenstock, C., and Niehrs, C. (1998). Gene expression screening in Xenopus identifies molecular pathways, predicts gene function and provides a global view of embryonic patterning. Mech Dev *77*, 95-141.

Genikhovich, G., Fried, P., Prunster, M.M., Schinko, J.B., Gilles, A.F., Fredman, D., Meier, K., Iber, D., and Technau, U. (2015). Axis Patterning by BMPs: Cnidarian Network Reveals Evolutionary Constraints. Cell Rep *10*, 1646-1654.

Gilardelli, C.N., Pozzoli, O., Sordino, P., Matassi, G., and Cotelli, F. (2004). Functional and hierarchical interactions among zebrafish vox/vent homeobox genes. Dev Dyn *230*, 494-508.

Giraldez, A.J., Mishima, Y., Rihel, J., Grocock, R.J., Van Dongen, S., Inoue, K., Enright, A.J., and Schier, A.F. (2006). Zebrafish MiR-430 promotes deadenylation and clearance of maternal mRNAs. Science *312*, 75-79.

Gistelinck, C., Kwon, R.Y., Malfait, F., Symoens, S., Harris, M.P., Henke, K., Hawkins, M.B., Fisher, S., Sips, P., Guillemyn, B.*, et al.* (2018). Zebrafish type I collagen mutants

faithfully recapitulate human type I collagenopathies. Proc Natl Acad Sci U S A *115*, E8037-E8046.

Glinka, A., Wu, W., Delius, H., Monaghan, A.P., Blumenstock, C., and Niehrs, C. (1998). Dickkopf-1 is a member of a new family of secreted proteins and functions in head induction. Nature *391*, 357-362.

Gonzalez, E.M., Fekany-Lee, K., Carmany-Rampey, A., Erter, C., Topczewski, J., Wright, C.V., and Solnica-Krezel, L. (2000). Head and trunk in zebrafish arise via coinhibition of BMP signaling by bozozok and chordino. Genes Dev *14*, 3087-3092.

Graff, J.M., Thies, R.S., Song, J.J., Celeste, A.J., and Melton, D.A. (1994). Studies with a Xenopus BMP receptor suggest that ventral mesoderm-inducing signals override dorsal signals in vivo. Cell *79*, 169-179.

Grandel, H., Lun, K., Rauch, G.J., Rhinn, M., Piotrowski, T., Houart, C., Sordino, P., Kuchler, A.M., Schulte-Merker, S., Geisler, R.*, et al.* (2002). Retinoic acid signalling in the zebrafish embryo is necessary during pre-segmentation stages to pattern the anterior-posterior axis of the CNS and to induce a pectoral fin bud. Development *129*, 2851-2865.

Green, D., Whitener, A.E., Mohanty, S., and Lekven, A.C. (2015). Vertebrate nervous system posteriorization: Grading the function of Wnt signaling. Dev Dyn *244*, 507-512.

Green, J.B., New, H.V., and Smith, J.C. (1992). Responses of embryonic Xenopus cells to activin and FGF are separated by multiple dose thresholds and correspond to distinct axes of the mesoderm. Cell *71*, 731-739.

Griffin, K.J., and Kimelman, D. (2003). Interplay between FGF, one-eyed pinhead, and T-box transcription factors during zebrafish posterior development. Dev Biol *264*, 456-466.

Grinblat, Y., Gamse, J., Patel, M., and Sive, H. (1998). Determination of the zebrafish forebrain: induction and patterning. Development *125*, 4403-4416.

Gritsman, K., Talbot, W.S., and Schier, A.F. (2000). Nodal signaling patterns the organizer. Development *127*, 921-932.

Gritsman, K., Zhang, J., Cheng, S., Heckscher, E., Talbot, W.S., and Schier, A.F. (1999). The EGF-CFC protein one-eyed pinhead is essential for nodal signaling. Cell *97*, 121-132.

Grotewold, L., Plum, M., Dildrop, R., Peters, T., and Ruther, U. (2001). Bambi is coexpressed with Bmp-4 during mouse embryogenesis. Mech Dev *100*, 327-330.

Hammerschmidt, M., Pelegri, F., Mullins, M.C., Kane, D.A., van Eeden, F.J., Granato, M., Brand, M., Furutani-Seiki, M., Haffter, P., Heisenberg, C.P.*, et al.* (1996a). dino and mercedes, two genes regulating dorsal development in the zebrafish embryo. Development *123*, 95-102.

Hammerschmidt, M., Serbedzija, G.N., and McMahon, A.P. (1996b). Genetic analysis of dorsoventral pattern formation in the zebrafish: requirement of a BMP-like ventralizing activity and its dorsal repressor. Genes Dev *10*, 2452-2461.

Harland, R., and Gerhart, J. (1997). Formation and function of Spemann's organizer. Annu Rev Cell Dev Biol *13*, 611-667.

Harvey, S.A., and Smith, J.C. (2009). Visualisation and quantification of morphogen gradient formation in the zebrafish. PLoS Biol *7*, e1000101.

Hashiguchi, M., and Mullins, M.C. (2013). Anteroposterior and dorsoventral patterning are coordinated by an identical patterning clock. Development *140*, 1970-1980.

Heasman, J. (2006). Patterning the early Xenopus embryo. Development *133*, 1205-1217.

Heasman, J., Kofron, M., and Wylie, C. (2000). Beta-catenin signaling activity dissected in the early Xenopus embryo: a novel antisense approach. Dev Biol *222*, 124-134.

Heisenberg, C.P., and Solnica-Krezel, L. (2008). Back and forth between cell fate specification and movement during vertebrate gastrulation. Curr Opin Genet Dev *18*, 311-316.

Hernandez, R.E., Putzke, A.P., Myers, J.P., Margaretha, L., and Moens, C.B. (2007). Cyp26 enzymes generate the retinoic acid response pattern necessary for hindbrain development. Development *134*, 177-187.

Hikasa, H., Ezan, J., Itoh, K., Li, X., Klymkowsky, M.W., and Sokol, S.Y. (2010). Regulation of TCF3 by Wnt-dependent phosphorylation during vertebrate axis specification. Dev Cell *19*, 521-532.

Hikasa, H., and Sokol, S.Y. (2013). Wnt signaling in vertebrate axis specification. Cold Spring Harb Perspect Biol *5*, a007955.

Hild, M., Dick, A., Rauch, G.J., Meier, A., Bouwmeester, T., Haffter, P., and Hammerschmidt, M. (1999). The smad5 mutation somitabun blocks Bmp2b signaling during early dorsoventral patterning of the zebrafish embryo. Development *126*, 2149-2159.

Holley, S.A., Jackson, P.D., Sasai, Y., Lu, B., De Robertis, E.M., Hoffmann, F.M., and Ferguson, E.L. (1995). A conserved system for dorsal-ventral patterning in insects and vertebrates involving sog and chordin. Nature *376*, 249-253.

Hopkins, D.R., Keles, S., and Greenspan, D.S. (2007). The bone morphogenetic protein 1/Tolloid-like metalloproteinases. Matrix Biol *26*, 508-523.

Houart, C., Caneparo, L., Heisenberg, C., Barth, K., Take-Uchi, M., and Wilson, S. (2002). Establishment of the telencephalon during gastrulation by local antagonism of Wnt signaling. Neuron *35*, 255-265.

Hur, M., Gistelinck, C.A., Huber, P., Lee, J., Thompson, M.H., Monstad-Rios, A.T., Watson, C.J., McMenamin, S.K., Willaert, A., Parichy, D.M.*, et al.* (2017). MicroCT-based phenomics in the zebrafish skeleton reveals virtues of deep phenotyping in a distributed organ system. Elife *6*.

Hwang, W.Y., Fu, Y., Reyon, D., Maeder, M.L., Tsai, S.Q., Sander, J.D., Peterson, R.T., Yeh, J.R., and Joung, J.K. (2013). Efficient genome editing in zebrafish using a CRISPR-Cas system. Nat Biotechnol *31*, 227-229.

Ikeya, M., Fukushima, K., Kawada, M., Onishi, S., Furuta, Y., Yonemura, S., Kitamura, T., Nosaka, T., and Sasai, Y. (2010). Cv2, functioning as a pro-BMP factor via twisted gastrulation, is required for early development of nephron precursors. Dev Biol *337*, 405-414.

Imai, Y., Gates, M.A., Melby, A.E., Kimelman, D., Schier, A.F., and Talbot, W.S. (2001). The homeobox genes vox and vent are redundant repressors of dorsal fates in zebrafish. Development *128*, 2407-2420.

Inomata, H., Shibata, T., Haraguchi, T., and Sasai, Y. (2013). Scaling of dorsal-ventral patterning by embryo size-dependent degradation of Spemann's organizer signals. Cell *153*, 1296-1311.

Isaacs, H.V., Pownall, M.E., and Slack, J.M. (1994). eFGF regulates Xbra expression during Xenopus gastrulation. EMBO J *13*, 4469-4481.

Itoh, K., Krupnik, V.E., and Sokol, S.Y. (1998). Axis determination in Xenopus involves biochemical interactions of axin, glycogen synthase kinase 3 and beta-catenin. Curr Biol *8*, 591-594.

Itoh, K., and Sokol, S.Y. (1997). Graded amounts of Xenopus dishevelled specify discrete anteroposterior cell fates in prospective ectoderm. Mech Dev *61*, 113-125.

Jasuja, R., Ge, G., Voss, N.G., Lyman-Gingerich, J., Branam, A.M., Pelegri, F.J., and Greenspan, D.S. (2007). Bone morphogenetic protein 1 prodomain specifically binds and regulates signaling by bone morphogenetic proteins 2 and 4. J Biol Chem *282*, 9053-9062.

Jasuja, R., Voss, N., Ge, G., Hoffman, G.G., Lyman-Gingerich, J., Pelegri, F., and Greenspan, D.S. (2006). bmp1 and mini fin are functionally redundant in regulating formation of the zebrafish dorsoventral axis. Mech Dev *123*, 548-558.

Jones, C.M., Kuehn, M.R., Hogan, B.L., Smith, J.C., and Wright, C.V. (1995). Nodal-related signals induce axial mesoderm and dorsalize mesoderm during gastrulation. Development *121*, 3651-3662.

Joseph, E.M., and Melton, D.A. (1997). Xnr4: a Xenopus nodal-related gene expressed in the Spemann organizer. Dev Biol *184*, 367-372.

Kamato, D., Burch, M.L., Piva, T.J., Rezaei, H.B., Rostam, M.A., Xu, S., Zheng, W., Little, P.J., and Osman, N. (2013). Transforming growth factor-beta signalling: role and consequences of Smad linker region phosphorylation. Cell Signal *25*, 2017-2024.

Kanki, J.P., and Ho, R.K. (1997). The development of the posterior body in zebrafish. Development *124*, 881-893.

Kawahara, A., Wilm, T., Solnica-Krezel, L., and Dawid, I.B. (2000). Antagonistic role of vega1 and bozozok/dharma homeobox genes in organizer formation. Proc Natl Acad Sci U S A *97*, 12121-12126.

Kelly, C., Chin, A.J., Leatherman, J.L., Kozlowski, D.J., and Weinberg, E.S. (2000). Maternally controlled (beta)-catenin-mediated signaling is required for organizer formation in the zebrafish. Development *127*, 3899-3911.

Kemp, H.A., Carmany-Rampey, A., and Moens, C. (2009). Generating chimeric zebrafish embryos by transplantation. J Vis Exp.

Kengaku, M., and Okamoto, H. (1995). bFGF as a possible morphogen for the anteroposterior axis of the central nervous system in Xenopus. Development *121*, 3121-3130.

Kettleborough, R.N., Busch-Nentwich, E.M., Harvey, S.A., Dooley, C.M., de Bruijn, E., van Eeden, F., Sealy, I., White, R.J., Herd, C., Nijman, I.J.*, et al.* (2013). A systematic genome-wide analysis of zebrafish protein-coding gene function. Nature *496*, 494-497.

Khokha, M.K., Yeh, J., Grammer, T.C., and Harland, R.M. (2005). Depletion of three BMP antagonists from Spemann's organizer leads to a catastrophic loss of dorsal structures. Dev Cell *8*, 401-411.

Kiecker, C., and Niehrs, C. (2001). A morphogen gradient of Wnt/beta-catenin signalling regulates anteroposterior neural patterning in Xenopus. Development *128*, 4189-4201.

Kim, C.H., Oda, T., Itoh, M., Jiang, D., Artinger, K.B., Chandrasekharappa, S.C., Driever, W., and Chitnis, A.B. (2000). Repressor activity of Headless/Tcf3 is essential for vertebrate head formation. Nature *407*, 913-916.

Kimelman, D., and Griffin, K.J. (2000). Vertebrate mesendoderm induction and patterning. Curr Opin Genet Dev *10*, 350-356.

Kimelman, D., and Martin, B.L. (2012). Anterior-posterior patterning in early development: three strategies. Wiley Interdiscip Rev Dev Biol *1*, 253-266.

Kimmel, C.B., Ballard, W.W., Kimmel, S.R., Ullmann, B., and Schilling, T.F. (1995). Stages of embryonic development of the zebrafish. Dev Dyn *203*, 253-310.

Kimmel, C.B., Warga, R.M., and Schilling, T.F. (1990). Origin and organization of the zebrafish fate map. Development *108*, 581-594.

Kishimoto, Y., Lee, K.H., Zon, L., Hammerschmidt, M., and Schulte-Merker, S. (1997). The molecular nature of zebrafish swirl: BMP2 function is essential during early dorsoventral patterning. Development *124*, 4457-4466.

Knecht, A.K., and Harland, R.M. (1997). Mechanisms of dorsal-ventral patterning in noggin-induced neural tissue. Development *124*, 2477-2488.

Knoetgen, H., Viebahn, C., and Kessel, M. (1999). Head induction in the chick by primitive endoderm of mammalian, but not avian origin. Development *126*, 815-825.

Kok, F.O., Shin, M., Ni, C.W., Gupta, A., Grosse, A.S., van Impel, A., Kirchmaier, B.C., Peterson-Maduro, J., Kourkoulis, G., Male, I.*, et al.* (2015). Reverse genetic screening reveals poor correlation between morpholino-induced and mutant phenotypes in zebrafish. Dev Cell *32*, 97-108.

Korchynskyi, O., and ten Dijke, P. (2002). Identification and functional characterization of distinct critically important bone morphogenetic protein-specific response elements in the Id1 promoter. J Biol Chem *277*, 4883-4891.

Korinek, V., Barker, N., Morin, P.J., van Wichen, D., de Weger, R., Kinzler, K.W., Vogelstein, B., and Clevers, H. (1997). Constitutive transcriptional activation by a beta-catenin-Tcf complex in APC-/- colon carcinoma. Science *275*, 1784-1787.

Kramer, C., Mayr, T., Nowak, M., Schumacher, J., Runke, G., Bauer, H., Wagner, D.S., Schmid, B., Imai, Y., Talbot, W.S.*, et al.* (2002). Maternally supplied Smad5 is required for ventral specification in zebrafish embryos prior to zygotic Bmp signaling. Dev Biol *250*, 263-279.

Kudoh, T., Concha, M.L., Houart, C., Dawid, I.B., and Wilson, S.W. (2004). Combinatorial Fgf and Bmp signalling patterns the gastrula ectoderm into prospective neural and epidermal domains. Development *131*, 3581-3592.

Kudoh, T., Wilson, S.W., and Dawid, I.B. (2002). Distinct roles for Fgf, Wnt and retinoic acid in posteriorizing the neural ectoderm. Development *129*, 4335-4346.

Kumano, G., and Smith, W.C. (2002). Revisions to the Xenopus gastrula fate map: implications for mesoderm induction and patterning. Dev Dyn *225*, 409-421.

Kuroda, H., Fuentealba, L., Ikeda, A., Reversade, B., and De Robertis, E.M. (2005). Default neural induction: neuralization of dissociated Xenopus cells is mediated by Ras/MAPK activation. Genes Dev *19*, 1022-1027.

Kwon, H.J., Bhat, N., Sweet, E.M., Cornell, R.A., and Riley, B.B. (2010). Identification of early requirements for preplacodal ectoderm and sensory organ development. PLoS Genet *6*, e1001133.

Labalette, C., Bouchoucha, Y.X., Wassef, M.A., Gongal, P.A., Le Men, J., Becker, T., Gilardi-Hebenstreit, P., and Charnay, P. (2011). Hindbrain patterning requires fine-tuning of early krox20 transcription by Sprouty 4. Development *138*, 317-326.

Lamb, T.M., and Harland, R.M. (1995). Fibroblast growth factor is a direct neural inducer, which combined with noggin generates anterior-posterior neural pattern. Development *121*, 3627-3636.

Lane, M.C., and Sheets, M.D. (2000). Designation of the anterior/posterior axis in pregastrula Xenopus laevis. Dev Biol *225*, 37-58.

Lane, M.C., and Sheets, M.D. (2002). Rethinking axial patterning in amphibians. Dev Dyn *225*, 434-447.

Lane, M.C., and Smith, W.C. (1999). The origins of primitive blood in Xenopus: implications for axial patterning. Development *126*, 423-434.

Langdon, Y.G., and Mullins, M.C. (2011). Maternal and zygotic control of zebrafish dorsoventral axial patterning. Annu Rev Genet *45*, 357-377.

Lapraz, F., Besnardeau, L., and Lepage, T. (2009). Patterning of the dorsal-ventral axis in echinoderms: insights into the evolution of the BMP-chordin signaling network. PLoS Biol *7*, e1000248.

Larrain, J., Oelgeschlager, M., Ketpura, N.I., Reversade, B., Zakin, L., and De Robertis, E.M. (2001). Proteolytic cleavage of Chordin as a switch for the dual activities of Twisted gastrulation in BMP signaling. Development *128*, 4439-4447.

Lee, H.X., Ambrosio, A.L., Reversade, B., and De Robertis, E.M. (2006). Embryonic dorsal-ventral signaling: secreted frizzled-related proteins as inhibitors of tolloid proteinases. Cell *124*, 147-159.

Lee, H.X., Mendes, F.A., Plouhinec, J.L., and De Robertis, E.M. (2009). Enzymatic regulation of pattern: BMP4 binds CUB domains of Tolloids and inhibits proteinase activity. Genes Dev *23*, 2551-2562.

Lekven, A.C., Thorpe, C.J., Waxman, J.S., and Moon, R.T. (2001). Zebrafish wnt8 encodes two wnt8 proteins on a bicistronic transcript and is required for mesoderm and neurectoderm patterning. Dev Cell *1*, 103-114.

Lele, Z., Bakkers, J., and Hammerschmidt, M. (2001). Morpholino phenocopies of the swirl, snailhouse, somitabun, minifin, silberblick, and pipetail mutations. Genesis *30*, 190-194.

Leung, T., Bischof, J., Soll, I., Niessing, D., Zhang, D., Ma, J., Jackle, H., and Driever, W. (2003). bozozok directly represses bmp2b transcription and mediates the earliest dorsoventral asymmetry of bmp2b expression in zebrafish. Development *130*, 3639-3649.

Leyns, L., Bouwmeester, T., Kim, S.H., Piccolo, S., and De Robertis, E.M. (1997). Frzb-1 is a secreted antagonist of Wnt signaling expressed in the Spemann organizer. Cell *88*, 747-756.

Li, Y., Allende, M.L., Finkelstein, R., and Weinberg, E.S. (1994). Expression of two zebrafish orthodenticle-related genes in the embryonic brain. Mech Dev *48*, 229-244.

Linville, A., Radtke, K., Waxman, J.S., Yelon, D., and Schilling, T.F. (2009). Combinatorial roles for zebrafish retinoic acid receptors in the hindbrain, limbs and pharyngeal arches. Dev Biol *325*, 60-70.

Little, S.C., and Mullins, M.C. (2004). Twisted gastrulation promotes BMP signaling in zebrafish dorsal-ventral axial patterning. Development *131*, 5825-5835.

Little, S.C., and Mullins, M.C. (2006). Extracellular modulation of BMP activity in patterning the dorsoventral axis. Birth Defects Res C Embryo Today *78*, 224-242.

Little, S.C., and Mullins, M.C. (2009). Bone morphogenetic protein heterodimers assemble heteromeric type I receptor complexes to pattern the dorsoventral axis. Nat Cell Biol *11*, 637-643.

Maegawa, S., Varga, M., and Weinberg, E.S. (2006). FGF signaling is required for {beta}-catenin-mediated induction of the zebrafish organizer. Development *133*, 3265-3276.

Mali, P., Esvelt, K.M., and Church, G.M. (2013). Cas9 as a versatile tool for engineering biology. Nat Methods *10*, 957-963.

Marom, K., Levy, V., Pillemer, G., and Fainsod, A. (2005). Temporal analysis of the early BMP functions identifies distinct anti-organizer and mesoderm patterning phases. Dev Biol *282*, 442-454.

Marques, G., Musacchio, M., Shimell, M.J., Wunnenberg-Stapleton, K., Cho, K.W., and O'Connor, M.B. (1997). Production of a DPP activity gradient in the early Drosophila embryo through the opposing actions of the SOG and TLD proteins. Cell *91*, 417-426.

Martyn, U., and Schulte-Merker, S. (2003). The ventralized ogon mutant phenotype is caused by a mutation in the zebrafish homologue of Sizzled, a secreted Frizzled-related protein. Dev Biol *260*, 58-67.

Mason, J.M., Morrison, D.J., Basson, M.A., and Licht, J.D. (2006). Sprouty proteins: multifaceted negative-feedback regulators of receptor tyrosine kinase signaling. Trends Cell Biol *16*, 45-54.

Massague, J., Seoane, J., and Wotton, D. (2005). Smad transcription factors. Genes Dev *19*, 2783-2810.

Mathieu, J., Griffin, K., Herbomel, P., Dickmeis, T., Strahle, U., Kimelman, D., Rosa, F.M., and Peyrieras, N. (2004). Nodal and Fgf pathways interact through a positive regulatory loop and synergize to maintain mesodermal cell populations. Development *131*, 629-641.

Matsuzaki, K. (2013). Smad phospho-isoforms direct context-dependent TGF-beta signaling. Cytokine Growth Factor Rev *24*, 385-399.

Maves, L., and Kimmel, C.B. (2005). Dynamic and sequential patterning of the zebrafish posterior hindbrain by retinoic acid. Dev Biol *285*, 593-605.

McGrew, L.L., Hoppler, S., and Moon, R.T. (1997). Wnt and FGF pathways cooperatively pattern anteroposterior neural ectoderm in Xenopus. Mech Dev *69*, 105-114.

McGrew, L.L., Lai, C.J., and Moon, R.T. (1995). Specification of the anteroposterior neural axis through synergistic interaction of the Wnt signaling cascade with noggin and follistatin. Dev Biol *172*, 337-342.

McMahon, J.A., Takada, S., Zimmerman, L.B., Fan, C.M., Harland, R.M., and McMahon, A.P. (1998). Noggin-mediated antagonism of BMP signaling is required for growth and patterning of the neural tube and somite. Genes Dev *12*, 1438-1452.

Meinhardt, H. (2015a). Dorsoventral patterning by the Chordin-BMP pathway: a unified model from a pattern-formation perspective for Drosophila, vertebrates, sea urchins and Nematostella. Dev Biol *405*, 137-148.

Meinhardt, H. (2015b). Models for patterning primary embryonic body axes: The role of space and time. Semin Cell Dev Biol *42*, 103-117.

Meinhardt, H., and Gierer, A. (2000). Pattern formation by local self-activation and lateral inhibition. Bioessays *22*, 753-760.

Melby, A.E., Beach, C., Mullins, M., and Kimelman, D. (2000). Patterning the early zebrafish by the opposing actions of bozozok and vox/vent. Dev Biol *224*, 275-285.

Melby, A.E., Clements, W.K., and Kimelman, D. (1999). Regulation of dorsal gene expression in Xenopus by the ventralizing homeodomain gene Vox. Dev Biol *211*, 293-305.

Meno, C., Gritsman, K., Ohishi, S., Ohfuji, Y., Heckscher, E., Mochida, K., Shimono, A., Kondoh, H., Talbot, W.S., Robertson, E.J.*, et al.* (1999). Mouse Lefty2 and zebrafish antivin are feedback inhibitors of nodal signaling during vertebrate gastrulation. Mol Cell *4*, 287-298.

Merino, R., Rodriguez-Leon, J., Macias, D., Ganan, Y., Economides, A.N., and Hurle, J.M. (1999). The BMP antagonist Gremlin regulates outgrowth, chondrogenesis and programmed cell death in the developing limb. Development *126*, 5515-5522.

Messeguer, X., Escudero, R., Farre, D., Nunez, O., Martinez, J., and Alba, M.M. (2002). PROMO: detection of known transcription regulatory elements using species-tailored searches. Bioinformatics *18*, 333-334.

Miller-Bertoglio, V., Carmany-Rampey, A., Furthauer, M., Gonzalez, E.M., Thisse, C., Thisse, B., Halpern, M.E., and Solnica-Krezel, L. (1999). Maternal and zygotic activity of the zebrafish ogon locus antagonizes BMP signaling. Dev Biol *214*, 72-86.

Mintzer, K.A., Lee, M.A., Runke, G., Trout, J., Whitman, M., and Mullins, M.C. (2001). Lost-a-fin encodes a type I BMP receptor, Alk8, acting maternally and zygotically in dorsoventral pattern formation. Development *128*, 859-869.

Mishima, Y., and Tomari, Y. (2016). Codon Usage and 3' UTR Length Determine Maternal mRNA Stability in Zebrafish. Mol Cell *61*, 874-885.

Molina, G.A., Watkins, S.C., and Tsang, M. (2007). Generation of FGF reporter transgenic zebrafish and their utility in chemical screens. BMC Dev Biol *7*, 62.

Monteiro, R.M., de Sousa Lopes, S.M., Korchynskyi, O., ten Dijke, P., and Mummery, C.L. (2004). Spatio-temporal activation of Smad1 and Smad5 in vivo: monitoring transcriptional activity of Smad proteins. J Cell Sci *117*, 4653-4663.

Moon, R.T., and Kimelman, D. (1998). From cortical rotation to organizer gene expression: toward a molecular explanation of axis specification in Xenopus. Bioessays *20*, 536-545.

Muller, P., Rogers, K.W., Jordan, B.M., Lee, J.S., Robson, D., Ramanathan, S., and Schier, A.F. (2012). Differential diffusivity of Nodal and Lefty underlies a reaction-diffusion patterning system. Science *336*, 721-724.

Mullins, M.C. (1998). Holy Tolloido: Tolloid cleaves SOG/Chordin to free DPP/BMPs. Trends Genet *14*, 127-129.

Mullins, M.C., Hammerschmidt, M., Kane, D.A., Odenthal, J., Brand, M., van Eeden, F.J., Furutani-Seiki, M., Granato, M., Haffter, P., Heisenberg, C.P.*, et al.* (1996). Genes establishing dorsoventral pattern formation in the zebrafish embryo: the ventral specifying genes. Development *123*, 81-93.

Muraoka, O., Shimizu, T., Yabe, T., Nojima, H., Bae, Y.K., Hashimoto, H., and Hibi, M. (2006). Sizzled controls dorso-ventral polarity by repressing cleavage of the Chordin protein. Nat Cell Biol *8*, 329-338.

Myers, D.C., Sepich, D.S., and Solnica-Krezel, L. (2002). Bmp activity gradient regulates convergent extension during zebrafish gastrulation. Dev Biol *243*, 81-98.

Nguyen, V.H., Schmid, B., Trout, J., Connors, S.A., Ekker, M., and Mullins, M.C. (1998). Ventral and lateral regions of the zebrafish gastrula, including the neural crest progenitors, are established by a bmp2b/swirl pathway of genes. Dev Biol *199*, 93-110.

Nguyen, V.H., Trout, J., Connors, S.A., Andermann, P., Weinberg, E., and Mullins, M.C. (2000). Dorsal and intermediate neuronal cell types of the spinal cord are established by a BMP signaling pathway. Development *127*, 1209-1220.

Nikaido, M., Tada, M., Takeda, H., Kuroiwa, A., and Ueno, N. (1999). In vivo analysis using variants of zebrafish BMPR-IA: range of action and involvement of BMP in ectoderm patterning. Development *126*, 181-190.

Nordstrom, U., Jessell, T.M., and Edlund, T. (2002). Progressive induction of caudal neural character by graded Wnt signaling. Nat Neurosci *5*, 525-532.

O'Connor, M.N., Salles, II, Cvejic, A., Watkins, N.A., Walker, A., Garner, S.F., Jones, C.I., Macaulay, I.C., Steward, M., Zwaginga, J.J.*, et al.* (2009). Functional genomics in zebrafish permits rapid characterization of novel platelet membrane proteins. Blood *113*, 4754-4762.

Oelgeschlager, M., Larrain, J., Geissert, D., and De Robertis, E.M. (2000). The evolutionarily conserved BMP-binding protein Twisted gastrulation promotes BMP signalling. Nature *405*, 757-763.

Oelgeschlager, M., Reversade, B., Larrain, J., Little, S., Mullins, M.C., and De Robertis, E.M. (2003). The pro-BMP activity of Twisted gastrulation is independent of BMP binding. Development *130*, 4047-4056.

Onichtchouk, D., Chen, Y.G., Dosch, R., Gawantka, V., Delius, H., Massague, J., and Niehrs, C. (1999). Silencing of TGF-beta signalling by the pseudoreceptor BAMBI. Nature *401*, 480-485.

Onichtchouk, D., Glinka, A., and Niehrs, C. (1998). Requirement for Xvent-1 and Xvent-2 gene function in dorsoventral patterning of Xenopus mesoderm. Development *125*, 1447-1456.

Peluso, C.E., Umulis, D., Kim, Y.J., O'Connor, M.B., and Serpe, M. (2011). Shaping BMP morphogen gradients through enzyme-substrate interactions. Dev Cell *21*, 375-383.

Pera, E.M., Ikeda, A., Eivers, E., and De Robertis, E.M. (2003). Integration of IGF, FGF, and anti-BMP signals via Smad1 phosphorylation in neural induction. Genes Dev *17*, 3023-3028.

Persson, U., Izumi, H., Souchelnytskyi, S., Itoh, S., Grimsby, S., Engstrom, U., Heldin, C.H., Funa, K., and ten Dijke, P. (1998). The L45 loop in type I receptors for TGF-beta family members is a critical determinant in specifying Smad isoform activation. FEBS Lett *434*, 83-87.

Perz-Edwards, A., Hardison, N.L., and Linney, E. (2001). Retinoic acid-mediated gene expression in transgenic reporter zebrafish. Dev Biol *229*, 89-101.

Piccolo, S., Agius, E., Lu, B., Goodman, S., Dale, L., and De Robertis, E.M. (1997). Cleavage of Chordin by Xolloid metalloprotease suggests a role for proteolytic processing in the regulation of Spemann organizer activity. Cell *91*, 407-416.

Piccolo, S., Sasai, Y., Lu, B., and De Robertis, E.M. (1996). Dorsoventral patterning in Xenopus: inhibition of ventral signals by direct binding of chordin to BMP-4. Cell *86*, 589-598.

Placinta, M., Shen, M.C., Achermann, M., and Karlstrom, R.O. (2009). A laser pointer driven microheater for precise local heating and conditional gene regulation in vivo. Microheater driven gene regulation in zebrafish. BMC Dev Biol *9*, 73.

Plouhinec, J.L., Zakin, L., Moriyama, Y., and De Robertis, E.M. (2013). Chordin forms a self-organizing morphogen gradient in the extracellular space between ectoderm and mesoderm in the Xenopus embryo. Proc Natl Acad Sci U S A *110*, 20372-20379.

Pomreinke, A.P., Soh, G.H., Rogers, K.W., Bergmann, J.K., Blassle, A.J., and Muller, P. (2017). Dynamics of BMP signaling and distribution during zebrafish dorsal-ventral patterning. Elife *6*.

Port, F., and Basler, K. (2010). Wnt trafficking: new insights into Wnt maturation, secretion and spreading. Traffic *11*, 1265-1271.

Pownall, M.E., and Isaacs, H.V. (2010). In FGF Signalling in Vertebrate Development (San Rafael (CA): Morgan & Claypool Life Sciences).

Pyati, U.J., Webb, A.E., and Kimelman, D. (2005). Transgenic zebrafish reveal stage-specific roles for Bmp signaling in ventral and posterior mesoderm development. Development *132*, 2333-2343.

Ramel, M.C., Buckles, G.R., Baker, K.D., and Lekven, A.C. (2005). WNT8 and BMP2B co-regulate non-axial mesoderm patterning during zebrafish gastrulation. Dev Biol *287*, 237-248.

Ramel, M.C., and Hill, C.S. (2013). The ventral to dorsal BMP activity gradient in the early zebrafish embryo is determined by graded expression of BMP ligands. Dev Biol *378*, 170-182.

Ramel, M.C., and Lekven, A.C. (2004). Repression of the vertebrate organizer by Wnt8 is mediated by Vent and Vox. Development *131*, 3991-4000.

Rebagliati, M.R., Toyama, R., Haffter, P., and Dawid, I.B. (1998). cyclops encodes a nodal-related factor involved in midline signaling. Proc Natl Acad Sci U S A *95*, 9932-9937.

Reichert, S., Randall, R.A., and Hill, C.S. (2013). A BMP regulatory network controls ectodermal cell fate decisions at the neural plate border. Development *140*, 4435-4444.

Reifers, F., Bohli, H., Walsh, E.C., Crossley, P.H., Stainier, D.Y., and Brand, M. (1998). Fgf8 is mutated in zebrafish acerebellar (ace) mutants and is required for maintenance of midbrain-hindbrain boundary development and somitogenesis. Development *125*, 2381-2395.

Rentzsch, F., Zhang, J., Kramer, C., Sebald, W., and Hammerschmidt, M. (2006). Crossveinless 2 is an essential positive feedback regulator of Bmp signaling during zebrafish gastrulation. Development *133*, 801-811.

Reversade, B., and De Robertis, E.M. (2005). Regulation of ADMP and BMP2/4/7 at opposite embryonic poles generates a self-regulating morphogenetic field. Cell *123*, 1147-1160.

Reynolds, S.D., Angerer, L.M., Palis, J., Nasir, A., and Angerer, R.C. (1992). Early mRNAs, spatially restricted along the animal-vegetal axis of sea urchin embryos, include one encoding a protein related to tolloid and BMP-1. Development *114*, 769-786.

Rhinn, M., and Dolle, P. (2012). Retinoic acid signalling during development. Development *139*, 843-858.

Rhinn, M., Lun, K., Luz, M., Werner, M., and Brand, M. (2005). Positioning of the midbrain-hindbrain boundary organizer through global posteriorization of the neuroectoderm mediated by Wnt8 signaling. Development *132*, 1261-1272.

Rogers, K.W., and Schier, A.F. (2011). Morphogen gradients: from generation to interpretation. Annu Rev Cell Dev Biol *27*, 377-407.

Ross, J.J., Shimmi, O., Vilmos, P., Petryk, A., Kim, H., Gaudenz, K., Hermanson, S., Ekker, S.C., O'Connor, M.B., and Marsh, J.L. (2001). Twisted gastrulation is a conserved extracellular BMP antagonist. Nature *410*, 479-483.

Row, R.H., and Kimelman, D. (2009). Bmp inhibition is necessary for post-gastrulation patterning and morphogenesis of the zebrafish tailbud. Dev Biol *329*, 55-63.

Rowan, A.M., Stern, C.D., and Storey, K.G. (1999). Axial mesendoderm refines rostrocaudal pattern in the chick nervous system. Development *126*, 2921-2934.

Sansom, S.N., and Livesey, F.J. (2009). Gradients in the brain: the control of the development of form and function in the cerebral cortex. Cold Spring Harb Perspect Biol *1*, a002519.

Santos, D., Luzio, A., and Coimbra, A.M. (2017). Zebrafish sex differentiation and gonad development: A review on the impact of environmental factors. Aquat Toxicol *191*, 141-163.

Sapkota, G., Alarcon, C., Spagnoli, F.M., Brivanlou, A.H., and Massague, J. (2007). Balancing BMP signaling through integrated inputs into the Smad1 linker. Mol Cell *25*, 441-454.

Schier, A.F. (2001). Axis formation and patterning in zebrafish. Curr Opin Genet Dev *11*, 393-404.

Schier, A.F. (2003). Nodal signaling in vertebrate development. Annu Rev Cell Dev Biol *19*, 589-621.

Schier, A.F. (2009). Nodal morphogens. Cold Spring Harb Perspect Biol *1*, a003459.

Schier, A.F., and Talbot, W.S. (2005). Molecular genetics of axis formation in zebrafish. Annu Rev Genet *39*, 561-613.

Schilling, T.F. (2008). Anterior-posterior patterning and segmentation of the vertebrate head. Integr Comp Biol *48*, 658-667.

Schmid, B., Furthauer, M., Connors, S.A., Trout, J., Thisse, B., Thisse, C., and Mullins, M.C. (2000). Equivalent genetic roles for bmp7/snailhouse and bmp2b/swirl in dorsoventral pattern formation. Development *127*, 957-967.

Schmierer, B., and Hill, C.S. (2007). TGFbeta-SMAD signal transduction: molecular specificity and functional flexibility. Nat Rev Mol Cell Biol *8*, 970-982.

Schohl, A., and Fagotto, F. (2002). Beta-catenin, MAPK and Smad signaling during early Xenopus development. Development *129*, 37-52.

Scholpp, S., and Brand, M. (2004). Endocytosis controls spreading and effective signaling range of Fgf8 protein. Curr Biol *14*, 1834-1841.

Schroeder, K.E., and Yost, H.J. (1996). Xenopus poly (A) binding protein maternal RNA is localized during oogenesis and associated with large complexes in blastula. Dev Genet *19*, 268-276.

Schulte-Merker, S., Lee, K.J., McMahon, A.P., and Hammerschmidt, M. (1997). The zebrafish organizer requires chordino. Nature *387*, 862-863.

Schumacher, J.A., Hashiguchi, M., Nguyen, V.H., and Mullins, M.C. (2011). An intermediate level of BMP signaling directly specifies cranial neural crest progenitor cells in zebrafish. PLoS One *6*, e27403.

Scott, I.C., Blitz, I.L., Pappano, W.N., Maas, S.A., Cho, K.W., and Greenspan, D.S. (2001). Homologues of Twisted gastrulation are extracellular cofactors in antagonism of BMP signalling. Nature *410*, 475-478.

Selleck, M.A., Garcia-Castro, M.I., Artinger, K.B., and Bronner-Fraser, M. (1998). Effects of Shh and Noggin on neural crest formation demonstrate that BMP is required in the neural tube but not ectoderm. Development *125*, 4919-4930.

Serpe, M., Umulis, D., Ralston, A., Chen, J., Olson, D.J., Avanesov, A., Othmer, H., O'Connor, M.B., and Blair, S.S. (2008). The BMP-binding protein Crossveinless 2 is a short-range, concentration-dependent, biphasic modulator of BMP signaling in Drosophila. Dev Cell *14*, 940-953.

Shi, Y., and Massague, J. (2003). Mechanisms of TGF-beta signaling from cell membrane to the nucleus. Cell *113*, 685-700.

Shimizu, N., Kawakami, K., and Ishitani, T. (2012). Visualization and exploration of Tcf/Lef function using a highly responsive Wnt/beta-catenin signaling-reporter transgenic zebrafish. Dev Biol *370*, 71-85.

Shimizu, T., Bae, Y.K., Muraoka, O., and Hibi, M. (2005). Interaction of Wnt and caudal-related genes in zebrafish posterior body formation. Dev Biol *279*, 125-141.

Shimizu, T., Yamanaka, Y., Nojima, H., Yabe, T., Hibi, M., and Hirano, T. (2002). A novel repressor-type homeobox gene, ved, is involved in dharma/bozozok-mediated dorsal organizer formation in zebrafish. Mech Dev *118*, 125-138.

Shimozono, S., Iimura, T., Kitaguchi, T., Higashijima, S., and Miyawaki, A. (2013). Visualization of an endogenous retinoic acid gradient across embryonic development. Nature *496*, 363-366.

Shoji, W., and Sato-Maeda, M. (2008). Application of heat shock promoter in transgenic zebrafish. Dev Growth Differ *50*, 401-406.

Simeone, A., Acampora, D., Mallamaci, A., Stornaiuolo, A., D'Apice, M.R., Nigro, V., and Boncinelli, E. (1993). A vertebrate gene related to orthodenticle contains a homeodomain of the bicoid class and demarcates anterior neuroectoderm in the gastrulating mouse embryo. EMBO J *12*, 2735-2747.

Sirbu, I.O., Gresh, L., Barra, J., and Duester, G. (2005). Shifting boundaries of retinoic acid activity control hindbrain segmental gene expression. Development *132*, 2611-2622.

Sirotkin, H.I., Dougan, S.T., Schier, A.F., and Talbot, W.S. (2000). bozozok and squint act in parallel to specify dorsal mesoderm and anterior neuroectoderm in zebrafish. Development *127*, 2583-2592.

Smith, S.M., and Maughan, P.J. (2015). SNP genotyping using KASPar assays. Methods Mol Biol *1245*, 243-256.

Smith, W.C., McKendry, R., Ribisi, S., Jr., and Harland, R.M. (1995). A nodal-related gene defines a physical and functional domain within the Spemann organizer. Cell *82*, 37-46.

Solnica-Krezel, L. (2005). Conserved patterns of cell movements during vertebrate gastrulation. Curr Biol *15*, R213-228.

Solnica-Krezel, L., and Driever, W. (2001). The role of the homeodomain protein Bozozok in zebrafish axis formation. Int J Dev Biol *45*, 299-310.

Stanganello, E., Hagemann, A.I., Mattes, B., Sinner, C., Meyen, D., Weber, S., Schug, A., Raz, E., and Scholpp, S. (2015). Filopodia-based Wnt transport during vertebrate tissue patterning. Nat Commun *6*, 5846.

Stern, C.D., Charite, J., Deschamps, J., Duboule, D., Durston, A.J., Kmita, M., Nicolas, J.F., Palmeirim, I., Smith, J.C., and Wolpert, L. (2006). Head-tail patterning of the vertebrate embryo: one, two or many unresolved problems? Int J Dev Biol *50*, 3-15.

Sun, Y., Tseng, W.C., Fan, X., Ball, R., and Dougan, S.T. (2014). Extraembryonic signals under the control of MGA, Max, and Smad4 are required for dorsoventral patterning. Dev Cell *28*, 322-334.

Suzuki, T., Hasso, S.M., and Fallon, J.F. (2008). Unique SMAD1/5/8 activity at the phalanx-forming region determines digit identity. Proc Natl Acad Sci U S A *105*, 4185-4190.

Tao, Q., Yokota, C., Puck, H., Kofron, M., Birsoy, B., Yan, D., Asashima, M., Wylie, C.C., Lin, X., and Heasman, J. (2005). Maternal wnt11 activates the canonical wnt signaling pathway required for axis formation in Xenopus embryos. Cell *120*, 857-871.

Thisse, B., Wright, C.V., and Thisse, C. (2000). Activin- and Nodal-related factors control antero-posterior patterning of the zebrafish embryo. Nature *403*, 425-428.

Thisse, C., and Thisse, B. (1999). Antivin, a novel and divergent member of the TGFbeta superfamily, negatively regulates mesoderm induction. Development *126*, 229-240.

Thomas, P., and Beddington, R. (1996). Anterior primitive endoderm may be responsible for patterning the anterior neural plate in the mouse embryo. Curr Biol *6*, 1487-1496.

Toyama, R., O'Connell, M.L., Wright, C.V., Kuehn, M.R., and Dawid, I.B. (1995). Nodal induces ectopic goosecoid and lim1 expression and axis duplication in zebrafish. Development *121*, 383-391.

Trindade, M., Tada, M., and Smith, J.C. (1999). DNA-binding specificity and embryological function of Xom (Xvent-2). Dev Biol *216*, 442-456.

Troilo, H., Zuk, A.V., Tunnicliffe, R.B., Wohl, A.P., Berry, R., Collins, R.F., Jowitt, T.A., Sengle, G., and Baldock, C. (2014). Nanoscale structure of the BMP antagonist chordin supports cooperative BMP binding. Proc Natl Acad Sci U S A *111*, 13063-13068.

Tsang, M., Kim, R., de Caestecker, M.P., Kudoh, T., Roberts, A.B., and Dawid, I.B. (2000). Zebrafish nma is involved in TGFbeta family signaling. Genesis *28*, 47-57.

Tuazon, F.B., and Mullins, M.C. (2015). Temporally coordinated signals progressively pattern the anteroposterior and dorsoventral body axes. Semin Cell Dev Biol *42*, 118-133.

Tucker, A.S., and Slack, J.M. (1995). Tail bud determination in the vertebrate embryo. Curr Biol *5*, 807-813.

Tucker, J.A., Mintzer, K.A., and Mullins, M.C. (2008). The BMP signaling gradient patterns dorsoventral tissues in a temporally progressive manner along the anteroposterior axis. Dev Cell *14*, 108-119.

Umulis, D., O'Connor, M.B., and Blair, S.S. (2009). The extracellular regulation of bone morphogenetic protein signaling. Development *136*, 3715-3728.

Umulis, D.M., and Othmer, H.G. (2013). Mechanisms of scaling in pattern formation. Development *140*, 4830-4843.

van Boxtel, A.L., Chesebro, J.E., Heliot, C., Ramel, M.C., Stone, R.K., and Hill, C.S. (2015). A Temporal Window for Signal Activation Dictates the Dimensions of a Nodal Signaling Domain. Dev Cell *35*, 175-185.

von der Hardt, S., Bakkers, J., Inbal, A., Carvalho, L., Solnica-Krezel, L., Heisenberg, C.P., and Hammerschmidt, M. (2007). The Bmp gradient of the zebrafish gastrula guides migrating lateral cells by regulating cell-cell adhesion. Curr Biol *17*, 475-487.

Wardle, F.C., Welch, J.V., and Dale, L. (1999). Bone morphogenetic protein 1 regulates dorsal-ventral patterning in early Xenopus embryos by degrading chordin, a BMP4 antagonist. Mech Dev *86*, 75-85.

Wawersik, S., Evola, C., and Whitman, M. (2005). Conditional BMP inhibition in Xenopus reveals stage-specific roles for BMPs in neural and neural crest induction. Dev Biol *277*, 425-442.

White, R.J., Nie, Q., Lander, A.D., and Schilling, T.F. (2007). Complex regulation of cyp26a1 creates a robust retinoic acid gradient in the zebrafish embryo. PLoS Biol *5*, e304.

White, R.J., and Schilling, T.F. (2008). How degrading: Cyp26s in hindbrain development. Dev Dyn *237*, 2775-2790.

Whitfield, T.T., and Hammond, K.L. (2007). Axial patterning in the developing vertebrate inner ear. Int J Dev Biol *51*, 507-520.

Wilson, P.A., Lagna, G., Suzuki, A., and Hemmati-Brivanlou, A. (1997). Concentration-dependent patterning of the Xenopus ectoderm by BMP4 and its signal transducer Smad1. Development *124*, 3177-3184.

Wolpert, L. (1969). Positional information and the spatial pattern of cellular differentiation. J Theor Biol *25*, 1-47.

Woo, K., and Fraser, S.E. (1997). Specification of the zebrafish nervous system by nonaxial signals. Science *277*, 254-257.

Xie, J., and Fisher, S. (2005). Twisted gastrulation enhances BMP signaling through chordin dependent and independent mechanisms. Development *132*, 383-391.

Xue, Y., Zheng, X., Huang, L., Xu, P., Ma, Y., Min, Z., Tao, Q., Tao, Y., and Meng, A. (2014). Organizer-derived Bmp2 is required for the formation of a correct Bmp activity gradient during embryonic development. Nat Commun *5*, 3766.

Yabe, T., Shimizu, T., Muraoka, O., Bae, Y.K., Hirata, T., Nojima, H., Kawakami, A., Hirano, T., and Hibi, M. (2003). Ogon/Secreted Frizzled functions as a negative feedback regulator of Bmp signaling. Development *130*, 2705-2716.

Yamaguchi, T.P. (2001). Heads or tails: Wnts and anterior-posterior patterning. Curr Biol *11*, R713-724.

Yu, S.R., Burkhardt, M., Nowak, M., Ries, J., Petrasek, Z., Scholpp, S., Schwille, P., and Brand, M. (2009). Fgf8 morphogen gradient forms by a source-sink mechanism with freely diffusing molecules. Nature *461*, 533-536.

Zagorski, M., Tabata, Y., Brandenberg, N., Lutolf, M.P., Tkacik, G., Bollenbach, T., Briscoe, J., and Kicheva, A. (2017). Decoding of position in the developing neural tube from antiparallel morphogen gradients. Science *356*, 1379-1383.

Zakin, L., and De Robertis, E.M. (2010). Extracellular regulation of BMP signaling. Curr Biol *20*, R89-92.

Zhang, J.L., Patterson, L.J., Qiu, L.Y., Graziussi, D., Sebald, W., and Hammerschmidt, M. (2010). Binding between Crossveinless-2 and Chordin von Willebrand factor type C domains promotes BMP signaling by blocking Chordin activity. PLoS One *5*, e12846.

Zhu, H., Kavsak, P., Abdollah, S., Wrana, J.L., and Thomsen, G.H. (1999). A SMAD ubiquitin ligase targets the BMP pathway and affects embryonic pattern formation. Nature *400*, 687-693.

Zimmerman, L.B., De Jesus-Escobar, J.M., and Harland, R.M. (1996). The Spemann organizer signal noggin binds and inactivates bone morphogenetic protein 4. Cell *86*, 599-606.

Zinski, J., Bu, Y., Wang, X., Dou, W., Umulis, D., and Mullins, M.C. (2017). Systems biology derived source-sink mechanism of BMP gradient formation. Elife *6*.

Zinski, J., Tajer, B., and Mullins, M.C. (2018). TGF-beta Family Signaling in Early Vertebrate Development. Cold Spring Harb Perspect Biol *10*.

Zinski, J., Tuazon, F., Huang, Y., Mullins, M., and Umulis, D. (2019). Imaging and Quantification of P-Smad1/5 in Zebrafish Blastula and Gastrula Embryos. Methods Mol Biol *1891*, 135-154.